POLYDOPAMINE-FUNCTIONALIZED AGAROSE MICROSPHERES FOR 3D ENGINEERED NEURONAL CULTURES

BY

HALLIE GRANT ARNOTT

A THESIS SUBMITTED TO THE UNIVERSITY OF OTTAWA

IN PARTIAL FULFILLMENT OF THE REQUIREMENTS FOR THE DEGREE OF

MASTER OF APPLIED SCIENCE IN BIOMEDICAL ENGINEERING

OTTAWA-CARLETON INSTITUTE FOR BIOMEDICAL ENGINEERING

FACULTY OF ENGINEERING

UNIVERSITY OF OTTAWA

ABSTRACT

Developing biomimetic 3D constructs to study neuronal networks and screen therapeutic agents *in vitro* is critical to address the limitations of conventional 2D cultures used in pre-clinical studies. Since substrate stiffness and culture dimensionality influence behaviour of neurons *in vitro,* using rigid 2D substrates limits translational potential and physiological accuracy. To improve physiological relevance of *in vitro* neuronal cultures, 3D constructs are engineered to recapitulate the material properties of the cerebral matrix which neuronal networks depend upon *in vivo*. Of particular importance is mimicking the low Young's modulus of the extracellular matrix in the brain, while providing regions for neuronal adhesion to promote viability and growth. To this end, a 3D microsphere-based strategy was investigated, where multiple microspheres collectively acting as a scaffold with high interconnected porosity were used to provide adhesive, 3D growth area. Specifically, agarose—a natural polysaccharide—was used to fabricate soft microspheres which are subsequently functionalized with the bio-inspired and adhesive polymer, polydopamine. Microfluidic technology yielded an agarose microsphere population of highly monodisperse diameters. Successful functionalization of the microspheres with polydopamine was verified through identification of the characteristic Raman spectra of polydopamine. Measured through atomic force nanoindentations in water, the Young's modulus of the agarose microsphere measured 4.9 ± 0.6 kPa –10^6 times lower than conventional culture-ware. The Young's modulus was found to increase to 26.8 ± 17.9 kPa after functionalization with polydopamine, where the large standard deviation was attributed to the nano- mechanical and -topographical non-homogeneity of the resulting surface due to polydopamine aggregation Microsphere stiffness followed the same trend while also increasing as a function of indentation depth. Functionalization of microspheres with polydopamine was also shown to significantly increase material surface adhesion compared to poly-D-lysine and laminin functionalized glass microspheres (a recently reported microsphere-based model). Finally, the microspheres were shown to provide embryonic cerebral neurons with 3D growth area while facilitating neural adhesion and neurite development. This work provides a 3D, soft and adhesive *in vitro* model for neuronal culture with improved biomimetics over current microsphere-based protocols, and ultimately rigid 2D culture-ware.

Keywords: 3D neuronal culture, agarose, biomimetics, microspheres, polydopamine

ACKNOWLEDGEMENTS

I would like to start by thanking my supervisor, Dr. Fabio Variola, for his guidance throughout the course of this thesis and the high-quality material characterization equipment he provided in his lab space for me to use. I am extremely grateful to have had the opportunity to dive deeper into the realm of material science within biomedical engineering field while working with the Variola Research Group.

I also owe sincere gratitude to Alexander Steeves, for teaching me all about atomic force microscopy and for being available and open for questions of any topic, at any time. Thank you also to David Lomboni who assisted in expediting 2D neuronal culture experiments during the pandemic. I would also like to thank my other lab mates, Michael Spracklin and Ryan Berthelot for their support and presence during my graduate studies.

Next, I would like to express my thanks to the collaborators in the Faculty of Medicine who took me in to complete the cell culture portions of this thesis. In particular, I am grateful to Dr. Sarah Schock for teaching me about neuronal culture, showing me how to harvest cerebral neurons, and for completing harvests for me to increase neuron yield for my experiments. I am also thankful for Dr. William Staines for sharing his laboratory space, textbooks and passion for neuroscience with me while in his lab. Also, I acknowledge the support of Dr. Chloe Van Oostende-Triple and all staff at the uOttawa CBIA Microscopy Core for training me on all the confocal microscopes.

Thanks also to my collaborators at the Godin Laboratory—where the agarose microsphere idea was born. Specifically, I would like to thank Nicholas Soucy for fabricating the microspheres at moments notice, and to Dr. Michel Godin, for fostering this collaboration without hesitation.

Finally, I would like to thank my family. It is always easier with you five in my corner. Particular thanks to Dad, for always being only a building over, whenever needed.

STATEMENT OF CONTRIBUTION

Microfluidic Device and Agarose Sphere Fabrication

To fabricate the agarose microspheres used in this thesis, a collaboration was made with the *Godin Laboratory* at the University of Ottawa. This laboratory specializes in fabricating agarose microspheres using microfluidic technology. Particularly, Nicholas Soucy, is responsible for fabricating the microfluidic devices and running polymers prepared by me through their device. This method is elaborated on in Section 3.2.2 of this thesis.

Embryonic Cerebral Neuron Harvest

The embryonic cerebral neurons used in this thesis which were harvested from mice (not those used from frozen vials) were generously shared with me by members of the Staines Laboratory from the Faculty of Medicine. The harvesting procedure outlined in Section 3.4.1 of this thesis is performed by Dr. Sarah Schock.

All Remaining Work

The remaining portions of work presented in this thesis was carried out by me, Hallie Arnott (author of this thesis). I am also responsible for all writing in this thesis.

TABLE OF CONTENTS

LIST OF FIGURES

LIST OF TABLES

LIST OF ABBREVIATIONS AND ACRONYMS

2D	Two-dimensional
3D	Three-dimensional
AFM	Atomic Force Microscopy
CGM	Complete growth media
DAPI	4', 6-Diamidino-2Phenylindole, Dihydrochloride
DIC	Differential interference contrast
DIV	Days in vitro
DMSO	Dimethyl sulfoxide
ECM	Extracellular matrix
FBS	Fetal bovine serum
FWHM	Full width half maximum
HBSS	Hanks balanced salt solution
MEA	Microelectrode array
ID	Inner diameter
OD	Outer diameter
PBS	Phosphate buffered saline
PDA	Polydopamine
PDL	Poly-D-lysine
PLGA	Poly (lactic-co-glycolic acid)
PLL	Poly-L-lysine
SLG	Soda-lime glass
TBS	Tris buffered saline

LIST OF SUPPLIERS

Bruker	Billerica, MA, USA
Charles River	Virginia, USA
Corning	Corning, NY, USA
Cospheric	Santa Barbra, CA, USA
MatTek	Ashland, MA, USA
Millipore-Sigma *(formerly Sigma-Aldrich)*	Burlington, MA, USA
OriginLabs	MA, USA
Thermo-Fisher Scientific	Waltham, MA, USA
QBM Cell Science	Ottawa, ON, Canada
WITec	Ulm, Germany
Zeiss	Germany

1 MOTIVATION, OBJECTIVES, AND HYPOTHESES

1.1 CONTEXT

Pathology and treatment of disease have evolved immensely in recent decades. Researchers continue to uncover disease mechanisms and develop pharmacological solutions to provide quality healthcare. However, an area of medicine that continues to present challenge is the etiology and pharmaceutical options for neurological disease [1]–[3]. This challenge can be largely due to the brain's intricacy, attributed to its complex connectome [4], [5] that has yet to be completely elucidated [6]. In addition, challenges associated with pharmaceutical development (pharmacokinetics, dosage, effective testing) limit clinical translation. Consequently, effective pharmacological intervention for those suffering from neurological diseases—particularly neurodegenerative diseases such as Alzheimer's, Parkinson's, and Multiple Sclerosis—presents an unmet clinical need. Currently, many neurological diseases are not curable; therefore, it is imperative that the available therapies are effective in supressing the life-altering symptoms associated with these diseases.

In Canada, neurological diseases, disorders and injuries are among the leading causes of disability [7], [8], with an estimated 3.6 million Canadians living with a neurological condition [9]. As the population grows and ages, prevalence of neurological diseases—which comprise a large part of the aforementioned statistic—is expected to increase. Unfortunately, most neurological diseases are associated with symptoms worsening with age, which speaks to the severity of the problem. A study conducted by Gaskin *et al* evaluated the burden of neurological conditions in Canada. Among the study's conclusions, authors state:

> *"a coordinated approach to etiologic research and treatment is required to reduce the associated burden of the disease".*

In other words, to improve the state of neurological disease, a synchronized effort toward a complete understanding of the pathology and effective treatments and therapies will ultimately improve this burden.

In pursuit of answers, researchers in the biomedical sciences community have worked to further unravel the complex molecular cascades and triggers involved in neurological diseases [10]–[12]. Although progression in this realm of research has been significant, clinical translation of target therapies based on the pre-clinical findings remains challenging [13]–[16]. For example, the FDA has only approved six drugs to medically treat Alzheimer's disease, which act only to control symptoms with varying effectiveness [17]. Currently, no drugs are proven to significantly alter or slow the progression of the disease.

The likely culprits responsible for limited clinical translational of these therapies are the preclinical screening models used as the read-out for putative therapeutic efficacy. These approaches are comprised mainly of two-dimensional (2D) cell culture methods and animal models. Although these approaches have provided platforms to elucidate disease mechanisms and evaluate neurotherapeutics, neither adequately mimics the key properties the *in vivo* environment for physiological accuracy. This limits our ability to study neurological disease for effective pharmacological intervention. Returning to the remark from Gaskin *et al* cited above, a coordinated approach is indeed the solution required to advance this field and improve the quality of life for those suffering with these incurable diseases. With an engineering take on their conclusion, collaboration between biomedical science and material engineering fields has emerged as a promising multidisciplinary approach to potentially improve the preclinical testing platforms used to evaluate therapies for these diseases [18]–[21].

1.2 MOTIVATION

To enhance the standard 2D cell culture techniques and reduce dependency on animal models to study and evaluate neuro-therapeutics, the field has turned to biomaterials for application in neuronal cell cultures. More specifically, three-dimensional (3D) *in vitro* modeling using biomaterials has begun to fill the gap that currently exists between 2D cell cultures and animal models. In doing so, biomaterials science has provided a key to generate a wide variety of scaffolds to improve the physiological relevance and breadth of conventional *in vitro* techniques, moving toward improved pre-clinical outcomes [22], [23]. Previous work in the space has shown microsphere-based geometry provides excellent 3D scaffolding for neuronal networks with multiple advantages over other 3D-scaffolding designs [20], [24], [25]. However, many of these

works employ stiff microspheres to construct the scaffold, which reduce physiological relevance of the model. In the few works that employ softer polymeric microspheres, a high polydispersity is observed, limiting ability to control culture growth area. Additionally, steps to functionalize the surface of the microspheres/scaffold tend to employ covalent chemical conjugation or physical adsorption which involve multistep processes in addition to plasma or chemical treatments [26]. These processes can be cytotoxic, material-specific, and lengthy.

The present work aims to contribute to this research space by improving 3D microsphere-based models for neuronal culture through utilization of soft microspheres functionalized with a single-step, bio-inspired strategy. In particular, the model is designed to mimic the Young's modulus of the neural extracellular matrix (ECM) through the use of agarose as the microsphere material, while adhesive properties for neuronal attachment and growth are provided through functionalization of the microsphere with polydopamine (PDA). Additionally, the microsphere fabrication method will capitalize on precise microfluidic technology to achieve monodisperse microsphere population for the construct. Atomic Force Microscopy (AFM) and Raman Spectroscopy are used to quantify the nanomechanical properties and chemical composition of the 3D construct, respectively, while neuronal adhesion and growth are assessed via confocal microscopy after culture with embryonic cerebral neurons.

1.3 OBJECTIVES

The main objectives of this work are as follows:

1. Assess agarose microsphere fabrication using microfluidic technology and compare method to established protocols including bulk emulsion or use of commercially manufactured microspheres
2. Evaluate successful PDA functionalization on 2D substates and assess bioaffinity (adhesion and growth) of neurons to PDA by comparing to the current gold standard (substrate functionalization with poly-D-lysine and laminin)
3. Translate the PDA functionalization strategy to 3D constructs consisting of agarose and glass microspheres
4. Quantify physiochemical and nanomechanical properties of PDA-functionalized agarose and glass microspheres and compare to physiological values and established methods

5. Validate the suitability of the proposed agarose-based constructs for 3D cultures through culture with embryonic cerebral neurons and compare them to established methods (i.e., glass microspheres functionalized with poly-D-lysine and laminin)

1.4 HYPOTHESES

The hypotheses of this work are:

1. The microfluidic microsphere fabrication approach will produce microspheres of comparable geometry to established methods and commercially manufactured microspheres
2. Agarose polysaccharide at low concentration in microsphere form, will possess a Young's modulus close to that of the neuronal ECM (1-2 kPa)
3. PDA will enable functionalization of the agarose microspheres and improve cell-surface interaction
4. PDA-functionalized agarose microspheres will serve as effective scaffolding for neuronal network growth *in vitro*

2 LITERATURE REVIEW

2.1 3D CELL CULTURE SYSTEMS FOR NEUROLOGICAL APPLICATIONS

The field is now at a stage where it is well known that cellular behaviours in 3D culture conditions mimic the native cell behaviour more closely, compared to conventional 2D cultures. For neurons, the additional dimension has been shown to impact neuronal electrophysiology, growth, and survival *in vitro* [18], [24], [27], which speaks to the necessity of 3D *in vitro* models when evaluating pharmaceutical potential for neurological disease therapies. Aside from the 3D nature of the human brain, there are other important properties of the neuro-environment *in vivo* that are essential to recapitulate *in vitro* for a physiologically relevant model. Figure 2.1 depicts the main differences between 2D and 3D cell cultures, outlining some of the important physiological features that control and guide cellular behaviour.

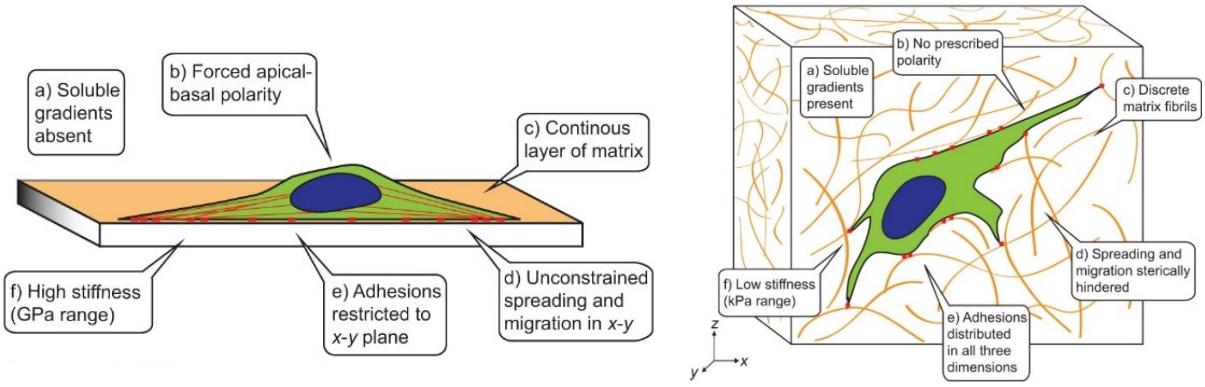

Figure 2.1 | Comparison between a cell cultured on a 2D substrate and cell cultured in a 3D matrix/scaffold. Adapted from [28].

On a planar surface, soluble gradients are absent, regions for cell adhesion are restricted to the x-y plane, forcing the direction of cellular polarity, which hinders growth in 3D. Additionally, 2D substrates are often accompanied by physiologically dissimilar stiffness and elastic moduli in the gigapascal (GPa) range. Conversely, 3D scaffolds and matrices provide soluble gradients, adhesive regions in all three directions and are commonly fabricated using softer viscoelastic materials with lower elastic moduli for a better recapitulation of brain tissue. However, almost no synthetic biomaterial inherently possesses these biochemical cues and mechanically optimal

microenvironments. As a result, biomaterial scaffolds are further manipulated and engineered beyond their three dimensionality to provide neuronal networks with topographical, mechanical, and chemical cues to mimic elements of native brain tissues. These engineered properties include the elastic modulus, stiffness, viscoelasticity, porosity, chemical stability, biocompatibility/cytotoxicity, and more. By modulating and optimizing these properties, 3D *in vitro* models can be tailored to mimic specific locations, pathways, or processes in the body. For example, engineering from a chemical approach, Wang *et al* designed and fabricated a biodegradable and biocompatible biomaterial scaffold synthesized from polypeptides containing neuron stimulate (glutamic acid) for nerve regeneration [29]. The peptides were shown to improve biocompatibility and neurite outgrowth, as well as guide anisotropic growth of the neurites within the 3D scaffold [29]. Focusing on a more mechanical- and structural-based engineering approach, a study by Tang-Schomer *et al* [30], capitalizes on the combination of both stiff and soft materials for cell adhesion and neurite outgrowth, respectively. Authors reported that the composite scaffolds exhibited viscoelastic behaviour similar to that of rat brain tissue with strains less than 20%, and compressive moduli ranging between 17-100 kPa [30].

Regardless of the engineering approach to fabricate biomaterials for neuronal tissue engineering, most materials seek to mimic the same cell support structure found in native tissues—the ECM. In most soft tissue engineering applications, a significant portion of the target areas of interest are occupied by the ECM, a 3D macromolecular structure which support cell networks both physically and chemically. As such, recapitulating the properties of the ECM is paramount to improve success of 3D *in vitro* models. Indeed, studies have shown that biomaterials with composition and structure similar to the native ECM result in cell growth [31], [32], differentiation [33], and behaviour [32] comparable to that *in vivo*. This suggests precise recapitulation of native ECM features are required for translational potential of *in vitro* models to address clinical need [34]. However, although this information is known, successfully mimicking all aspects of the ECM in a single *in vitro* environment has proven to be challenging [34].

2.1.1 Mimicking the Neural Extracellular Matrix

In the central nervous system, a notable portion (20-30%) of neural tissue is comprised of the ECM, which, like in many other tissues in the body, supports cellular networks and plays a major role in regulating tissue function [32], [35]. Surrounding the ECM and making up most of the

remaining percentage of the neural tissue, are dense networks of neurons and glial cells which rely on the ECM to function. Although the ECM accounts for less volume in the brain compared to the cellular network, a slight change in ECM properties—whether chemical, mechanical or biological—can result in significant behavioural and morphological changes in the cells, impacting overall function of the neuronal network [36]. For example, alterations and deficits in ECM structure and function have been associated with neuropathologies including Alzheimer's [37], traumatic brain injury [38], and epilepsy [39]. Unsurprisingly, cellular response to synthetic/engineered ECM substitutes *in vitro* is no different. Indeed, in search for biomaterial scaffolds to mimic the native ECM and support neuronal networks *in vitro*, studies have shown slight changes in biomaterial elasticity, composition, porosity and topography, among others, can have significant effects on cell-matrix adhesion, network electrophysiology, and long-term culture viability [20], [29], [32]. Ideally, the 3D scaffolds should function as biomimetic entities of the ECM so that the neuronal networks mimic *in vivo* behaviours through interactions at the cell-scaffold interface. Since the ECM is a macromolecular structure with complex tissue mechanics and molecular pathways, there are many factors to consider when recapitulating the structure *in vitro.* From a materials engineering standpoint, material stiffness and adhesive properties at the cell-material interface are two features imperative to for recapitulation of the neuronal ECM. Although not the only material properties important to be considered for *in vitro* models, substrate stiffness is a parameter shown to heavily influence behaviour of neuronal cultures, while cell adhesion is imperative for a viable culture. As such, these properties are used as measurable and quantities to assess material biomimetics in this work.

2.1.2 Mechanical Cues – Substate Stiffness

Of primary interest in numerous studies aimed at recapitulating the ECM *in vitro* is the influence of mechanical cues on neuronal network behaviour, since neurons are known to be mechanosensitive [40]–[42]. Of these mechanical properties, stiffness of a substate has shown to influence neuronal networks significantly [40]. Due to the high concentration of glycosaminoglycans, proteoglycans, and glycoproteins in neural ECM and its lack of fibrillar proteins, such as collagen and fibronectin, the elastic modulus of brain tissue is significantly lower than other tissues [43]. For instance, the elastic modulus of white matter (outer layer consisting of cell bodies, dendrites, unmyelinated axons, and ECM) and grey matter (consisting of primarily

myelinated axons and ECM) ranges between 1-2 kPa and from ~90-230 kPa in the spinal chord [44]. Figure 2.2 illustrates the elastic moduli of various tissues compared to agarose and glass culture-ware, clearly showing the difference between elasticity of materials currently used for *in vitro* cell culture (glass or plastic dishes) and physiological brain tissue.

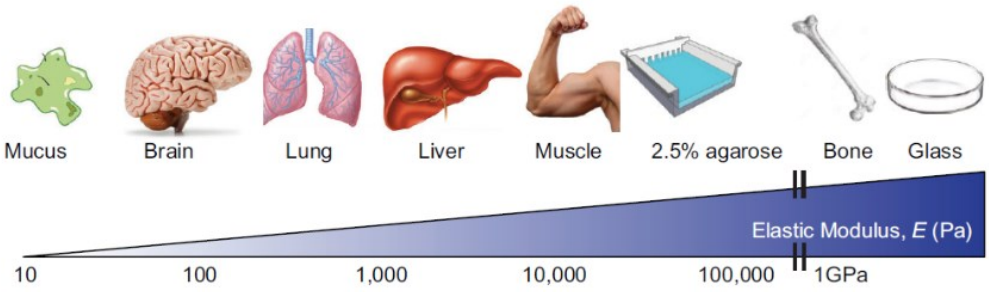

Figure 2.2 | Rough range of elastic modulus of physiological tissues compared to cell culture glassware. Glass and plastic cell culture-ware has comparable elastic moduli to bone ($E \geq 10^9$ Pa), muscle and liver tissues are in an intermediate range ($E \geq 10^4$ Pa), brain and lung tissue have the lowest elastic modulus ($E \leq$1-2 kPa), as a biomaterial reference, a 2.5% agarose gel (relatively stiff and high concentration) is approximately 35 kPa [43].

Investigating the impact of substrate stiffness on neural behaviour, Tanaka *et al* [45], explored how the elasticity of polyacrylamide gel substrates effects neuritogenesis (process in which neurites form to eventually develop into axons and dendrites) in hippocampal neurons cultured *in vitro*. The softest substrates had elastic moduli of 1700 Pa and 2.2kPa (physiological brain tissue stiffness <1-2 kPa), and the stiffest gels had elastic moduli between 3.2-3.8 kPa. Figure 2.3 shows fluorescent images, highlighting the effect of increased substrate stiffness on neurogenesis and neurite elongation after 20 hours in culture. Statistically significant differences were found between the number of neurons developed after 26 hours in culture on the soft (1700 Pa) gel and the stiff (3.2 kPa) gels used to culture the neurons. Although neurons were cultured on 2D substrates, the study provides clear insight on the importance of finely tuned scaffold stiffness when progressing with 3D culture.

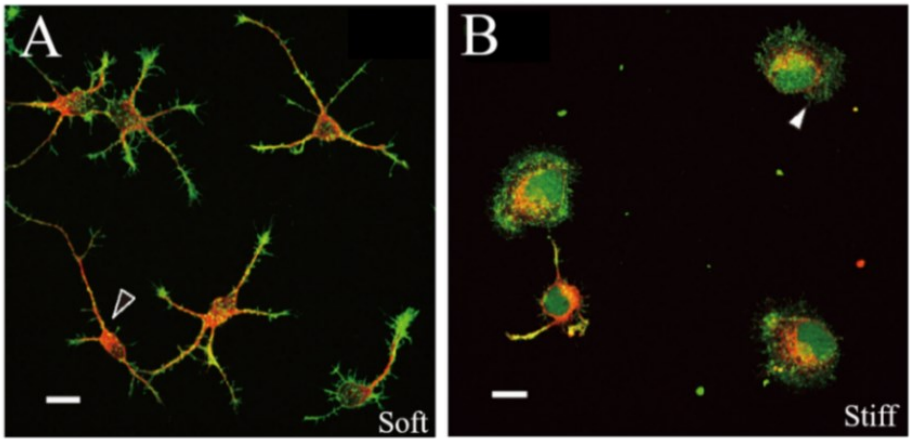

Figure 2.3 | Effect of substrate stiffness on neural development

A) and B): Immunofluorescent images of hippocampal neurons on **(A)** soft and **(B)** stiff substrates after 20 hours in culture. Red: β-III tubulin, Green: F-actin [45] .

2.1.3 CELL ADHESION

In an *in vivo* environment, the ECM plays the role of providing anchorage points for neurons during maturation and growth. When attempting to culture neurons outside of the body, providing these anchorage points on engineered biomaterials is of critical importance [46]. Indeed, adhesion of cells to the culture substrate or scaffold is imperative for a successful *in vitro* model. True for many cell types, once seeded on a surface, whether in 2D or 3D, the cells will need to adhere within the first few hours for a viable culture. For successful cell adhesion during those first few critical hours in culture, biomaterials are commonly functionalized with adhesive molecules derived from, or similar to those found in, the ECM—poly-D-lysine (PDL) and laminin being the most widely used for neuronal culture (see Section 2.4.1 and 2.4.2).

2.2 MICROSPHERE-BASED 3D SCAFFOLDS

To date, many methods have been used to fabricate 3D scaffolds for neuronal culture to mimic the ECM. Each fabrication technique, like anything else, comes with its own set of advantages and disadvantages, and although the field is broadening and improving the biomimetics of the 3D scaffolds, there is currently no gold standard in 3D for neuronal cell culture [47]. A brief overview of various 3D scaffold fabrication techniques is outlined in Table A.2 of Appendix A.

Although not exhaustive, the brief overview of current techniques in Appendix A helps visualize the multiple scaffold fabrication methods that have been developed to improve our ability to study neuronal networks in 3D *in vitro* environments. However, interestingly, many of these techniques rely on stochastic methods which typically result in uncontrolled parameters, including pore size,

interconnectivity, growth area, and structure [48]. This can ultimately limit translational potential of these scaffolds since it is known these parameters need to be precisely tuned and be reproduceable with high throughput for preclinical use. This observation along with publications by Frega, Tedesco *et al* [20], [24] guided the context and inspired the methods of this work. The following sections close in on the microsphere-based model—a scaffold-based strategy that does not succumb to fabrication method-induced stochastics. Specifically, the scaffold's origin, the microsphere fabrication methods and its use in 3D neuronal culture is discussed.

2.2.1 ORIGIN

Microspheres are spherical particles with diameters in the micrometer range (1 μm-1000 μm) that are manufactured from natural or synthetic materials using a variety of techniques. To date, the majority of work involving microspheres in the biomedical engineering field is targeted toward drug delivery and cell encapsulation for *in vivo* therapy and tissue regeneration [49]–[52]. For these applications, microspheres act as vehicles that control release and site-specific delivery of therapeutic agents both *in vivo* and *in vitro* via injection, implantation, or embedment in scaffolding [53], [54]. However, microspheres have proven themselves multifaceted due to their increasing use as 3D scaffolding for *in vitro* cell culture [20], [24], [25], [55]–[57].

Prior to their use for 3D *in vitro* scaffolding, microsphere-based scaffolds first emerged in orthopedics for purpose *in vivo*. In the late 90's and early 2000's the microsphere-based scaffold—also termed colloid model—was coined in the orthopedic community by C.T Laurencin and his research team to overcome a persisting limitation involving insufficient mechanical properties in synthetic 3D scaffolding for use as bone graft substitutes [58], [59]. Using the well-established emulsion solvent evaporation technique, the group fabricated gel and sintered poly(lactic-co-glycolic acid) (PLGA) microspheres and bound them together to produce an '*inverse'* of the scaffolds that were currently being used for bone grafts. By simply creating an *inverse*, or *negative* of the scaffolds accepted at the time, the authors improved structural integrity of the scaffold for a mechanically comparable bone graft alternative. In both initial publications outlining the novel method, [58], [59], the PLGA microspheres were formed using emulsion in polyvinyl alcohol and stirring. In [58], 3D scaffold was established by fusing the microspheres together using three different approaches: sintered method, solvent cast method and gel method. In successive publications, the authors maintained work with the sintered and gel methods [59]. Briefly,

fabricating the 3D sintered matrix involved heating the PLAGA microspheres above glass transition temperature allowing polymer chains to intertwine and connect with adjacent microspheres to establish a rigid matrix (Figure 2.4). The gel method involved the addition of sodium chloride and hyaluronic acid followed by air-drying, freeze-drying, rehydrating with salt-leaching and freeze-drying.

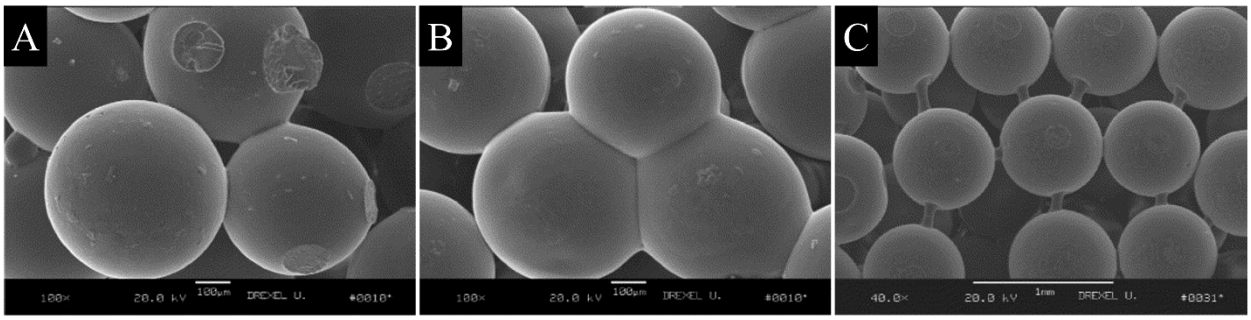

Figure 2.4 | Electron micrographs of the sintered poly(lactide-co-glycolide) microspheres (425-590 μm) after heating above glass transition temperature (62°C) for **(A)** 24 hr and **(B)** 72 hr. **(C)** microsphere bonds are pulled apart after 72 hr heating to visualize polymeric entanglement between neighbouring microspheres [59]

The Laurencin group published another paper a few years after their pioneering discovery reporting human osteoblast adhesion and proliferation in 3D throughout the microsphere system [60]. Over the next decade, researchers in the orthopedic community used the microspheric scaffolding approach for various osteo and osteochondral tissue engineering efforts [61]–[66], which ultimately broadened for use in several other tissue and regenerative engineering applications, including skin regeneration [67], cardiovascular tissue engineering [68], and many others [69], [70].

2.2.2 FABRICATION METHODS

Microsphere fabrication for biomedical application is a large and extremely active area of research, with the majority of the efforts targeted toward drug delivery and cell encapsulation for *in vivo* therapy and tissue regeneration [49]–[52]. As a result, researchers have been quite successful with the engineering of the size, surface, mechanical, and chemical properties of these microspheres. In this thesis, the fabrication of the microspheres is not the main area of research, therefore, a collaboration was made with a laboratory *(Godin Laboratory; Department of Physics, University of Ottawa)* specializing in the fabrication of microspheres. Consequently, fabrication methods of the microspheres are not elaborated on extensively. However, to acquaint the reader with the

fabrication methods, a brief overview of the main methods currently used for cell culture and regenerative medicine is provided below, including the method used in this thesis. For additional information on this topic, the reader is directed to [71], [72].

Techniques used to fabricate polymeric microspheres for biomedical application most commonly capitalize on emulsion. For solid homogeneous microspheres, single emulsions are used, and to fabricate a microcapsule an addition emulsion is required. For 3D microspheric scaffolds, only a single emulsion is needed. A single emulsion occurs by mixing two immiscible solvents, which, as shown below in Figure 2.5A-C, can be done using various methods. Rather than mixing two solvents in bulk (Figure 2.5A), the polymer solution can be added in a dropwise fashion to the emulsification phase to control microsphere diameter and reduce diameter variance, as shown in Figure 2.5B [20], [73]. To further narrow the microsphere diameter range produced, additional devices can be used to control parameters at the extrusion outlet, such as air flowmeters to control coaxial [55], [74] or ambient pressures [20] (Figure 2.5B).

Manually mixing or dropwise addition to form microspheres via emulsion is simple and works relatively well, as evidenced by the works mentioned in the previous paragraph. However, these methods can yield low numbers of microspheres with large deviations from a mean diameter (further discussed in Section 2.2.3.3). Consequently, these methods would not provide the high throughput, tight tolerances, and batch to batch reproducibility required for translational potential important in pre-clinical studies. As a result, microfluidic technologies have been applied to the pre-clinical research space as an alternative to bulk and manual emulsion. The microfluidic devices employed for cell culture and *in vivo* therapeutics are designed using flow-focusing nozzles equipped with a perpendicular flow of oil, creating a T-junction, resulting the formation microspheres due to the Rayleigh-Plateau instability phenomenon. The continuous oil phase compresses the dispersed aqueous polymeric phase into a thin flow column that breaks apart into monodisperse droplets—or microspheres [75], [76].

In a recent publication by Kanda *et al* [77], a flow focusing microfluidic device was used to encapsulate heart explant-derived cells in a nanoporous gel microsphere of agarose and ECM proteins (fibronectin and fibrinogen) for intramyocardial injection to stimulate endogenous repair in damaged heart tissue. The flow focusing and emulsion with an oil phase within the microfluidic device is depicted in Figure 2.5CI. Since the microsphere matrix was predominately composed of

agarose, the inlet and outlet of the microfluidic device were maintained at a temperature of ~37 ºC and ~4 ºC, respectively, creating a temperature gradient along the device to prevent premature agarose gelation at the inlet, and ensure gelation prior to the microsphere's arrival at the device outlet where the microspheres are collected on ice (Figure 2.5CII). Alongside the studies findings related to cardiac repair and regeneration, the microsphere fabrication technique using microfluidics was compared against the manual vortex mixing approach (bulk emulsion) for the application. Diameter of microspheres formed with the microfluidic platform proved to be more monodisperse with only 5% variation from the mean, and varying flow pressure ratios within the microfluidic device allowed precise control of the microsphere diameter enabling fabrication of small and large size microspheres in addition to batch-to-batch reproducibility [77]. AFM was also performed to evaluate microsphere stiffness and revealed no significant differences between microspheres formed using the two methods. Ultimately, the microspheres fabricated using the precisely engineered microfluidic technology were superior to the microspheres formed using the manual mixing approach for this study's application. The research group responsible for fabrication of the microspheres using the microfluidics in [77], is the same research group that is involved in the microsphere fabrication in this thesis.

In addition to these innovative fabrication methods, commercially available microspheres exist for similar application (food processing, pharmaceutical, biomedical). Therefore, in lieu of fabricating polymeric microspheres using the manual or microfluidic methods previously described, researchers have also have reported success using commercially available microspheres in biomedical application, including *in vitro* use as 3D scaffolding for neuronal networks [24], [56], [57]. However, it should be noted that the commercially available microspheres are most commonly fabricated from hard plastics, ceramics, or glass—materials that have been established to provide physiologically irrelevant environments for *in vitro* cell cultures (high stiffness).

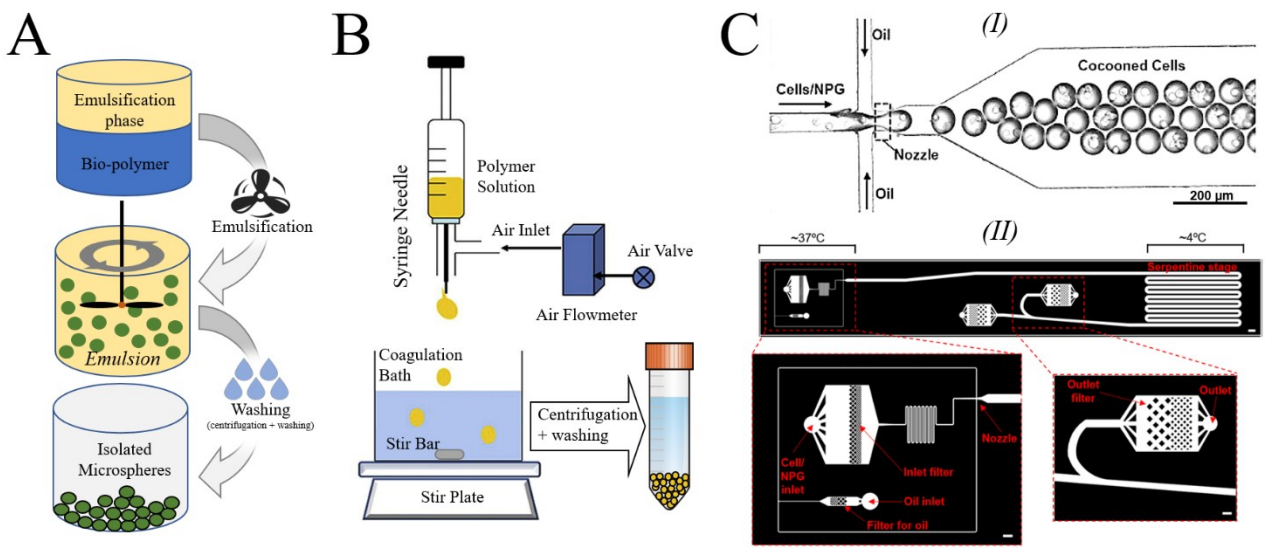

Figure 2.5 | Polymeric microsphere fabrication methods

(A) Emulsion of an aqueous polymer phase with an immiscible solution (e.g.: oil) resulting in polymeric microspheres when mixed. Resulting microspheres can be isolated via centrifugation and washing to remove oil; **(B)** Fabrication of polymeric microspheres via emulsion where polymeric solution is added in a dropwise fashion to a continuously stirred emulsification phase (coagulation bath), followed by centrifugation and washing to isolate microspheres; **(CII)** Microfluidic device nozzle area depicting the aqueous polymeric phase + cells (dispersed phase) and the two perpendicular oil flows (continuous phase) creating a T-junction, resulting the formation microspheres [77]; **(CII)** top view Schemata of microfluidic chip (*scale bar: 800 µm)*. Magnified panel (*scale bar: 400µm*) highlight key areas on the microfluidic chip. The inlet and the outlet were maintained at a temperature of ~37ºC and ~4ºC, respectively [77].

2.2.3 3D Microspheric Scaffolds for Neuronal Cultures

The following sections outline the advantages of the 3D microsphere scaffold, specifically for neuronal culture, highlighting its advantageous structural properties in addition to its use to date in the field. The use of the model in the field to date has been segregated into two sections based on stiffness of the microspheres used.

2.2.3.1 Advantages for 3D Neuronal Cultures

A main advantage of the microspheric scaffold is its precisely tunable growth area and predictable volume of interstitial space, with both parameters governed by microsphere diameter. The model also permits unrestricted gas exchange with the ambient environment in addition to uniform diffusion of nutrients and additives throughout the culture. These characteristics—inherent for the microspheric model—are commonly encountered obstacles for the other 3D scaffolding designs. The widely used continuous matrix 3D hydrogels or spheroid models have shown to result in necrotic regions at the center of the cultures due to poor gas exchange and nutrient delivery, and

metabolic waste buildup during incubation [78], [79]. This is particularly seen in 3D cultures over a few hundred microns in size, since as the culture becomes larger, efficient gaseous exchange becomes hindered. As the microsphere model becomes larger, it can also be subject to the same issue, but due to the high interconnectivity provided by the microsphere interstitial space, this would occur at a much lower rate than a continuous hydrogel, thus permitting the 3D culture to become quite large before encountering any gas exchange issues. Since uniform diffusion of additives and nutrients in an *in vitro* model becomes increasingly important in the context of disease models for therapeutic screening. For pharmacological agents to be evaluated effectively, it is imperative the therapy be delivered to the entirety of the cellular network and not discrete regions. The ability to increase the 3D culture size without diffusion/gas exchange issues would also allow the addition of microsphere layers in the z-direction to further model physiology of the brain, including structures such as the blood brain barrier, further improving the model's overall mimetics. For these reasons and among others, the microsphere-based scaffold provides a structurally ideal 3D construct to study neuronal networks and screen therapies *in vitro.*

2.2.3.2 RIGID MICROSPHERES: STATE-OF-THE-ART, ADVANTAGES AND LIMITATIONS

To our knowledge, the first study to interface microspheres with neurons *in vitro* for the purpose of replicating *in vivo* physiology was in 2005 by Baksh *et al* [80]. In this work, authors did not use the microspheres to construct a 3D scaffold, but rather used the microspheres (silica, SiO_2) coated with synthetic fluid lipid bilayer membranes to model the neurexin-neuroligin signaling pathway (neurexin expressed by the neuron, and neuroligin expressed by the non-neuronal cell). This publication provided the field with evidence of successful functionalization of silica microspheres and interaction with neurons *in vitro*. Contributing authors S. Pautot and E.Y Isacoff in [80] continued work with functionalization of silica microspheres, expanding the application to using the microspheres as supports in 3D neuronal network growth [56]. In particular, 45 μm-diameter silica microspheres were functionalized with poly-L-lysine (PLL) and interfaced with rat hippocampal neurons; over a 4-day period, the microspheres with neurons and glia cells adhered to the surface were assembled into 3D hexagonal (close packed) arrays [56]. Authors reported neuronal process growth crossing to and from adjacent microspheres within the scaffolds interstitial space after 3-week culture period (Figure 2.6A). Authors mentioned that the microspheric structure became woven together as a result of the multiple neural processes extending from cell bodies creating a stable structure. Additionally, it was reported that the neuron

health remained consistent regardless of the location within the assembly (Figure 2.6A)—which as mentioned previously, is likely due to unrestricted gas exchange throughout the culture (a common obstacle for 3D scaffolds with a continuous matrix). In [56], Pautot *et al* also determined the optimal microsphere diameter (~45 μm) for neuronal culture viability and growth, with a seeding density of 75,000 cells/cm^2, or 5 cells/microsphere, which laid the foundation for succeeding publications in the field, including [24], [25], [57], as well as in this work.

Frega *et al* [24] improved upon the microsphere model reported in [56] by coupling PDL and laminin-functionalized glass microspheres, to a microelectrode array (MEA). Authors reported an interconnected and functional 3D network of hippocampal neurons grown on, and within the interstitial space of the functionalized microspheres after 3-4 weeks *in vitro*. Further, spontaneous bursting activity of the network and its response to electrical stimulus was recorded, highlighting stark differences between 3D cultures and 2D controls [24]. Evidenced by immunofluorescent imaging, network connectivity was observed in z-stacks over 200 μm in height, where some cell bodies adhered to the glass microsphere surface, and others remained encapsulated within the interstitial space between microspheres [24]. From an electrophysiological standpoint, the group's work demonstrated that the neuronal network formed within the 3D microspheric scaffold resulted in higher percentage of random spiking, and higher network burst duration when compared to electrophysiological behaviour of a neuronal network cultured on a 2D substrate. The results provided insight on the significant differences in neuronal network electrophysiology between 2D and 3D cultures while also demonstrating successful use of the 3D functionalized glass microsphere scaffold coupled to a MEA for 3D *in vitro* modeling of the CNS.

Demonstrating the potential use of microspheric scaffolds *in vivo*, Park *et al* [25] reported that the use of growth factor-loaded heparin/poly-L-lysine nanoparticles adhered to the surface of PLGA microspheres enabled neuronal adhesion, stimulation and growth for potential implantation to repair damaged nerves (Figure 2.6C). Rather than the commercially available silica microspheres, the PLGA microspheres were fabricated using solvent evaporation in an oil-in-water emulsion. Since the authors utilized PLGA, as the base microsphere material, the PLGA will degrade over time such that the space initially occupied by the microsphere will be replaced by regenerated tissues [25]. Although the PLGA microspheres present favorable characteristics for application *in vivo,* a biodegradable scaffold for neuronal culture is not feasible since neuronal cultures require a

supporting matrix for culture periods ranging from 2-weeks to a few months. Should long term (multiple months) *in vitro* culture be required, use of a degradable microsphere material can be considered, ensuring degradation rate of the material agrees with ECM deposition rate by neurons.

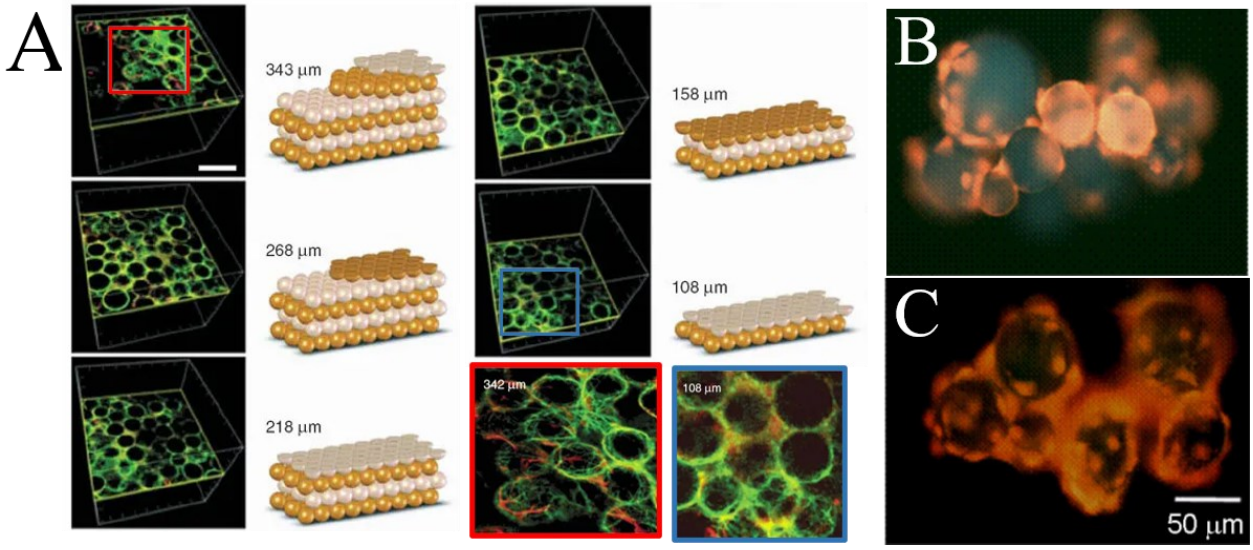

Figure 2.6 | Microsphere based approaches for 3D cell culture

(A) Primary hippocampal neurons cultured on 3D (450 x 450 x 388 µm) assembly of 45 µm silica microspheres functionalized with PLL. Neural processes are visualized at various heights in the scaffold using confocal microscopy and staining with neuron-specific antibody to α-tubulin (green) and glial-specific antibody to GFAP (red) after 3-week culture [56]; **(B-C)** Fluorescent images of propidium iodide stained PC12 cells adhered to PLGA pretreated with polyethyleneimine and coated with growth factor loaded heparin/PLL nanoparticles. Micrographs show cell adhesion on microsphere surfaces and proliferation in scaffold between 3 days (left) and 5 days (right) in culture. [25]

Although the microsphere model possesses many advantages over other models and has demonstrated potential for both *in vitro* and *in vivo* neuro applications, it also faces certain limitations which present opportunity for improvement. In the majority of studies to date which employ the microspheric model for culturing 3D neuronal networks [24], [25], [81], the microspheres are fabricated from materials such as borosilicate glass or plastic, resulting in a model with high stiffness. Of note, the Young's Moduli of these materials measure over six orders of magnitude larger than the physiological value of brain tissue [43]. As mentioned in Section 2.1.2, substrate stiffness is an important property that influences the behaviour of cells, and as a result, these rigid microspheres limit the physiological accuracy and translational potential of the microspheric 3D model.

2.2.3.3 SOFT MICROSPHERES: STATE-OF-THE-ART, ADVANTAGES AND LIMITATIONS

To improve the physiological relevance of the microspheric scaffolds, researchers in the space have fabricated microspheres using softer biomaterials to better mimic the stiffness of brain tissue. By using softer microspheres to construct the model, the desirable scaffold structure and geometry which enable uniform diffusion of nutrients and gas exchange in the culture is preserved while the stiffness of the scaffold is dramatically reduced. Authors from the previously mentioned paper [24], reporting 3D neuronal network growth and physiologically similar electrophysiology on PDL and laminin-functionalized glass microspheres, have improved (reduced) their scaffold stiffness by replacing the functionalized glass microspheres with soft 1-2% chitosan microspheres coated with PDL and laminin [20]. The chitosan microspheres were fabricated using a commercially available pressurized extrusion device (Nisco Encapsulation Unit Var J30). Microspheres were collected in a bath of gelling solution (H_2O_{dd} 40%, ethanol 60% and NaOH 2% w/v) continuously stirred at 200 rpm and interfaced with hippocampal neurons for up to 25 days. Immunofluorescent and transmission electron microscopy revealed well interconnected 3D networks of neurons, with dense networks of axons and dendrites on the profiles of the chitosan microspheres with smaller dendrites penetrating the microspheres [20]. Similar to their preceding publication [24], Tedesco *et al* also coupled the chitosan microsphere scaffold to MEAs and found similar electrophysiological network patterns to those observed with neuronal networks cultured on glass microspheres in [24]. Although similar patterns were observed, there was an increase of random network spikes with the 3D chitosan microsphere cultures compared to 3D glass microsphere networks, with the networks cultured on the 1% chitosan microspheres showing more synchronous bursts than on the 2% chitosan microspheres, indicating formation of dense network and high degree of connectivity. Additionally, a lower number of active electrodes were found with the chitosan microsphere scaffolds, which could be due to higher bio affinity of chitosan than the microsphere surface.

In terms of the scaffold characterization, authors encountered difficulties when evaluating the stiffness of the 1% chitosan microspheres using AFM, they were in fact unable to reliably determine the stiffness of the 1% chitosan microsphere, and thus approximated the microsphere's elastic modulus through extrapolation of stiffness measurements from 2% chitosan microspheres. Although the 1% chitosan microsphere was noted by authors to have concentration comparable to the stiffness of brain tissue (Young's modulus measuring ~15-24 kPa), when developing

biomimetic platforms to study neurological disease and potential therapies, it is imperative that biomaterial characterization to assess physiological relevance is carried out with accuracy. This extrapolation presents error and possibly discredits the reliability of the reported values.

Similar to Tedesco *et al* [20], Skop *et al* fabricated multifunctional chitosan microsphere scaffolding to improve neural precursor cell transplantation for traumatic brain injury repair [55]—again, demonstrating the use of the microsphere scaffold for both *in vitro and in vivo* neuro-application. Authors fabricated 3% chitosan microspheres using by extruding the chitosan solution through a syringe equipped with either a 23-gauge needle charged with 25kV of current or a 30-gauge needle subject to coaxial air pressure, and into a basic coagulation bath (2.5 M sodium hydroxide-methanol-water; 30:20:50 v/v). Both the applied coaxial air pressure and the electric current were effective at reducing the size of the microspheres. Fibronectin was then adsorbed to the surface of the microspheres. Surface chemistry was further enhanced by covalently linking heparin to the surface of the microspheres for the purpose of immobilizing fibroblast growth factor-2. Radial glial cells (RG3.6 cell line) were then seeded onto the microspheres. Results showed cells adhered to the surface of the microspheres after 18 hours, and excellent proliferation and survival after 10 days in culture. Further, authors demonstrated the transplantation of the microspheres with RG3.6 cells adhered to their surface into a neocortical lesion cavity via a syringe, 7 days post cortical impact (simulating impact causing TBI). 3-days post transplantation, RG3.6 cells were identified within the neocortical lesion cavity, with some cells still adhered to the microspheres, and some cells far from the microspheres in adjacent tissue. This work highlights the adaptability of the soft microspheres for use beyond *in vitro* application, specifically, their ability to serve as transplantable vehicles, and the microspheres ability to be functionalized with multiple biomolecules. It should be noted however, that in this work, the microsphere stiffness was not determined.

Evidenced by the work by Tedesco *et al*, and Skop *et al*, the soft microspheric scaffold for 3D neuronal culture is a push in the right direction in terms of improving physiological relevance of the model while preserving the desirable structure/geometry of the original design. However, there is much more to be explored in this research space. This includes evaluating the efficacy of other biomaterials to fabricate the soft microspheres in addition to alternative or additional functionalization options. Also, the methods through which the mechanical properties of the

microspheres are evaluated can be improved since the microsphere reported to possess the most similar to elastic modulus of neuronal ECM was determined through extrapolation [20]. Finally, from the literature, it was observed that the studies which have chosen softer materials to fabricate the microspheres have used methods which generate relatively large variance in microsphere diameter. For example, in [20], Tedesco *et al* report microsphere diameters ranging from 40-90 μm, with an average of 66 ± 20 μm, for 1% chitosan, while for 2% chitosan microsphere diameters ranged from 40-160 μm, with an average of 100 ± 40 μm (Figure 2.7A-B). Similarly, work by Skop *et al* [55] reported a large range of 3% chitosan microsphere diameters ranging from 30-100 μm using the electrospraying fabrication method (Figure 2.7C). These variances are relatively large in comparison to the small variances in microsphere diameter achieved through commercial suppliers due to the tight manufacturing tolerances, or with fabrication using precisely designed microfluidic technology. As such these large variances in microsphere diameter in the literature to date present space for improvement in the microsphere models for neuronal culture.

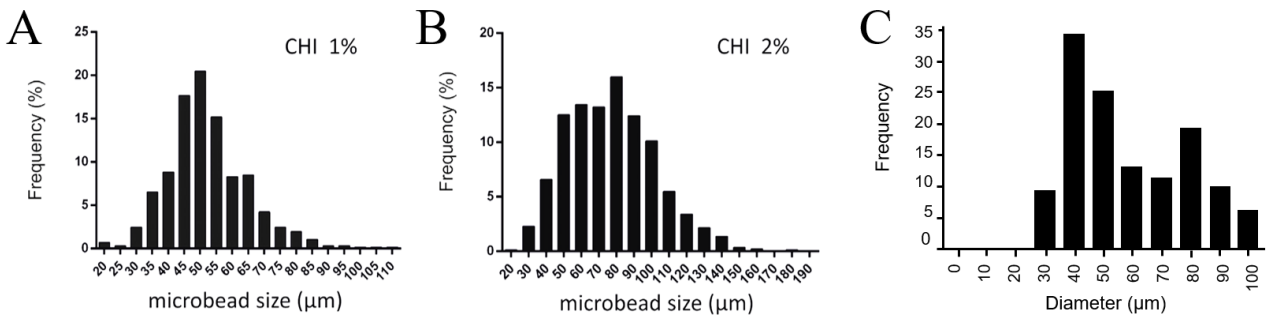

Figure 2.7 | Microsphere diameter histograms. Microsphere size distribution for **(A)** 1% chitosan microspheres and **(B)** 20% chitosan microspheres fabricated via dropwise emulsion [20]; **(C)** Microsphere size distribution for 3% chitosan microspheres fabricated via electrospraying

2.3 AGAROSE: A VERSATILE BIOMATERIAL

As mentioned in Section 2.1.1, 3D scaffolds for neuronal culture aim to mimic the natural properties of the neural ECM. Since the emergence of 3D scaffolds for *in vitro* studies, many synthetic, natural, and composite biomaterials have been investigated to mimic the neural ECM. Table A.1 in Appendix A outlines some biomaterials used as 3D scaffolding for neuronal culture, highlighting their advantages and the types of scaffolds they have been used in.

Of the biomaterials reviewed in literature, the natural polysaccharide agarose was chosen as the microsphere material in this work. This choice was motivated by the fact that agarose offers

properties that are attractive for its use in 3D cultures, including thermal hysteresis, low and easily tuned stiffness, and inherent biocompatibility. Additionally, agarose microspheres were previously shown to be successfully fabricated using microfluidic technology [77]. However, the main limitation of agarose for neuronal culture is that it does not readily offer moieties for cell adhesion—a deficiency that has restricted use in its native form. The following sections outline the chemistry and mechanical properties of the agarose polysaccharide, highlighting in detail its advantages and disadvantages for use as a material in 3D neuronal cell culture.

2.3.1 Chemical Structure and Gelation Mechanism

Agarose is a natural, high molecular weight, linear polysaccharide purified from the cell walls of agar or agar-bearing red marine algae. The polymer is composed of a repeating agarobiose disaccharide unit, (D-galactose and 3,6-anhydro-L-galactopyranose) connected in an alternating fashion by α-(1→3) and ß-(1→4) glycosidic bonds. Figure 2.8 shows the chemical structure of the repeating agarobiose unit in agarose.

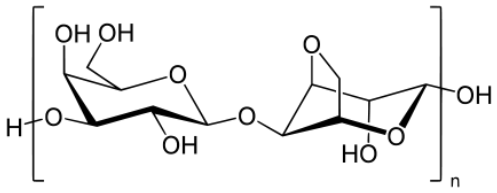

Figure 2.8 | Chemical structure of repeating agarobiose unit in agarose

In the biomedical field, agarose is commonly used in hydrogel form. One of the challenges with the use of hydrogels for biomaterial applications is gelation behaviour. To achieve a durable hydrogel with bio-functionalities, chemical crosslinking is commonly used. However, crosslinking agents are generally cytotoxic and thus reduce biocompatibility of the resulting material [82], [83]. Since agarose is a thermo-reversible, self-gelling polymer as a result of hydrogen bonding, and electrostatic interaction, crosslinking agents are not needed for gelation [84]. These gels are sometimes referred to as 'physical gels', where polymeric entanglement defines the porous network [85].

An important gelation property of agarose is the thermal hysteresis the hydrogel exhibits in its sol-gel transition, causing agarose hydrogels melt and gel at different temperatures [86]. Agarose is soluble in water or neutral buffer at ~90 °C; when cooled, gelation is initiated via crosslinking of

the polymer chains with hydrogen bonds to form double helices. The resulting gel is composed of aggregated double helices. Due to thermal hysteresis, the thermo-reversible hydrogel must be heated to 90 °C to re-enter its sol and sol-gel state. This gelation behaviour is depicted in Figure 2.9. Natural agarose melting and gelling temperatures are around 40 °C and 90 °C, respectively, but engineered hydroxyethylated agarose can reduce the gelling temperature to room temperature. This synthetic, ultra-low gelling temperature agarose is used in biomedical research enabling mixing with cells and ease of biomaterial fabrication, both at room temperature.

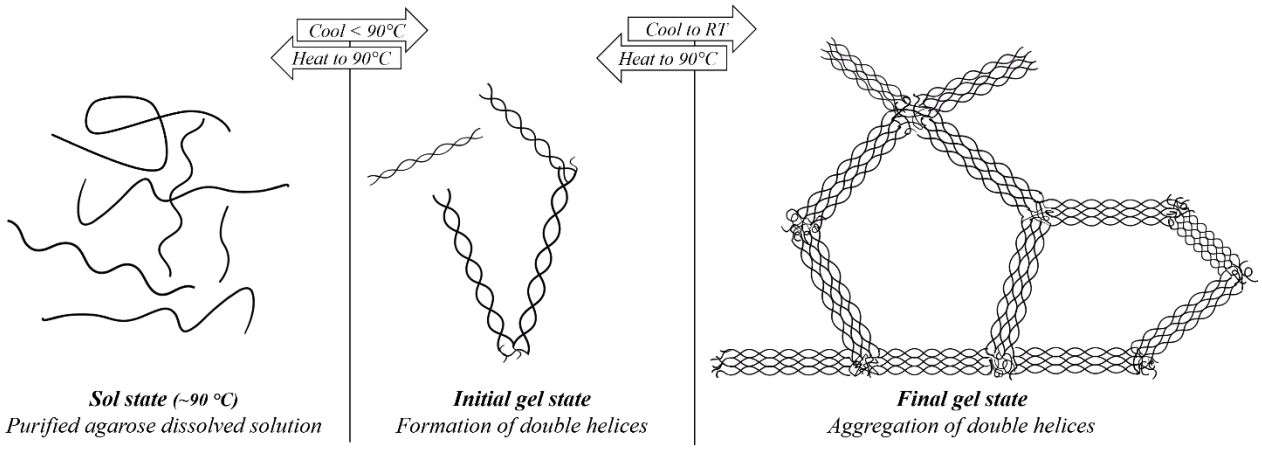

Figure 2.9 | Agarose gelation mechanism. Agarose is dissolved in solution at 90°C and enters its gelation state via hydrogen bonding of polymer chains when cooling is initiated. An agarose hydrogel exhibits a final molecular structure of aggregated double helices when completely gelled. Due to thermal hysteresis, the thermo-reversible hydrogel is heated to 90 °C to re-enter its sol and sol-gel states.

The phenomenon of thermal hysteresis in agarose gelation becomes an important property when interfacing this polymer with cells. For application in *in vitro* cell culture, the hydrogel will need to experience and withstand physiological temperature (37 °C) to mimic the *in vivo* environment. As a result of thermal hysteresis, once gelled, agarose can be heated to physiological temperature without melting or loss of structural integrity.

2.3.2 MECHANICAL PROPERTIES

The agarose polysaccharide is commonly used in hydrogel form for biomedical applications and therefore adopts viscoelastic and concentration dependent mechanical properties [87], [88]. Like other natural polymers in their hydrogel form, increasing the concentration of agarose in the hydrogel is associated with a higher stiffness since the polymer chains are more densely entangled. We also know that this stiffness can be further increased through use of crosslinking agents which

provide additional crosslinking within the polymer structure. As previously mentioned, agarose does not require the use of a crosslinking agent to gel, however the stiffness of an agarose hydrogel can be increased by introducing covalent bonding using a crosslinker instead of increasing the agarose concentration. In this section, only the Young's (elastic) moduli of agarose hydrogels reported in literature determined using AFM will be considered since the elastic modulus of the agarose at the nanoscale is of interest.

The majority of work reporting the Young's modulus of agarose hydrogels seem to comply with one another, with only minimal variance and/or discrepancies. Data from literature on this property is summarized in Table 2.1 for agarose concentrations from 1-3% (i.e., 1-3 g / 100 ml).

Table 2.1 | Agarose hydrogel Young's (elastic) moduli

Agarose Concentration (%)	Young's Moduli ± error	Indentation depth	Tip Geometry and cantilever stiffness	Reference
1	3.5 ± 0.7 kPa *(mean)*	400-1000 nm	Tip-less, equipped with 5.3µm melamine bead, k=0.1 N/m	[88]
1.5	5.6 ± 0.9 kPa *(mean)*	400-1000 nm	Tip-less, equipped with 5.3µm melamine bead, k=0.1 N/m	[88]
1.5	9.8 ± 1.5 kPa	100 nm	Pyramidal (k=0.06N/m)	[89]
2.0	10.6 ± 2.7 kPa *(mean)*	400-1000 nm	Tip-less, equipped with 5.3µm melamine bead, k=0.1 N/m	[88]
2.0	9.3 ± 2.3 kPa *(1 Hz dynamic)*	600 nm	Polystyrene spherical (k=0.32)	[90]
2.5	22 kPa	300 nm	Pyramidal (k=0.06N/m)	[91]
3.0	20.9 ± 4.9 kPa	600 nm	Pyramidal (k=0.1 N/m)	[92]
3.0	17.5 ± 3.0 kPa	600 nm	Spherical (k=0.32N/m)	[92]

Since neurons are mechanosensitive, an agarose hydrogel used for scaffolding is required to be similar to the mechanical properties of the ECM in order to elicit natural cell behaviour within the 3D culture. Young's moduli reported in Table 2.1 are evidently closer to the moduli of brain tissue, which ranges from a few hundred pascals [93] to a few kilopascals [44], in comparison to the conventional tissue culture substrates, glass and plastic. Although the elastic moduli of these agarose hydrogels in these concentrations, are slightly higher stiffness than physiological brain

tissue, they still provide significant improvement upon glass and plastic substates. Additionally, given the nature of hydrogels there is a minimum concentration required for the hydrogel to maintain its 'gel' form such that it can be manipulated and handled during fabrication, cell seeding, media changes etc. This requirement makes it difficult for hydrogels—like agarose—to be used at low concentrations that perfectly match the physiological range of brain tissue elasticity.

2.3.3 AGAROSE FOR NEURONAL CELL CULTURE

The physiochemical features and inherent biocompatibility of the agarose hydrogel elect its use in a many of tissue engineering and regenerative medicine applications. For readers interested in exploring these applications, see recent review by Zarrintaj et al [94]. Among the widespread use in the field, the agarose hydrogel has been used for neurological applications due to the aforementioned properties and its tunable elastic modulus which can be manipulated to mimic that of native brain tissue.

For example, Yoo *et al* used an agarose hydrogel at a concentration of 0.7%, coupled to nylon micromesh, functionalized with either PDL or a polyelectrolyte multilayer [95]. E18 rat hippocampal neurons were seeded on the nylon micromeshes and mixed within the agarose hydrogel. The agarose/cell suspension and micromeshes were layered to create 3D scaffolding. Results showed excellent cell viability at 9 days *in vitro* (DIV) on both PDL and polyelectrolyte functionalized micromeshes in addition to neuronal growth within the agarose hydrogel. Authors mentioned that the neurons tended to cluster within the agarose, forming thick fibre bundles as a result of the gel not being functionalized for adhesion. This demonstrates that an agarose hydrogel without functionalization would not provide a suitable for long term neuronal cultures due to excessive clustering and clumping of cells. It should be noted that authors did not confirm the mechanical properties of the scaffold.

Also capitalizing on the physiochemical characteristics of agarose, Struzyna *et al* [21] fabricated 1% agarose microcolumns (OD = 398μm; ID = 198 μm; L = 6-20 mm) and filled them with an 'ECM cocktail' composed of various collagens, laminins, esters, and other bonding/crosslinking agents. The 3D microconduits were fabricated for use *in vitro* to study the nigrostriatal pathway which is damaged in the pathophysiology of Parkinson's and *in vivo* to potentially reconstruct damaged pathway. Dopaminergic, striatal or hESCs neurons were aggregated (~3,200 cells per aggregate) and inserted into one (unidirectional) or both (bidirectional) ends of the microcolumns.

Evidenced by immunofluorescent staining, authors identified axonal outgrowth from aggregates extended 6 mm at 9 DIV and 9 mm by 28 DIV. Additionally, cyclic voltammetry revealed dopamine release in the aggregate and at the distal end of the microcolumn after 24 DIV [21]. However, similar to Yoo *et al* [95], the mechanical properties of the resulting 3D biomaterial were not investigated.

Conversely, Cao *et al* [96] did measure the mechanical properties—namely the stiffness—of their agarose-based scaffold for 3D neuronal culture by using rheological methods. 1% agarose was blended with 0-3% chitosan to promote neural adhesion to the 3D scaffold. Their results showed scaffold stiffness similar to stiffness of brain tissues, measuring on the order of 100 Pa, in addition to neural adhesion to the scaffold with chitosan concentrations between 0.66-1.5%. In addition to these three studies, there are many other studies which have reported successful results with agarose as a base material in a 3D scaffold for neuronal culture [97]–[100].

2.3.3.1 Limitations and Outlook for 3D Neuronal Culture

As demonstrated through studies mentioned above, agarose alone is unfortunately unable to facilitate neuronal adhesion and growth since it is essentially electrostatically neural. Although the agarose polysaccharide contains charged groups of pyruvate and sulfate (giving it a slight negative charge), the molecular biology grade, low melting temperature agarose has very low electroendosmosis values (below 0.12) meaning the number of sulfate and pyruvate residues present on the agarose is almost negligible. This results in a polysaccharide virtually neutral in charge. In neuronal cell culture, the commonly used surface functionalization to enable neuronal adhesion and growth on a glass or plastic substrates, such as poly-lysines and proteins), require a negatively charged surface to bind to. Therefore, the widely used functionalization methods for plastic and glass culture-ware cannot be used with agarose as the underlying substrate. To overcome this limitation, agarose is commonly blended and crosslinked with other polymers, such as chitosan [96], alginate [100], or collagen [19], [52], where the agarose serves as the mechanical tuner and the additional polymer provides binding sites or adhesive properties for cell retention However, with blended hydrogels, the surface of the resulting material will still have neutral regions of agarose that cells will not adhere to, and as previously mentioned, chemical crosslinking agents can be cytotoxic and thus reduce biocompatibility of the material.

While many studies have established agarose as an excellent scaffold material once blended or crosslinked with other bioactive materials [97]–[99], to our knowledge, the implementation of a material-independent surface coating to functionalize the entire surface of the agarose polysaccharide for use as a 3D scaffold in neuronal culture has yet to be investigated. Since agarose is inherently inert, completely covering its surface with a thin, and continuous bioactive polymeric coating would provide an ideal interface for cell adhesion and growth while preserving the desired mechanical properties provided by the agarose. This approach would be advantageous for cell attachment and growth since the entire surface area of the agarose would become functionalized rather than only discrete regions, while mitigating the need for cytotoxic crosslinking agents.

2.4 Surface Functionalization of Synthetic (Bio)materials

Surface modification is used to improve how a material interacts with its environment, without majorly altering its bulk properties. These modifications can be chemical, topographical, or biological in nature, altering a surface's chemical composition, appearance, reactivity, and more. By modifying the surface of a material, we can protect a material from its environment, like coating steel with zinc (i.e. galvanized steel) to prevent rusting. However, in the context of biomaterials, most materials are not often designed to be shielded from their environment—in fact, it is commonly the exact opposite. Depending on the biomedical application, surface modifications are used to achieve a surface that is biomimetic in its chemistry, topography, and mechanical properties for seamless integration with the environment. In the case of biomedical applications, the environment we are working with is the cell-laden human physiology. By using and designing materials that interface well with the body, or *in vitro* biological environments, the resident cells will not flag the material as a foreign; this prevents molecular cascades which lead to cell death and ultimately, necrotic cultures or tissues. When designing and fabricating 3D biomaterials for use in neuronal culture, it is therefore important to carefully engineer the surface of the material to promote cell attachment and growth for an overall viable culture long term.

Specific to *in vitro* neuronal cultures used for pre-clinical studies, multiple surface modifications exist to optimize cell attachment, neurite growth and culture longevity. Among them, some modification techniques employ the use topographical cues, biomolecule immobilization or adsorption and surface patterning. Some of the most commonly used surface modifications for

neuronal culture on conventional culture-ware is immobilization of the biomolecules, PDL and laminin [101]–[103]. For this reason, PDL (Section 2.4.1) and laminin (Section 2.4.2) functionalization on glass is used as a study control, while the functionalization of interest, namely the bio-inspired polymer PDA (Section 2.4.3) is evaluated for its ability to functionalize physiologically inert glass and agarose substates for 3D neuronal culture.

2.4.1 POLY-D-LYSINE

PDL is a positively charged amino acid polymer used extensively in both 2D and 3D neuronal cell culture [101]–[103]. Serving as a non-specific attachment factor, PDL enhances the electrostatic interaction between the negatively charged ions of the cell membrane and the culture substrate, promoting cell adhesion, and thus culture viability. Coating of a culture substrate with PDL is the most common initial preparation step prior to neuronal culture. To functionalize a surface with PDL, PDL is added to the substrate and incubated overnight at room temperature, followed by washing and in some cases, addition of another cell adhesion molecule. Due to its extensive use in the field for decades [104], PDL is used in the present study as a control with a basement membrane protein (laminin) coating on top of it.

2.4.2 LAMININ

Laminin is a protein found in the basement membrane of the central nervous system ECM. The basement membrane is an amorphous layer at the interface of the central nervous system and the circulatory system. Similar to fibronectin, laminins provide mechanical stability for cells while also regulating their differentiation, survival and motility [105]. Laminin has multiple domains in which binding can occur, which ultimately promotes cell adhesion. For these reasons, laminin commonly serves as an additional functionalization step after overnight incubation with PDL (Section 2.4.1) in neuronal cell culture. After PDL functionalization, culture substrate is immersed in laminin solution for two hours, followed by a wash with a neutral buffer. Due to the extensive use of this cell adhesion protein for *in vitro* neuronal studies, laminin from Engelbreth-Holm-Swarm murine sarcoma basement membrane is used in conjunction with PDL as a control in the present work.

2.4.3 POLYDOPAMINE

PDA is a polymer inspired by the composition of adhesive proteins of sessile mussels that enable them to adhere to rocks in the ocean for long periods of time, taking on even the strongest of storms (Figure 2.10A) [106]. After the *Mytilus edulis* foot protein 5 (Mefp-5) was found to play a critical role in the mussel's adhesive abilities, synthesizing mimetic materials to capitalize on nature's creation for applications that benefit from adhesive surfaces was attempted. First reported in 2007 [107], Lee *et al* identified the amino acid composition at the adhesive interface of the mussel to be rich in 3,4-dihydroxy-L-phenylalanine (DOPA) and lysine amino acids, which sparked the hypothesis that a molecule combining both catechol (DOPA) and amine (lysine) groups would facilitate adhesion on any surface—organic or inorganic. This led to the identification of dopamine as a possible candidate since it contained both catechol and amine functionalities [107]. Authors show self-polymerization of dopamine HCl in solution buffered to a typical marine pH (Figure 2.10B) resulted in spontaneous deposition of PDA onto a wide range of organic and inorganic surfaces. Prior to this discovery, coating organic surfaces with polymers was not a simple, single-step task. PDA film thickness was found to be a function of immersion time, depositing a homogeneous layer on the nanometer scale, increasing to 50 nm after 24 hours (Figure 2.10C).

Since first reported [107], the uses and applications for PDA functionalized surfaces expanded in many directions, ranging from use in energy and environmental industries to use in the biomedical field [108]. The reason PDA quickly became an attractive functionalization method is due to its simplicity and versatility; PDA is unique in the sense that it is one of the only single-step, material-independent functionalization schemes. However, despite its successful synthesis, and extensive use, the exact mechanism in which PDA is polymerized, and the factors that influence it, are still widespread research questions and topics of scientific debate [109]. Although the polymerization and structure are still being investigated, PDA has nonetheless become widely used in the biomedical industry because of its adhesive, antibacterial, and biocompatible properties [110]–[113].

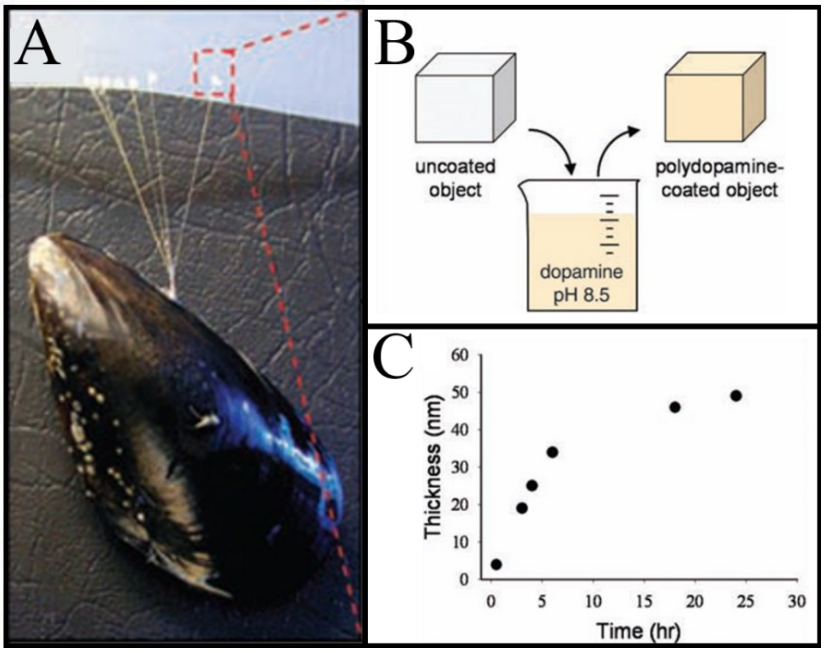

Figure 2.10 | First report of mussel-inspired PDA functionalization **(A)** Photograph of a mussel attached to commercial PTFE; **(B)** A schematic illustration of thin film deposition of polydopamine by dip-coating an object in an alkaline dopamine solution; **(C)** Thickness evolution of polydopamine coating on Si as measured by AFM of patterned surfaces. *Image and caption adapted from* [107]**.**

2.4.3.1 Polydopamine in Neuronal Culture

Although PDA coatings have made their way into the biomedical industry, their application in neuronal cell culture is relatively recent—especially in comparison to the widespread use of PDL and laminin for over four decades [104], [114]. Neuronal networks cultured *in vitro* are notoriously high maintenance and picky about the substate functionalization scheme used, which is why many 2D studies continue to use PDL and laminin coatings. However, now that neuronal culture has evolved and is beginning to employ soft 3D materials as scaffolds instead of the conventional 2D glass and plastic cell culture substates, the material functionalization schemes also need to be broadened to promote neuronal attachment and growth on any material. As such, PDA is an attractive candidate to functionalize substrates or scaffolds for neural culture due to its ability to functionalize any surface in a single step. Additionally, since it is rich in catechol and amine groups, it provides numerous secondary reaction sites for attachment of biomolecules (like PDL and laminin) after it polymerizes [107]. The PDA functionalization scheme is therefore advantageous over other biomolecule immobilization methods including covalent chemical conjugation and physical adsorption which can involve multistep processes or functionalization steps requiring plasma or chemical treatments [26]. In fact, the PDA functionalization scheme has been shown to immobilize serum proteins fundamental for cell adhesion, while also eliciting serum independent effects on cell behaviour, likely induced through surface properties of PDA [115].

The PDA surface functionalization was first introduced into neuronal cell culture as an intermediate immobilization step to enable addition of biomolecules essential for neuronal network survival on a substrate. However, since then, PDA has shown to promote neuronal attachment and growth even when used alone [26], [116], [117], suggesting PDAs efficiency as a single functionalization step without the need for additional biomolecule functionalization. PDA has also been shown to improve culture longevity in 3D *in vitro* models and increase adhesion within the culture [118]. Furthermore, PDA has been used successfully to functionalize neuron-electrode interfaces, such as MEAs used for *in vitro* electrophysiological recordings of 2D and 3D neural cultures without reducing the electrical properties of the electrodes [111], [119], [120]. Since the native electrophysiological signature of neuronal networks has distinguishable patterns, an electrophysiological readout from a microelectrode array can inform any biophysical effects on the neuronal culture due to a PDA surface functionalization scheme. This baseline would be important to establish before assessing neuronal response to therapeutic additives.

In literature to date, PDA used as a functionalization in neuronal culture (either as an immobilization step or as a single functionalization step) is prepared at a concentration of 2mg/ml in tris buffered saline (TBS) at alkaline pH 8.5. Self-polymerization of the dopamine occurs immediately after dopamine hydrocholoride is added to TBS. The scaffold or culture substrate is therefore immediately submerged in the PDA solution where the PDA spontaneously deposits on the surface of the scaffold or substrate. The scaffold or substate is left to rest in the PDA solution for a static deposition or placed on a shaker for a dynamic deposition. Dynamic depositions have been associated with higher numbers of PDA aggregates on a surface increasing in height with longer deposition time [110]. Both static and dynamic depositions are carried out at room temperature for different lengths of time which change depending on the application. The longer the deposition, the thicker the resulting polymeric film (Figure 2.10C), and larger the number (and larger the size) of polymeric aggregates [110], [115].

2.5 BIOMATERIAL CHARACTERIZATION

Once a biomaterial has been successfully fabricated, it is imperative that the chemical, mechanical and physical properties of the resulting material are characterized. This is to

ensure the material meets the design requirements, and to establish the reproducibility of the material and fabrication process. In the present work, AFM and Raman spectroscopy are used.

2.5.1 Atomic Force Microscopy

By using AFM for characterization, non-invasive nanoscale measurements can be made on biomaterials, providing information on the nanomechanics (e.g: Young's moduli) and adhesion which are important for comparison to physiological values. Indeed, these physical and mechanical measurements have become standard practice in evaluating the success of a biomaterial, as it is now well-established that nano-structured features and mechanical properties greatly influence biological response [45], [121], [122]. Additionally, the AFM technique can be carried out in aqueous environments, and therefore allows the user to accurately replicate physiological and culture conditions during measurements. Ensuring measurements can be taken in a physiologically relevant environment is essential for accurate characterization of a biomaterial. This is especially relevant for polymers as it is well established that polymer stiffness and geometry can change dramatically when characterized in ambient conditions in comparison to an aqueous buffer [123], [124]. AFM has also been extensively used in the field due to its ability to measure soft materials without damage which previously limited mechanical testing on biomaterials. For these reasons, AFM is used in the present study to analyze microsphere stiffness and the Young's modulus in an aqueous environment to assess mechanical mimetics of physiological brain tissue. The background and working principles of AFM is elaborated on in Appendix B for non-familiar readers.

2.5.2 Raman Spectroscopy

To characterize the chemical composition of the surface of the material, Raman spectroscopy is used. As a sensitive, non-invasive, non-destructive, and label-free analytical method, Raman spectroscopy allows us to easily identify chemical and molecular fingerprints. Most importantly, the method can also be carried out in an aqueous environment. In this work, Raman is used to confirm deposition of the PDA functionalization on culture substrates (planar and microspheric glass and agarose). Additionally, we aim to identify any differences in the molecular composition of the PDA functionalization deposited on agarose compared to on glass and 2D surface compared to 3D microspheres. The background and working principles of Raman is elaborated on in Appendix B for non-familiar readers.

3 MATERIALS AND METHODS

3.1 2D SUBSTRATE PREPARATION

3.1.1 GLASS FUNCTIONALIZED WITH POLYDOPAMINE

2 mg/ml PDA solution was prepared by polymerizing dopamine hydrochloride (Millipore Sigma; H8502) in 10 mM TBS (Millipore Sigma; T6664) according to previously published protocols [107], [111]. The solution was then immediately added to the substate to be functionalized:

3.1.1.1 FOR MATERIAL CHARACTERIZATION (RAMAN AND AFM)

The prepared 2 mg/ml PDA solution was added to 50 mm petri dishes containing No. 1, 24 mm square glass coverslips. The dishes were placed on a shaker for 2 hours at room temperature at medium speed to generate a film of PDA on the surface of the glass. After 2 hours, PDA solution was aspirated, and the coverslips were washed vigorously 4 times with 1X-phosphate buffered saline (PBS; Corning; 21-040-CV). The unfunctionalized side of the coverslips was immobilized to the bottom of a 100 mm parafilm-lined petri dish (3 coverslips per dish), and 20 ml of 1X-PBS was subsequently added to the petri dish.

3.1.1.2 FOR CELL CULTURE

The prepared 2 mg/ml PDA solution was sterile filtered and immediately added to a glass-bottom 96-well plate (MatTek; P96G-1.5-F) in sextuplet. The 96-well plate was placed on a shaker for 2 hours at room temperature on medium speed to generate a film of PDA on the surface of the glass. After 2 hours, the PDA solution was aspirated, and the glass-bottom wells were washed vigorously 4 times with 1X-PBS. To prevent drying, 1X-PBS was left in functionalized wells until cells were ready to be seeded.

3.1.2 AGAROSE GEL (FOR MATERIAL CHARACTERIZATION: RAMAN AND AFM)

A 1.5% agarose stock solution was prepared in a 15 ml conical tube by adding sterile, ultra-low gelling temperature agarose (Millipore Sigma; A2576) to pre-warmed 1X-PBS. The resulting solution was heated to ~95 °C in a microwave for 10 seconds, followed by brief vortex mixing; these two steps were repeated until the agarose was completely dissolved (~2 minutes). 10 ml of

agarose solution was then deposited into a 100 mm petri dish and placed at 4 °C to gel. 20 ml of 1X-PBS was added to the dish after gelation to prevent dehydration of the hydrogel.

3.1.3 Glass Functionalized with Poly-D-Lysine and Laminin (for cell culture)

Under sterile conditions, 0.1 mg/ml PDL (Millipore Sigma; P6407) solution was added to a glass bottom 96-well plate (Mattek; P96G-1.5-F) in sextuplet and incubated overnight at room temperature. PDL is aspirated and wells were washed once with 1X-PBS. 20 µg/ml laminin (Millipore Sigma; L2020) solution is added on top of the PDL functionalization and left for 2 hours at room temperature. Laminin solution is aspirated, and wells were washed a final time in 1X-PBS. To prevent drying, 1X-PBS was added to wells until cells are ready to be seeded.

3.2 Microsphere Preparation

3.2.1 Glass Microsphere Sterilization

Commercially available soda-lime glass (SLG) microspheres in the 42-47 µm diameter range (Cospheric; SLGMS-2.5 42-47) were added into a 1.5 ml microcentrifuge tube and sterilized in 70% ethanol for 2 hours under cyclical rotation every 20 minutes. Microspheres were washed with 1X-PBS 3 times and kept in 1X-PBS until the subsequent functionalization step.

3.2.2 Agarose Microsphere Fabrication – Single Emulsion in Oil Phase

The following procedure is illustrated in Figure 3.1. The 1.5% agarose solution was prepared as described in Section 3.1.2, and agarose microspheres were fabricated according to a previously established protocol [125]. In brief, without allowing the 1.5% agarose solution to cool to room temperature (gelling temperature), 150 µL of agarose solution was added to a glass insert (VWR; 46610-702 0.15 ml 5 mm CS100) and placed in a 2 ml glass vial. Mineral oil (Sigma; M5904-500) containing 1.5% nonionic surfactant (Span 80; Sigma; s6760-250) was added to a separate 2 ml glass vial. In the microfluidic device (prepared by N.Soucy as described in [77], [126]), the oil phase was run perpendicular to the aqueous (agarose) phase, and a temperature control system was used to generate a temperature gradient along the microfluidic device. The temperature was controlled with a heating block and cooling block at the device inlet and outlet, respectively. The heating block was maintained at 40 °C to prevent gelation of agarose at inlet, and the cooling block was used to maintain the serpentine channel at 4 °C to gel agarose microspheres after emulsion.

Inlet pressure of the aqueous (agarose) and oil phases were adjusted to achieve an average microsphere diameter of 48 µm. Agarose microspheres were collected in a 1.5 ml microcentrifuge tube and centrifuged for 3 minutes at 0.3 G, and oil in the supernatant was aspirated; this step was repeated until no oil remained in the sample. Sample was transferred to a fresh vial and kept at 4°C until further processing.

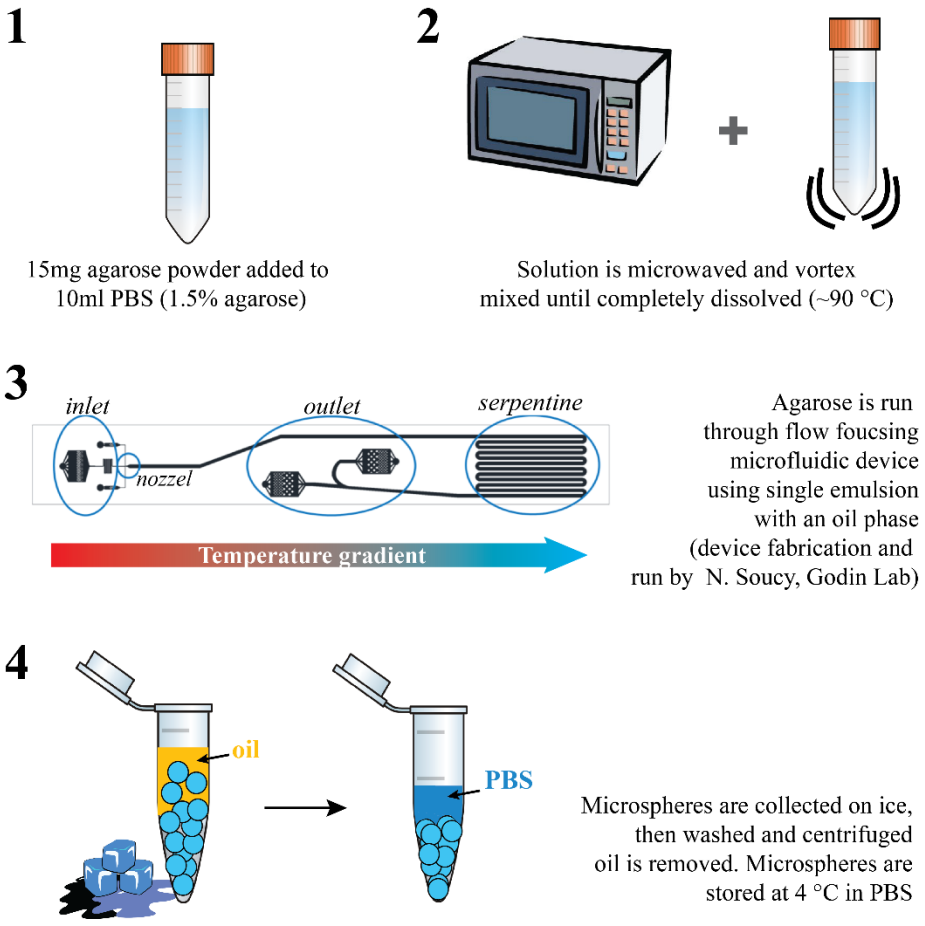

Figure 3.1 | Agarose microsphere fabrication steps. Step 3 is done by N. Soucy in the Godin Laboratory. Microfluidic chip schematic by N. Soucy [126].

3.2.3 Polydopamine Functionalization on Glass and Agarose Microspheres

The following procedure is illustrated in Figure 3.2. Two (2) mg/ml PDA solution was prepared as previously described in Section 3.1.1. Agarose and sterilized glass microspheres were immersed in the freshly prepared (and sterile filtered if microspheres are intended for cell culture) PDA solution and placed on a shaker plate for 2 hours, to generate a film of PDA on the microspheres.

After the 2-hour deposition, microsphere-PDA suspensions were centrifuged to pellet the microspheres. The supernatant was then aspirated, and the microspheres were resuspended in 1X-PBS and mixed vigorously. This washing step was repeated 4 times.

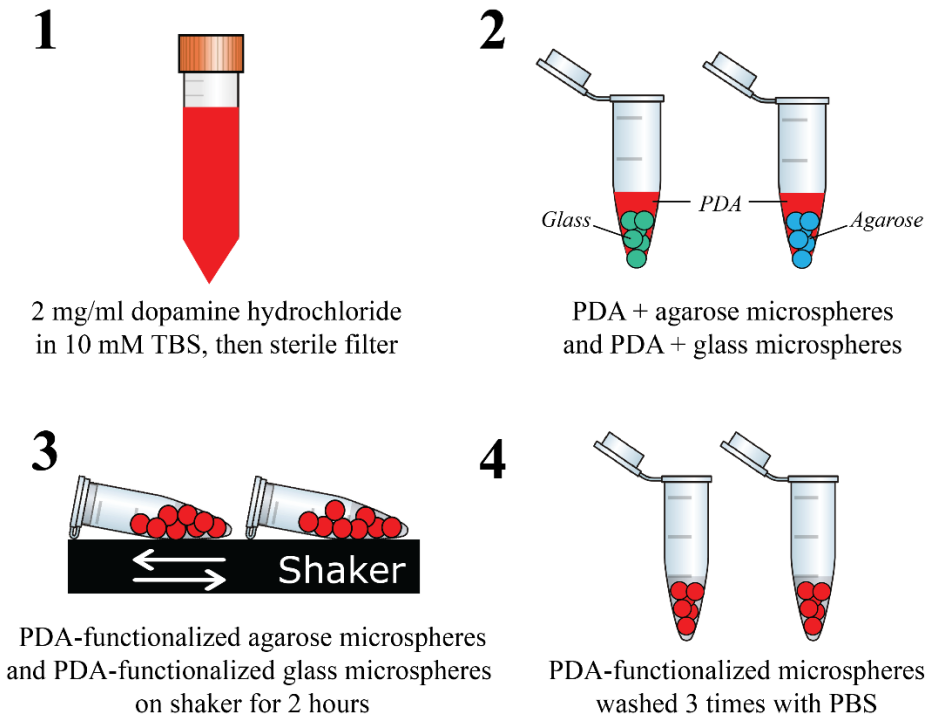

Figure 3.2 | Functionalizing glass and agarose microspheres with PDA

3.2.4 Poly-D-Lysine and Laminin Functionalization on Glass Microspheres

Sterilized glass microspheres were functionalized with PDL (Millipore Sigma; P6407) and laminin (Millipore Sigma; L2020). Under sterile conditions, microspheres were immersed in a 0.1 mg/ml PDL solution overnight at room temperature. Microspheres were then washed in 1X-PBS and immersed in 20 µg/ml laminin solution for 2 hours at room temperature, followed by a final wash in 1X-PBS. The microspheres were held in 1X-PBS until further processing. PDL and laminin functionalized glass microspheres served as the experimental control in cell culture as a result of their previously reported success [24], [56].

3.2.4.1 Microsphere Immobilization for Material Characterization (Raman and AFM)

Prior to Raman and AFM procedures, all microspheres were immobilized on PDA-functionalized coverslips. Briefly, No. 1-24 mm square glass coverslips were immersed in a solution of 2 mg/ml dopamine hydrochloride in 25 mM TBS (pH=8.5) for 2 hours at room temperature (static deposition) to create a thin adhesive film. Coverslips were then washed vigorously with sterile water 4 times and immobilized to the bottom of a 100 mm parafilm-lined petri dish (3 coverslips per dish, unfunctionalized side down). Microspheres suspended in PBS were deposited onto the surface of the PDA-functionalized coverslips and left overnight to adhere to the substrate. The following day, 20 ml of PBS was added to the petri dish, and material characterization procedures (Raman imaging and AFM nanoindentations) were performed.

3.3 Material Characterization

3.3.1 Microsphere Size Distribution

To evaluate the size distribution of microsphere population, 20 microspheres per experiment were imaged with a spinning-disk (Quorum Technologies) inverted confocal microscope (Leica DMI6000B) equipped with an sCMOS camera, using infrared light source for differential interference contrast (DIC) images, or by using the video camera capabilities on the Alpha300 RSA system (WITec; Germany). 20 microspheres per experiment (n=4) were measured using ImageJ software (NIH).

3.3.2 Raman Spectroscopy

Raman spectra of sample surfaces were acquired using the Raman module of the Alpha300 RSA system (WITec). Spectra were collected through a 20X water immersion objective (0.5 NA, water; Zeiss) with excitation by a 785 nm laser (*130.1 mW* measured at the objective, integration time = 4 seconds). During measurements, samples were immersed in 1X-PBS to replicate culture and physiological conditions. For 2D samples, single spectra were acquired in 7 random locations on each sample surface. On microspheres, single spectra were acquired from the surface of 10 different microspheres in each sample. Baseline subtraction was performed on each spectrum using OriginPro software (Origin Labs Corp., USA). After processing, the PDA Raman fingerprint,

characterized by two broad peaks (consistently used in literature to confirm the presence of PDA [110], [127]) at ~1370 cm^{-1} and ~1570 cm^{-1} were identified.

3.3.3 Atomic Force Microscopy – Nanoindentation

To quantify sample stiffness and adhesion, AFM was used. Nanoindentations of samples immersed in 1X-PBS were performed using the AFM module on an Alpha300 RSA system (WITec; Germany). MLCT-BIO probes, cantilever E and F (Bruker; USA) were used for all measurements. The MLCT-BIO, cantilevers E and F are characterized by a tetrahedral tip and a triangular silicon nitride cantilever with a reflective gold coating (see Appendix C for specifications). All AFM probes used were calibrated prior to use to determine the cantilever spring constant and sensitivity (Section 3.3.3.1).

3.3.3.1 Probe Calibration

Spring Constant

The spring constant of the AFM probe cantilever was determined experimentally using the thermal noise method and Sader Method tool [128]. Three user inputs were required for the Sader tool, including cantilever model (for geometry), cantilever resonance frequency (in air) and quality factor (in air). Resonant frequency of the cantilever was determined through an automated frequency sweep performed more than 1 cm away from sample surface by the WITec Control Software (WITec, Germany); amplitude-frequency graph was subsequently extracted and processed in OriginPro software. Specifically, a baseline subtraction was performed, followed by non-linear Gaussian curve fitting to determine the full width half maximum (FWHM) frequency (Figure 3.3B). Quality factor was subsequently determined using the following equation:

$$Q = \frac{f_0}{\Delta f} \qquad \text{Eq 1}$$

where f_0 is the resonant frequency, and Δf is the FWHM. Using the Sader tool, the MLCT (Bruker) probe model was selected, resonance frequency and quality factor were specified, and the experimental spring constant was calculated.

Sensitivity

The sensitivity was determined experimentally. The AFM probes were approached and retracted from a silicon sample and their resulting voltage-distance curve extracted. The inverse of the slope of the approach portion of the curve after tip-surface contact was calculated:

$$S = \frac{d}{V_p} \qquad \text{Eq 2}$$

where S, is the sensitivity, d, is the indentation distance, and V_P, is the measured voltage from the photodiode. Graphically, the sensitivity can be represented as shown in Figure 3.3A.

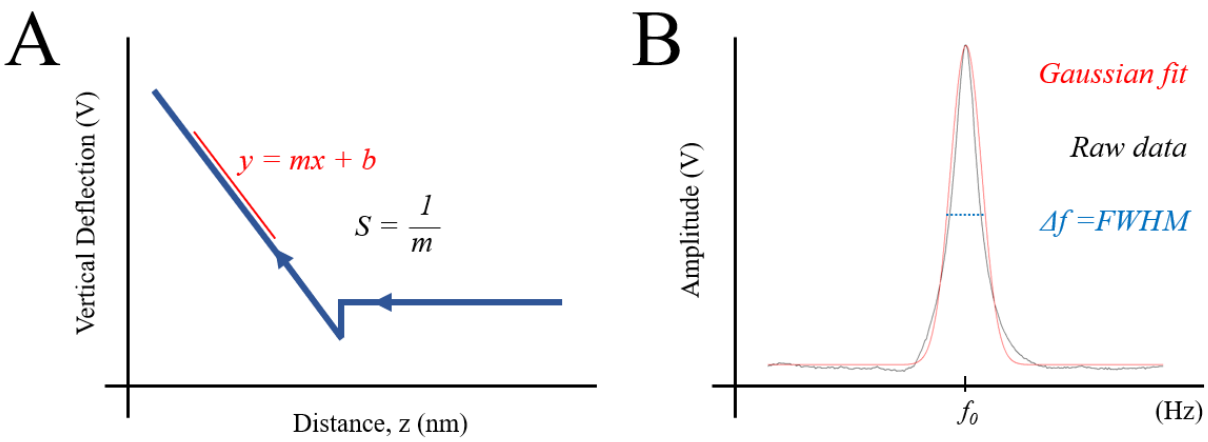

Figure 3.3 | Probe calibration. **(A)** Inverse of the slope (1/m) of the linear region of the approach portion of a nanoindentation curve will yield the tip sensitivity. Sensitivity is used in the process to convert vertical deflection, measured in volts by the AFM photodiode, to a force in nanonewtons; **(B)** Amplitude-Frequency graph acquired after frequency sweep >1cm from sample surface and fit with Gaussian function to determine FWHM.

3.3.3.2 NANOINDENTATIONS

2D substrates

2D samples were subjected to indentation at a rate of 0.5 µm s^{-1} in 10 random locations on the surface area of samples in triplicate, per experiment (n=3). Indentation data was processed using OriginPro to obtain sample stiffness, adhesion and Young's Modulus.

Microspheres

Microspheres were subjected to indentation at a rate of 0.5 µm s^{-1} performed at the microspheres approximate center of mass. 15 microspheres per condition, per experiment (n=3) were subject to indentation. Indentation data was processed using OriginPro to obtain sample stiffness, adhesion, and Young's Modulus.

3.3.3.3 *Curve Conversion*

The output curve after a nanoindentation is expressed with voltage, *V*, on the y-axis (Figure 3.4). Using properties of the AFM probe, this voltage was converted into force—the unit of measure required to assess material stiffness, elasticity, and adhesion. To convert the voltage to force, the following equation was used:

$$F = S \cdot k \cdot V_p \qquad \text{Eq 3}$$

where *F[nN],* represents the applied force, *S [nm/V],* represents the tip sensitivity, *k [nN/nm],* represents the cantilever spring constant, and V_p *[V]* represents the measured voltage from the photodiode throughout the indentation.

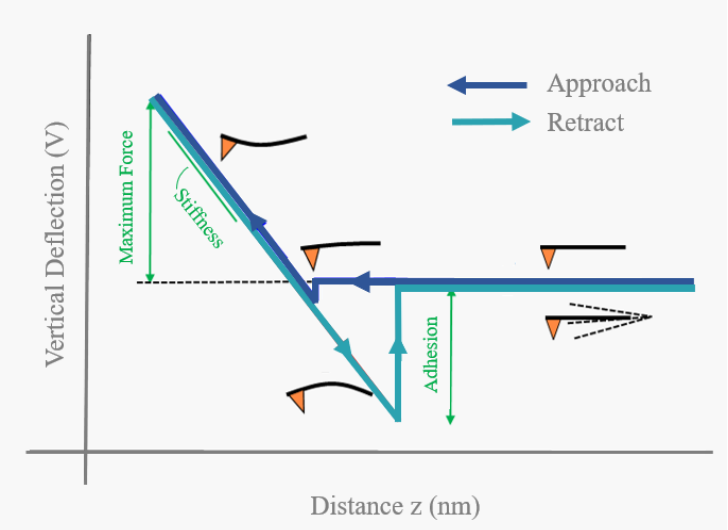

Figure 3.4 | Force-distance curve [129]

3.3.3.4 *Material Property Calculation*

Stiffness

Sample stiffness was calculated as a function of indentation depth in 300 nm increments from the approach portion of the force-indentation curves after conversion. Each curve was fit with a linear regression within each 300 nm increment, up to 900 nm to determine the slope of each segment. The slope represents sample stiffness at each indentation depth (Figure 3.4). One-way ANOVA and post-hoc Tukey test was performed in to determine statistical significance between conditions.

Young's Modulus

The Young's Modulus of the samples was estimated by fitting converted force-indentation curves with the Hertz model adapted for a tetrahedral indenter (also known as Sneddon extended model [130]) for the first 300 nm of indentation. The model is described by,

$$F = \frac{E}{1-\nu^2} \cdot \frac{\tan\alpha}{\sqrt{2}} \delta^2 \qquad \text{Eq 4}$$

where F is the force applied to the sample, E, the Young's modulus, α, is the face angle of the tip used, δ, is the indentation depth, and ν, is the Poisson ratio of the sample. A custom function was created in Origin Pro software to reflect the parameters of the Hertz model for an MLCT-bio tip *(α=35°)* and agarose (*ν=0.5*). All force-indentation (*F-δ*) curves were subsequently fit until convergence for the Young's Modulus, *E*. One-way ANOVA and post-hoc Tukey test was performed to determine statistical significance between conditions.

Adhesion

Sample adhesion was determined by identification of the minimum value in the retraction portion of force-indentation curves after conversion. One-way ANOVA and post-hoc Tukey test was performed to determine statistical significance between conditions.

3.4 NEURONAL CELL CULTURE AND IMAGING

3.4.1 ISOLATION OF PRIMARY NEURONS

Pregnant female (E18) CD-1 mice (Charles River) were euthanized by cervical dislocation. Placing the mouse supine, a 3-inch incision was made in the ventral area through the epidermis and dermis, exposing the embryonic sacs. Embryo sacs were removed and placed in hanks balanced salt solution (HBSS; Corning; 21-021-CV). Embryos were removed from their sacs and cervical dislocation was performed. Using curved forceps, the two most superficial meninges layers (dura, and arachnoid mater) were removed exposing the cerebral cortex, allowing its removal. Next, the two hemispheres of the cerebral cortex were unraveled, and the striatum was removed. The cortex was removed from the remaining meninge (pia matter) and placed in 15 ml conical tube on ice containing HBSS. The suspension was centrifuged at 200 G for 5 minutes. Under sterile conditions, supernatant was aspirated, and cell pellet was resuspended in 5 ml of Neurobasal™ medium (ThermoFisher; 21103049) supplemented with 2% B-27™ Supplement (ThermoFisher;

17504044), 1% GlutaMAX (ThermoFisher; 35050061), 1% 100 Uml^{-1} penicillin streptomycin—this media formulation is abbreviated 'complete growth media' (CGM). Cell suspension was counted using a hemocytometer at 20X magnification to determine cell concentration, with dead cells identified by trypan blue staining. Cell suspension was finally diluted to the desired concentration of 400,000 cells/ml in CGM.

3.4.2 Thawing Cryopreserved Neurons

One vial of embryonic cortical neurons isolated from an E14-15 CD-1 mouse (QBM Cell Science, Ottawa, ON; M-Cx-400 (CD-1)) was removed from liquid nitrogen and placed in a water bath at 37 °C for 2.5 minutes. The entire 1 ml volume contained in the vial was gently transferred to a 15 ml centrifuge tube using a 1 ml pipette with the tip cut to reduce shear on cells. Using a serological pipette, 9 ml pre-warmed CGM with 10% fetal bovine serum (FBS; ThermoFisher, 2614007), was added to the 15 ml tube in a drop-wise fashion while rotating the tube by hand to prevent osmotic shock. The final concentration of the cell suspension was 400,000 cells/ml.

3.4.3 Microsphere Seeding for Neuronal Cell Culture

Functionalized microsphere suspensions were mixed. For each condition 40 µl of microsphere suspension was collected and added to wells of a glass bottom 96-well plate (Mattek; P96G-1.5-F) to achieve a uniform layer with regions of multiple layers of microspheres. Microspheres were assessed under 20X magnification after each addition to ensure complete well coverage. Excess 1X-PBS was aspirated immediately prior to cell seeding.

3.4.4 Cell Seeding and Incubation

200 µl of cell suspension was added on top of a microsphere monolayer or on 2D substates, at a concentration of 80,000 cells/well. Non-functionalized wells and microspheres were used as a control to ensure growth was not occurring on the un-functionalized surfaces. The 96-well plate was then placed in a humidified incubator at 37 °C and 5% CO_2. Three quarters of CGM was removed from the wells 7 days after plating and replaced with fresh, prewarmed CGM; the plate was subsequently returned to humidified incubator at 37 °C with 5% CO_2. Three quarters of CGM was changed every 3-4 days thereafter until fixation.

If the neurons plated were previously cryopreserved, the first media change was carried out 4 hours after plating to remove any traces of dimethyl sulfoxide (DMSO). Three quarters of the CGM with 10% FBS was removed from each well and replaced with fresh, prewarmed CGM, without FBS. Plate was returned to humidified incubator at 37 °C with 5% CO_2. Three quarters of CGM was changed every 3-4 days thereafter until fixation.

3.4.5 IMMUNOFLUORESCENCE IMAGING

3.4.5.1 SAMPLE PREPARATION (STAINING)

All CGM was removed from the wells and washed once with 1X-PBS. Cells were fixed in Lana's fixative (4% paraformaldehyde with 7% picric acid) for 20 minutes at room temperature, followed by 3 washes with 1X-PBS. To visualize the β-III microtubules formed during culture, fixed cultures were exposed to the antibody TUJ-1 (neuron-specific class III beta-tubulin), diluted 1:10 in 1X-PBS+0.3% Triton-X at 4 °C overnight. Cells were washed once with 1X-PBS and exposed to the secondary antibody, donkey/goat anti-mouse IgG conjugated with Alexa Fluor 594 (ThermoFisher, A-11032) or Alexa 488 (ThermoFisher, A11001) diluted 1:400 in 1X-PBS+0.3% Triton-X for 35 minutes at 37 °C. Cells were then washed with 1X-PBS. Finally, cell nuclei were stained with 4', 6-Diamidino-2Phenylindole, Dihydrochloride (DAPI; ThermoFisher, D1306) diluted 1:50 in 1X-PBS for 20 minutes at 4 °C and then washed with 1X-PBS.

3.4.5.2 IMAGE ACQUISITION FOR 2D SUBSTRATES

Multichannel images of cortical neurons cultured on functionalized planar substates were acquired using an inverted epiluorescence microscope (Axio Observer D1; Zeiss) equipped with a AxioCam MRm CCD camera. The Zen Blue 2.3 software was configured to activate two excitation wavelengths: DAPI/Blue (460 nm), and Alexa 488/Green (525 nm). Images were acquired in 3 different locations in 3 wells for each condition using a 20X objective (0.80 NA, Air, Plan-Apo; Zeiss) to confirm cell adhesion and growth of β-III microtubule networks on culture substrates. Quantification of nuclei number and growth area of microtubule networks on each substrate were achieved using background subtraction, thresholding, and particle analysis functions in ImageJ. One-way ANOVA and post-hoc Tukey test was performed in OriginPro to determine statistical significance between conditions.

3.4.5.3 IMAGE ACQUISITION FOR MICROSPHERES

Multichannel z-stack images of cortical neurons cultured on functionalized microspheres were acquired using a spinning-disk (Quorum Technologies) inverted confocal microscope (Leica DMI6000B) equipped with an sCMOS camera. Metamorph software (Molecular Devices, LLC) was configured to activate an sCMOS noise filter, two excitation wavelengths: confocal Cy3/Red (605 nm), confocal DAPI/Blue (460 nm), and an infrared light source for DIC images. Z-stack images were acquired in 3 different locations of 3 wells for each condition. A 20X objective (0.7 NA, Air, HC Plan APO; Zeiss) was used to assess connectivity of βIII microtubule networks within the microspheres and 40X oil immersion objective (1.3 NA, Oil, PL APO; Zeiss) was used to evaluate adhesion of neuronal cell bodies and accompanying microtubules to the surface of the microsphere surface area. Additionally, a laser scanning confocal microscope (Zeiss; LSM-800) was used to obtain high-resolution images with a smaller field of view to highlight regions of interest using 20X objective (0.8 NA, Air, Plan-Apo; Zeiss). For presentation, images were focus stacked, followed by a background subtraction using ImageJ. Z-stacks were 3D rendered using ImageJ Volume Viewer to visualize the neuronal networks in 3D.

3.5 METHODS SUMMARY AND CONDITION RATIONALE

For clarity,

Table 3.1 outlines the methods carried out for each condition evaluated. The rationale for using each method for each condition is as follows:

- **Nanoindentation for Stiffness and Young's Modulus**: Only carried out on soft samples (agarose) since glass is incompressible. 2D agarose sample measured to assess if any differences in the nanomechanical properties arise after agarose is run through microfluidic device to form microspheres.
- **Nanoindentation for Adhesion**: Carried out on all microspheres with and without functionalization to assess tip-surface interaction strength.
- **Raman**: Carried out on all PDA functionalized samples to ensure successful PDA-functionalization.
- **2D cell culture**: Carried out only on functionalized glass substrates since only bioaffinity of neurons to PDA in comparison to PDL and laminin is to be assessed.
- **3D cell culture**: Carried out on all functionalized microsphere conditions to validate potential of the proposed 3D strategy.

Table 3.1 | Method summary and rationale

		2D SUBSTRATES			**MICROSPHERES**			
	Base Material →	**Glass**		**Agarose**	**Agarose**		**Glass**	
	Functionalization →	*PDL+Laminin*	*PDA*	*None*	*None*	*PDA*	*PDL+Laminin*	*PDA*
NANOINDENTATION ***(AFM)***	Stiffness			✓	✓	✓		
	Young's Modulus			✓	✓	✓		
	Adhesion				✓	✓	✓	✓
RAMAN	PDA spectra		✓			✓		✓
2D CULTURE WITH EMBRYONIC CEREBRAL NEURONS	Neural adhesion, growth, culture viability	✓	✓					
3D CULTURE WITH EMBRYONIC CEREBRAL NEURONS	Neural adhesion, growth, culture viability					✓	✓	✓

4 RESULTS

4.1 MATERIAL CHARACTERIZATION

4.1.1 MICROSPHERE SIZE DISTRIBUTION

The microfluidic fabrication method yielded a highly monodisperse distribution of spherical agarose microspheres. The average microsphere diameter was 48 ± 1 µm. The histogram in Figure 4.1A shows the distribution of microsphere diameter: data were collected from a total number of 80 microspheres, during 4 independent experiments with 20 microspheres each (n=4). Figure 4.1B-E display agarose microspheres with (C-E) and without (B) PDA functionalization.

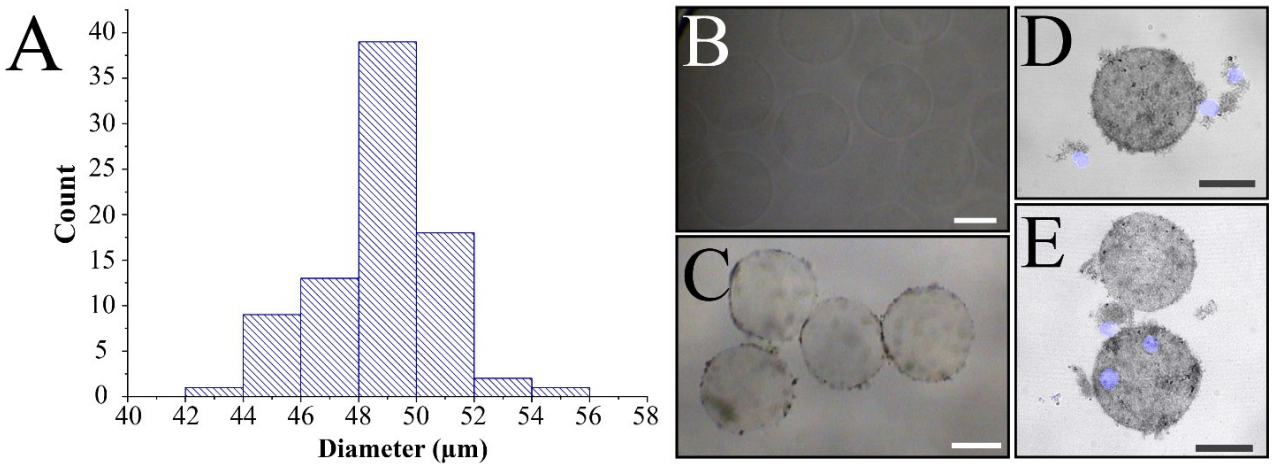

Figure 4.1 | Agarose microsphere diameter and PDA functionalization; **(A)** Size distribution; **(B)** As-fabricated agarose microspheres, *scale bar: 30 µm*; **(C)** PDA-functionalized agarose microspheres (2-hour deposition), *scale bar: 30 µm*; **(D-E)** PDA-functionalized agarose microspheres (18-hour deposition), with DAPI stained nuclei adhered to surface, *scale bar: 25 µm*.

4.1.2 POLYDOPAMINE FUNCTIONALIZATION

The presence of PDA on 2D glass substrates as well as on glass and agarose microspheres was confirmed by Raman spectroscopy. Figure 4.2A shows representative Raman spectra of PDA-functionalized agarose and glass microspheres, along PDA-functionalized 2D glass substrates and glass and agarose controls. Figure 4.2B and C show brightfield images of PDA-functionalized agarose microspheres, and PDA-functionalized glass microspheres, respectively. The PDA Raman

fingerprint, characterized by peaks at ~1380 and 1570 cm^{-1} due to catechol stretching and deformation, respectively, [110], [131], were visible in all spectra, thus confirming the successful deposition of PDA on the surface of all samples.

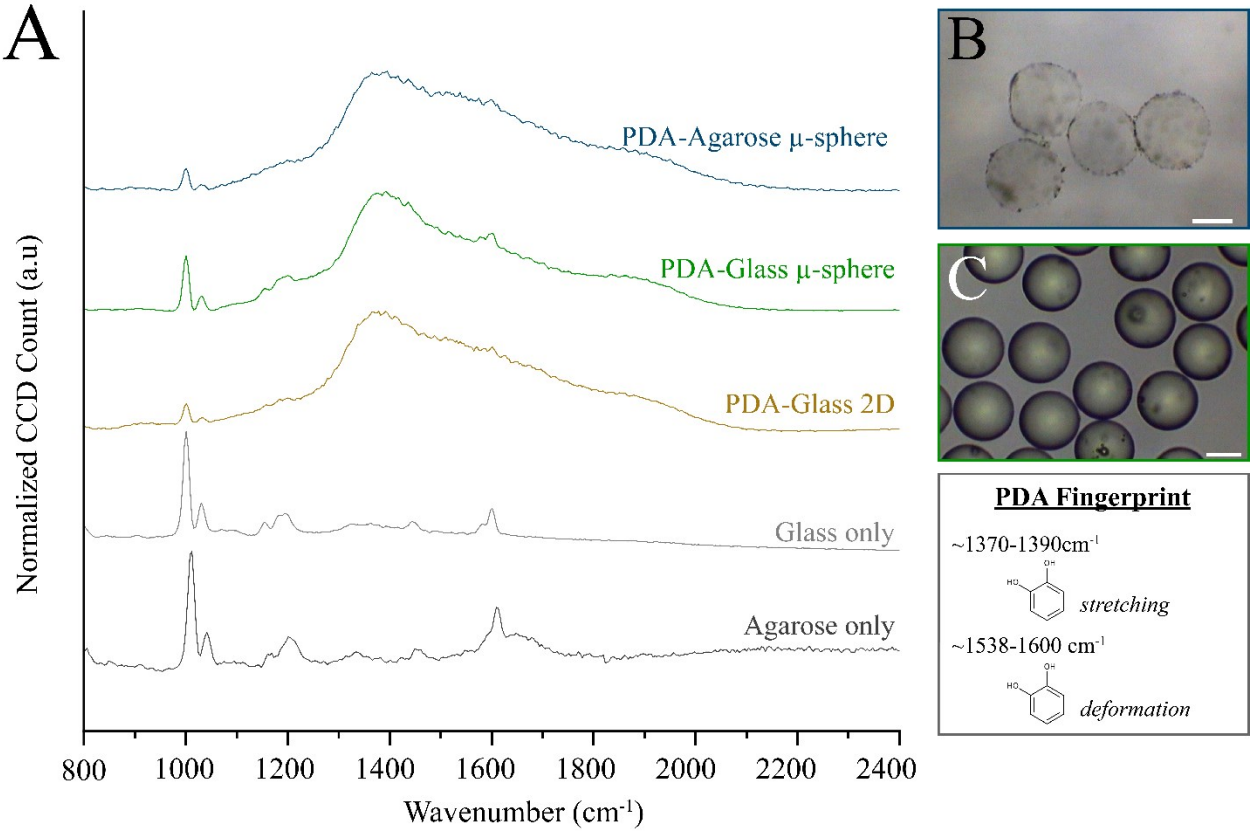

Figure 4.2 | Raman spectra of PDA identified on agarose and glass microspheres and 2D glass substrates; **(A)** Representative Raman spectrum (normalized 0-1) of PDA-functionalized glass *(green),* agarose microspheres *(blue)* and 2D glass substrates *(yellow)* and glass only *(light grey)* and agarose only *(dark grey)* controls; **(B)** Brightfield image of PDA-agarose microspheres (2 hour deposition*), scale bar: 30 µm*; **(C)** Brightfield image of PDA-Glass microspheres (2 hour deposition), *scale bar: 30 µm*; Spectra offset for clarity

4.1.3 NANOMECHANICAL PROPERTIES

4.1.3.1 STIFFNESS

The stiffness of soft samples was determined through AFM nanoindentation measurements in an aqueous environment. The slope of the approach portion of the force-indentation curve after contact represents the stiffness of the microspheres. Mean stiffness is reported as a function of

indentation depth in increments 300 nm. Figure 4.3A shows mean stiffness of samples at 0-300, 300-600, and 600-900 nm indentation depth. Figure 4.3B shows mean force-indentation curves (bold lines) from data used to determine stiffness, along with their standard deviations (shaded regions delimited by fine lines). For clarity, means and respective standard deviations are presented in Table 4.1. Results show increase in stiffness in all conditions with respect to indentation depth. PDA-functionalized microspheres possessed the highest stiffnesses in all indentation increments, followed by unfunctionalized agarose deposited as a 2D substrate; unfunctionalized agarose microspheres were shown to have the lowest stiffness. Stiffness of the unfunctionalized agarose microsphere and the PDA-functionalized agarose microsphere were found to be significantly different in the 600-900 nm indentation depth increment (One-way ANOVA; $*p < 0.05$).Considerable standard deviation between measurements existed in the PDA-functionalized agarose microsphere condition, whereas nanoindentation on agarose microspheres and 2D agarose substrates were found to have much narrower data distribution associated with the mean force-indentation curves (Figure 4.3B), and thus stiffnesses (Figure 4.3A).

Table 4.1 | Sample stiffness as a function of indentation depth measured through AFM nanoindentation

	STIFFNESS (× 10^{-3} N/m)		
	0 – 300 nm	*300 – 600 nm*	*600 – 900 nm*
PDA-Agarose Microspheres	4.8 ± 3.3	8.5 ± 4.8	11.1 ± 5.5
Agarose Microspheres	0.8 ± 0.2	1.8 ± 0.5	2.8 ± 0.5
2D Agarose	2.5 ± 0.5	6.7 ± 1.1	9.8 ± 1.0

Mean ± standard deviation

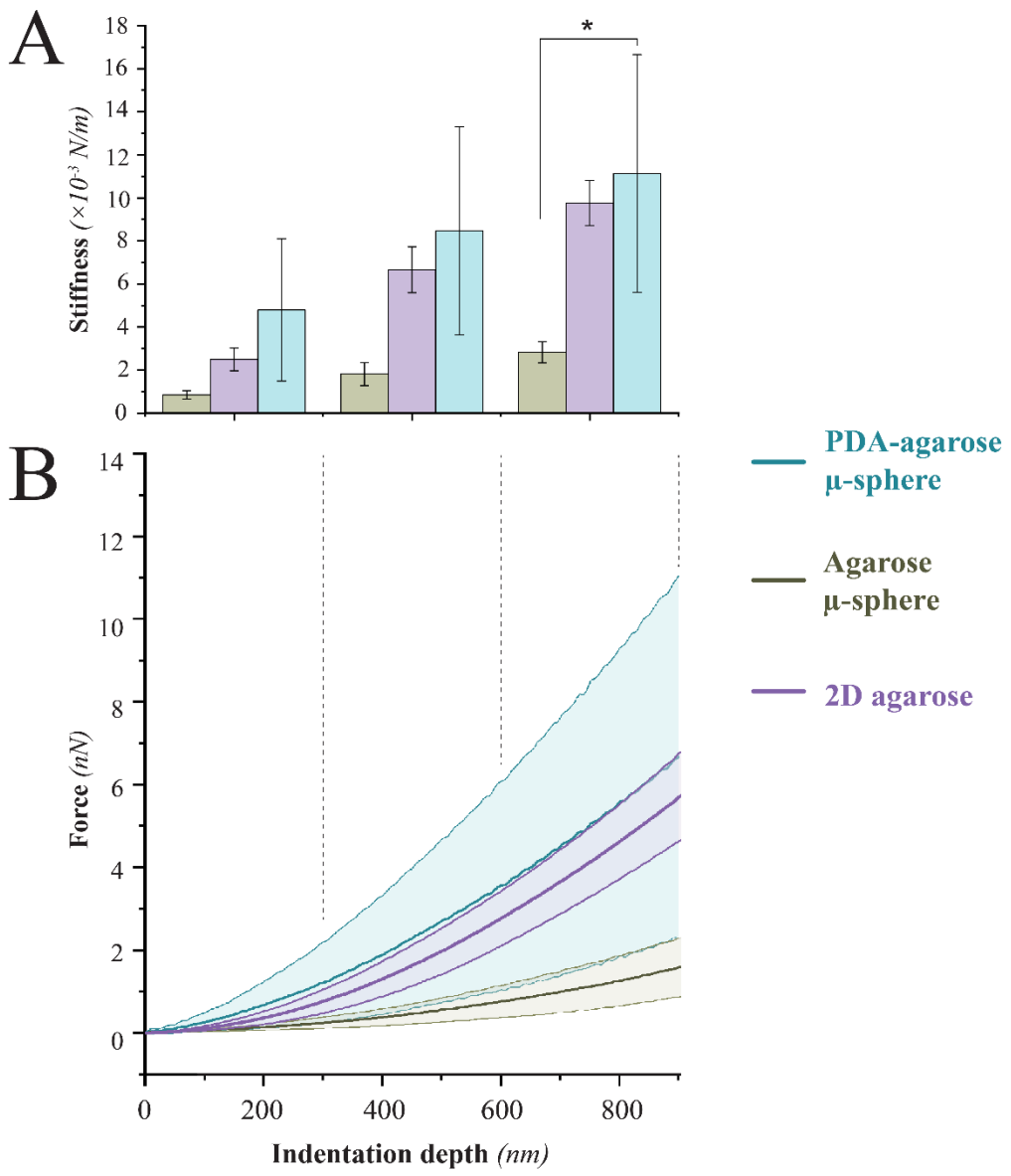

Figure 4.3 | Sample stiffness as a function of indentation depth in 300 nm increments **(A)** Mean sample stiffness ± standard deviation. Indentation depth increments aligned with x-axis in B [One-way ANOVA test; **: $p<0.05$*]; **(B)** Average (bold line) force-indentation curve (normalized to zero at contact point) for each condition ± standard deviations (shaded region delimited by fine lines)

4.1.3.2 Young's Modulus

Young's modulus of soft samples was quantified by fitting the first 300 nm of force-indentation curves obtained through nanoindentations to the Hertz model adapted for a tetrahedral indenter. An indenter face angle of 35° and a Poisson ratio of 0.5 were used to reflect geometry of the MCLT-Bio tetrahedral indenter and material properties of agarose, respectively. Expectantly, the

trend observed between conditions for the Young's modulus followed that of the stiffness; PDA-functionalized microspheres possessed the highest modulus of 26.8 ± 17.9 kPa, followed by 2D agarose with a modulus of 13.4 ± 2.9 kPa, then agarose microspheres with a modulus of 4.9 ± 0.6 kPa (Figure 4.4A). Means were not found to be significantly different at the 0.05 level (One-way ANOVA). However, similar to calculated stiffnesses, considerable standard deviation between measurements existed in the PDA-functionalized agarose microsphere condition. Fitting of representative force-indentation curves with the Hertz model is shown in Figure 4.4B for each condition.

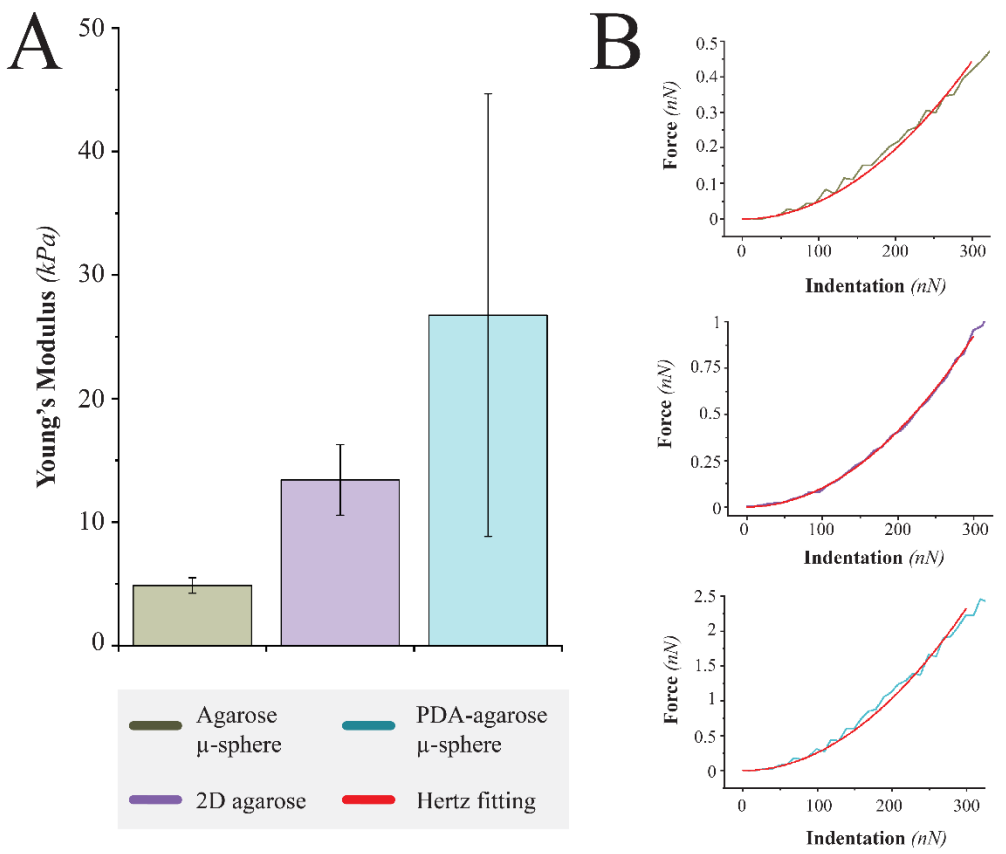

Figure 4.4 | Young's Modulus estimated by fitting to Hertz Model measured in kilopascal (kPa) **(A)** Mean Young's Modulus ± standard deviation. **(B)** Force-indentation curve fitting with Hertz model from 0-300 nm indentation depth

4.1.3.3 SURFACE ADHESION

The tip-sample adhesion strength on all functionalized samples was determined through analysis of the retraction portion of the nanoindentation curves obtained using AFM. Minimum value prior to tip snap-off was determined for each sample condition and their means were compared. Results showed the force required to detach the AFM tip from PDA-functionalized microspheres was the largest, with the PDA-functionalized glass microspheres requiring a larger force for detachment than PDA-functionalized agarose microspheres; mean adhesion forces were 5.1 ± 2.8 nN and 2.1 ± 0.9 nN, respectively. PDL and laminin-functionalized glass microspheres followed, with a mean adhesion force of 1.6 ± 0.6 nN, while agarose microspheres without any functionalization required the lowest force for tip detachment, with a mean adhesion force of 0.3 ± 0.05 nN. Means were found to be statistically different between PDA-functionalized glass microspheres and unfunctionalized agarose microspheres at the 0.05 level (One-way ANOVA, $*p < 0.05$). Similar to stiffness measurements, large standard deviation was associated with PDA-functionalized samples.

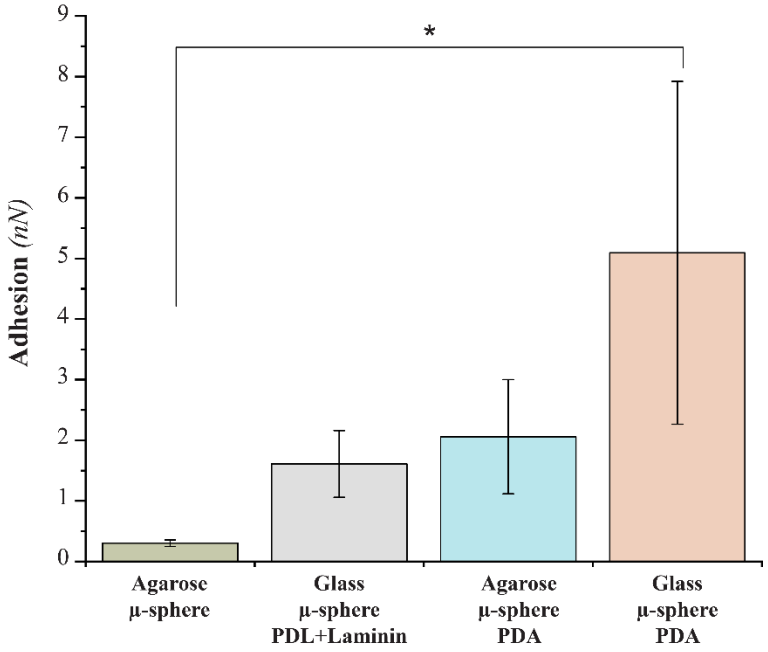

Figure 4.5 | Surface adhesion comparison between glass and agarose microspheres with PDA or PDL and laminin functionalization. Error expressed as a standard deviation [One-way ANOVA test; *$: p < 0.05$].

4.2 2D Polydopamine-Functionalized Substrates

As a fundamental prerequisite prior to 3D neuronal culture, the response of neurons to the PDA was assessed. A standard 2D culture model was adopted for this purpose, where embryonic cerebral neurons were seeded directly onto the surface of PDA-functionalized glass substrates and cultured for 14 days. Figure 4.6 shows representative immunofluorescent images of neurons cultured on glass only (negative control), PDA-functionalized glass, and PDL and laminin-functionalized glass (positive control). Morphological development of the neuronal networks on PDA was similar to the PDL and laminin functionalization (current gold standard in neuronal cultures), however, higher density networks were achieved with PDL and laminin due to increased number of neuronal cell bodies adhered to the substrate after seeding. As expected, neurons cultured on glass with no functionalization formed clusters with minimal neuronal processes (neurites) developed after 14 days.

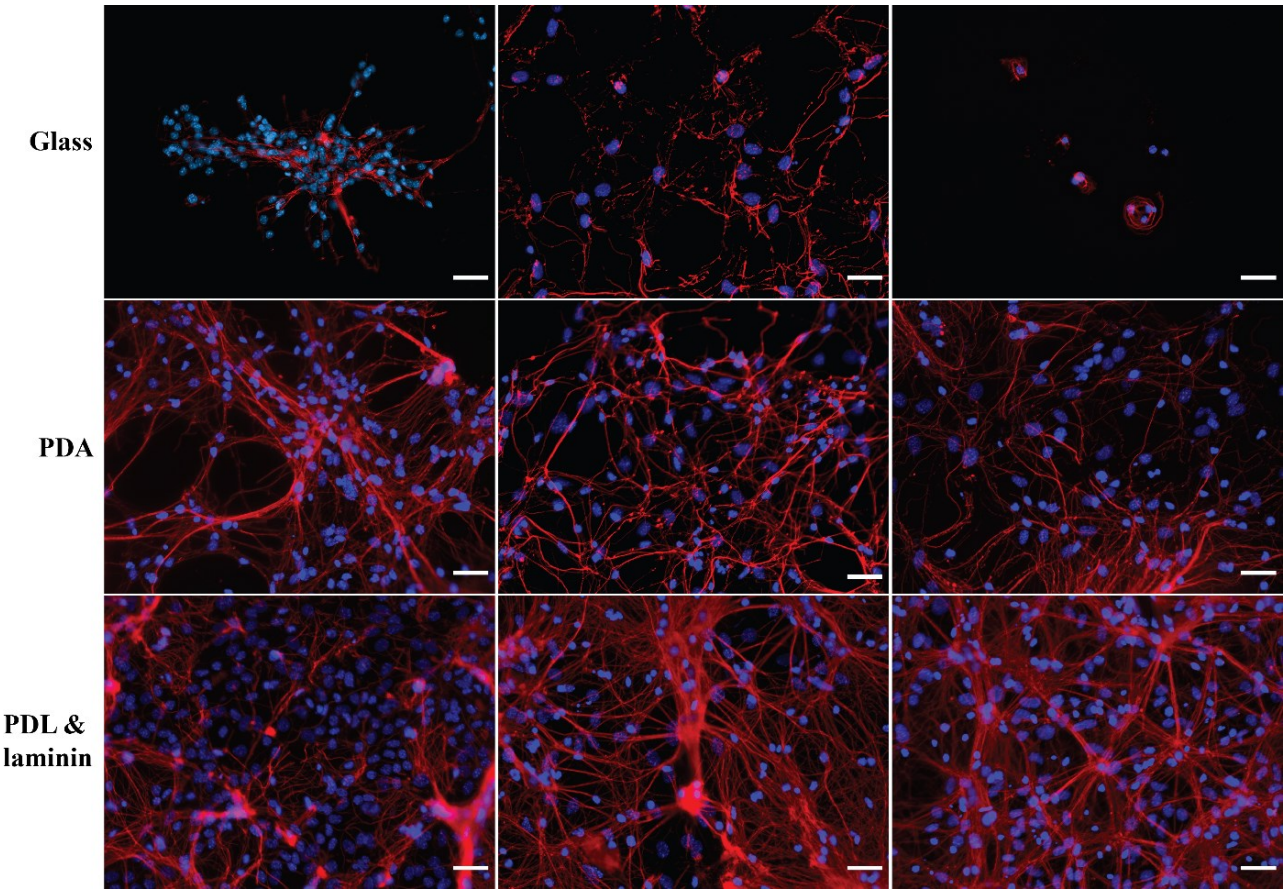

Figure 4.6 | Immunofluorescent images of 2D neuronal networks at 14 DIV on glass (top row), PDA functionalized glass (middle row), and PDL and laminin-functionalized glass (bottom row). βIII-tubulin *(red)*, DAPI *(blue)*; *Scale bars: 40 µm.*

Quantitative analysis was performed on βIII-tubulin and nucleic fluorescence to assess neuronal adhesion and neurite growth on PDA-functionalized substrates compared the standard methods (PDL and laminin functionalization). Results show a larger neurite growth area on PDA-functionalized substrates compared to substates functionalized with PDL and laminin. The mean neurite growth area normalized to number of nuclei was calculated to be 405.4 ± 28.4 μm^2 and 302.6 ± 19.1 μm^2 on PDA-functionalized, and PDL and laminin-functionalized substrates, respectively (Figure 4.7A). The difference between conditions was found to be statistically significant (t-test; *: $p<0.05$). Conversely, PDL and laminin substates were found to have a higher cell retention/neural adhesion, with ~15 ± 4 nuclei adhered to the substate per 10^4 μm^2 compared to ~8 ± 2 nuclei adhered to the PDA-functionalized substates per 10^4 μm^2 (Figure 4.7B). This difference was also found to be statistically significant (t-test; *: $p<0.05$).

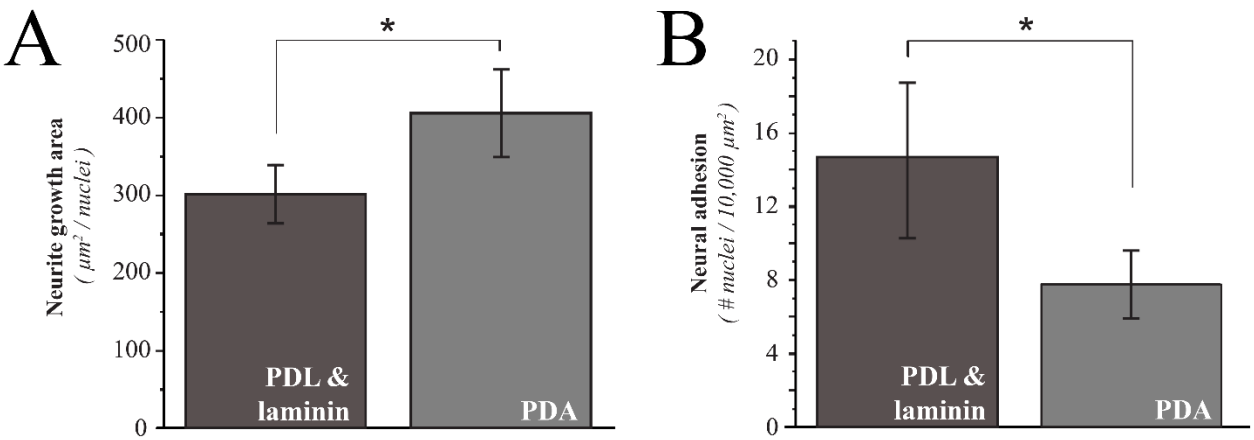

Figure 4.7 | Neurite outgrowth and neuronal adhesion at 14 DIV on 2D substates functionalized with PDA or PDL and laminin; error bars: standard deviation; [t-test, *: $p<0.05$, equal variance not assumed (Welch Correction)]; **(A)** Neurite growth area normalized to number of nuclei; **(B)** Neuronal adhesion evaluated by number of nuclei adhered to substrate per 10^4 μm^2

4.3 POLYDOPAMINE FUNCTIONALIZED MICROSPHERES

4.3.1 CONFOCAL MAX PROJECTIONS

The 3D neuronal networks cultured on functionalized microspheres were fixed and immunolabeled for tubulin markers after 14 DIV. Figure 4.8 shows DIC and fluorescent (βIII-tubulin) images in addition to the resulting composite image for visualization of neural processes on the microspheres.

DIC images revealed non-homogenous glass microsphere monolayers resulting in unoccupied regions in the culture wells (Figure 4.8B-C). Both glass and agarose microspheres showed regions in wells where additional layers of microspheres were deposited, creating multi-layer regions within the culture. This provided neuronal networks with additional growth area in the z-direction. Although this occurred with both microsphere types, it can be seen more clearly in the agarose microsphere images where the microspheres in the second layer have a visually darker perimeter attributed to their different focal plane (Figure 4.9A, *column 1*).

Fluorescent images of neuronal networks show different neurite localization on glass microspheres (Figure 4.8B-C) compared to agarose microspheres (Figure 4.8A, Figure 4.9). For both PDA and PDL and laminin functionalization on glass microspheres, neuronal projections are shown to wrap around the top portion of each sphere, where interconnected networks are not clearly defined within the monolayer. The composite and fluorescent images in Figure 4.8B-C show neurite growth confined to each microsphere separately, but with multiple neurites distinguishable on each glass microsphere. Conversely, neuronal networks cultured on PDA-functionalized agarose microspheres show complex, interconnected networks within the microsphere monolayer, however, neuronal projection over the top of the microspheres is not as frequent within the network compared to networks cultured on glass microspheres (Figure 4.8A; Figure 4.9). It was also observed that neuronal growth on glass microspheres, regardless of functionalization, was sparse, and lacking complex connections across the culture (Figure 4.8B-C) in comparison to the wide stretching neuronal networks formed within the PDA-functionalized agarose microspheres (Figure 4.8A; Figure 4.9). Figure 4.9C magnifies a region of interest (delimited by the red dashed line in Figure 4.9 A and B). The magnified region of interest shows high-density cell adhesion and neurite growth within multi-layers of microspheres—this region of interest is further discussed in Section 4.3.2 using 3D rendering of z-stack confocal images.

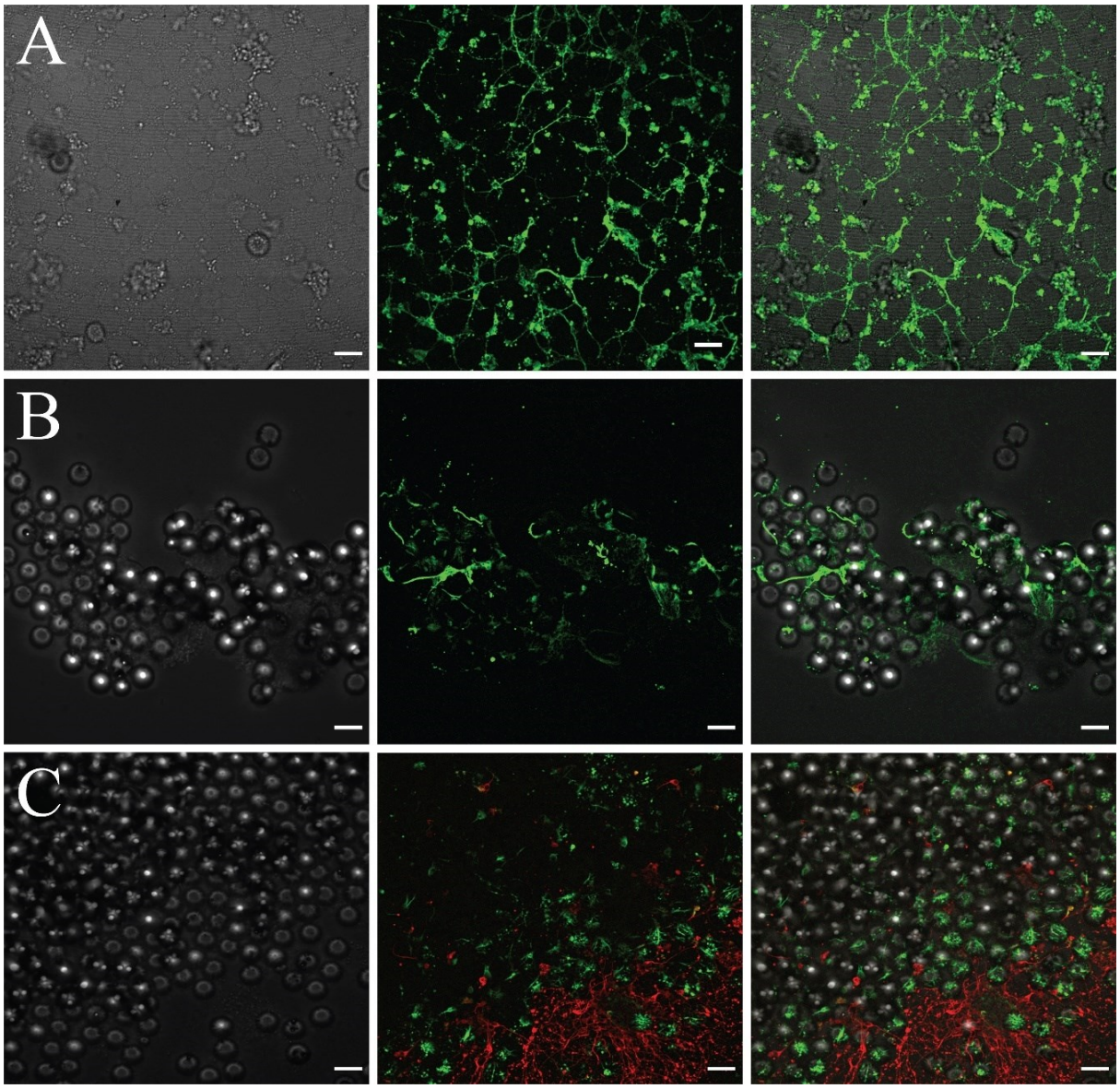

Figure 4.8 | Maximum projected immunofluorescent confocal images of 3D neuronal networks at 14 DIV cultured on functionalized microspheres and immunolabeled for βIII-tubulin *(green/red)*; **(Row A)** PDA-functionalized agarose microspheres; **(Row B)** PDA-functionalized glass microspheres; **(Row C)** PDL and laminin-functionalized glass microspheres; βIII-tubulin on surface of microspheres *(green)*; βIII-tubulin on planar substate/bottom of well *(red)*; ***Column 1:*** DIC image*;* ***Column 2:*** βIII-tubulin fluorescent image*;* ***Column 3:*** Composite image *(column 3); Scale bars: 50 µm*

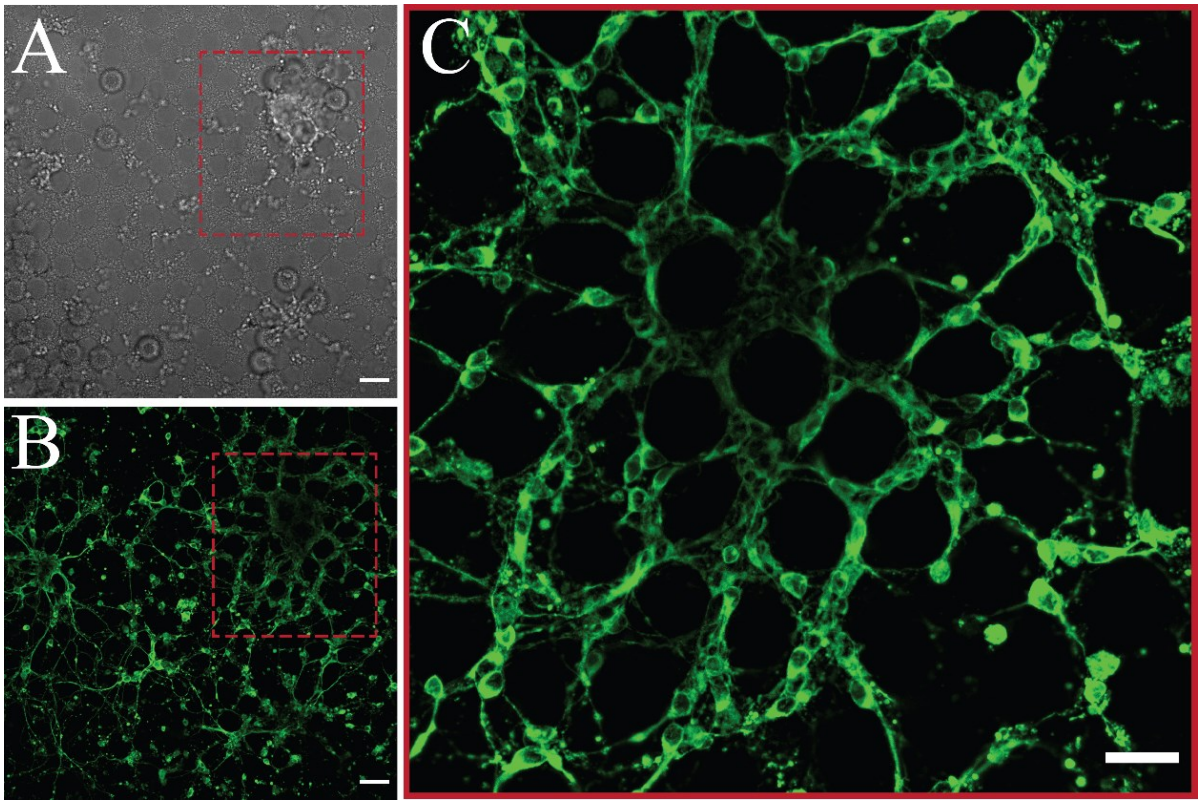

Figure 4.9 | Maximum projected immunofluorescent confocal images of 3D neuronal networks at 14 DIV cultured on PDA-functionalized agarose microspheres; **(A)** DIC image. *Scale bar: 50 µm*; **(B)** Fluorescent image immunolabeled for βIII-tubulin *(green)*; *Scale bar: 50 µm*; **(C)** Red boxed region of interest identified in A and B; *Scale bar: 30 µm*

4.3.2 3D RENDERING

Z-stack confocal images of neuronal networks after 14 DIV were 3D rendered to visualize network growth in 3D. Due to optical clarity, only networks on PDA-functionalized agarose microspheres were able to be 3D rendered using *Volumetric Viewer* plugin on ImageJ. Both volumetric reconstruction and orthogonal views of a representative 3D network on PDA-functionalized agarose microspheres and its regions of interest is shown in Figure 4.10-Figure 4.12, providing a comprehensive view of the network. A wide field of view (658.10 × 658.10 µm) of the network is achieved through a 20X objective of a spinning disk confocal microscope (Figure 4.10), highlighting the level of interconnectivity of the network. The orthogonal view of the x-z and y-z axis in Figure 4.10C show the βIII-tubulin marker occupying space in the third dimension provided by the microspheres.

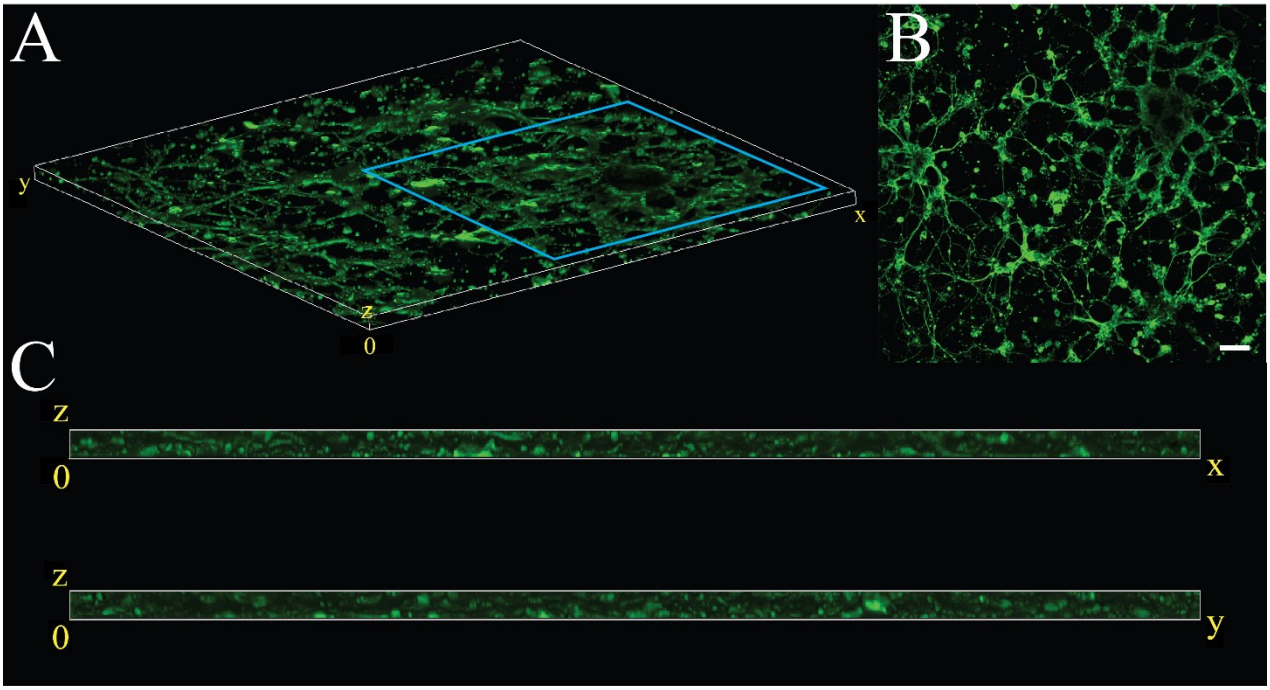

Figure 4.10 | Volume Viewer 3D rendering of neuronal networks on PDA functionalized agarose microspheres after 14 DIV labeled for βIII-tubulin; **(A)** Volumetric representation *(x,y = 658.10 µm, z =24.60 µm)*; blue square delimits agarose microsphere aggregation; **(B)** Maximum projection of z-stack (x-y plane); *scale bar: 50 µm*; **(C)** x-z, and y-z orthogonal view of 3D volume *(x,y = 658.10 µm, z = 24.60 µm)*

To further investigate the neurites within the multi-layered aggregation of microspheres (delimited by blue square in Figure 4.10A), the region was imaged under additional magnification as shown in Figure 4.11. The orthogonal views of the x-z and y-z axis in Figure 4.11B-C show the neuronal processes extending over 91 µm into z-axis indicating neurite growth on the surface of the functionalized agarose microspheres in the third dimension. The orthogonal view in the x-z plane also suggests neurite extension past 91 µm since the network remains dense at this height. The areas on the top left- and right-hand corners of the x-z plane are not fluorescent as there is not a second layer of microspheres to allow neurons to adhere and grow in those regions.

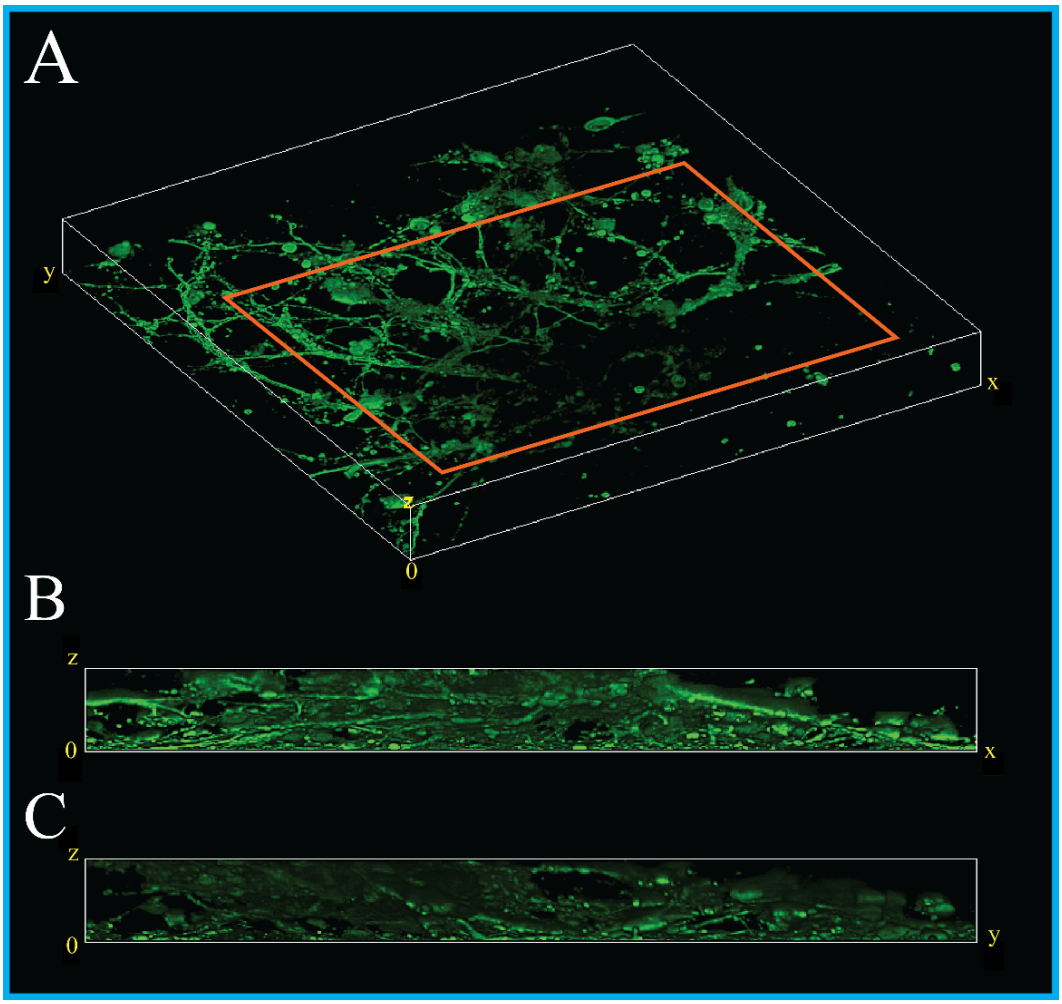

Figure 4.11 | Volumetric representation of PDA-functionalized agarose microsphere aggregation (region of interest delimited by blue square in Figure 4.10) at increased magnification **(A)** 3D view *(x,y = 324.83 µm, z =91.29 µm)*; **(B-C)** x-z, and y-z orthogonal view of 3D volume *(x,y = 324.83 µm, z =91.29 µm)*; **(C)** Maximum projection of z-stack (x-y plane)

As shown in Figure 4.12, imaging the βIII-tubulin marker through excitation of the fluorophore with the laser scanning confocal microscope resulted in high resolution of neurite development on the surface of the microspheres. The higher resolution indirectly provided an outline of the microspheres acting as scaffolding for growth. The non-fluorescent areas within the network, outlining the geometry of the PDA-functionalized agarose microspheres were found to measure considerably smaller in diameter than the target diameter during microfluidic fabrication. The average diameter of the 10 clearly measurable microspheres in Figure 4.12 is ~33.90 µm, which is almost 15 µm smaller than the mean calculated in Section 4.1.1. Considering the small standard deviation in microsphere diameter achieved with the microfluidic fabrication approach, the decrease in measured diameter here can be attributed to neuronal processes covering the top surface of the microspheres at multiple heights in the z-stack.

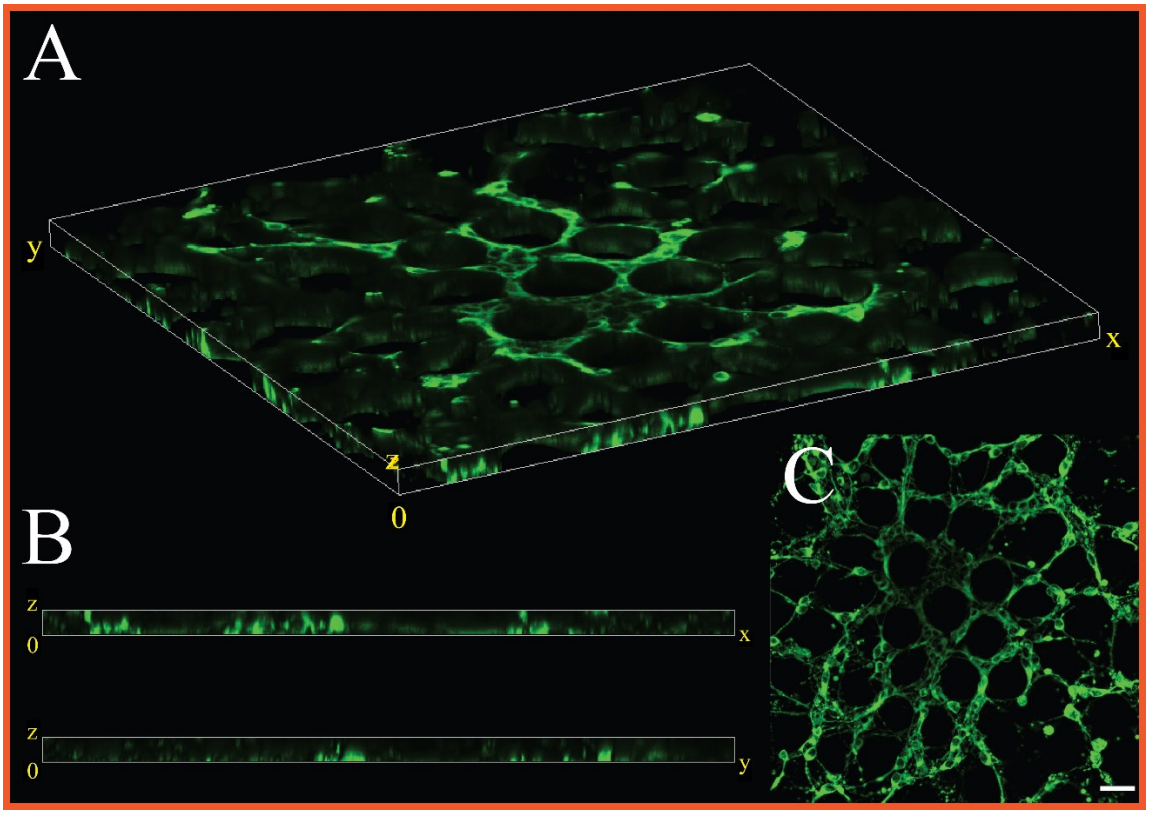

Figure 4.12 | Volumetric representation of PDA-functionalized agarose microsphere aggregation (region of interest delimited by orange square in Figure 4.11) using laser scanning confocal microscope **(A)** 3D view *(x,y = 319.45 µm, z =11.25 µm);* **(B)** x-z, and y-z orthogonal view of 3D volume *(x,y = 319.45 µm, z =11.25 µm)*; **(C)** Maximum projection of z-stack (x-y plane), *scale bar: 30 µm*

5 DISCUSSION

In the following sections, the use of PDA-functionalized agarose microspheres for 3D neuronal cultures is discussed, and compared to existing literature to highlight contribution of this work to the research field. Microsphere fabrication using microfluidics and the PDA-functionalization scheme is reviewed, while effective recapitulation of the soft and adhesive properties of the neuronal ECM in the model is assessed. Specifically, agarose microsphere fabrication reproducibility, PDA performance, microsphere adhesion, stiffness and Young's modulus is elaborated on. Finally, evaluation of the model after 14-day culture with embryonic cerebral neurons is discussed. Additionally, methodological limitations are addressed throughout.

5.1 MICROSPHERES

The microfluidic fabrication method coupled with the easily manipulated agarose polysaccharide provided a high-throughput, and facile pipeline to fabricate soft microspheres with precise geometry. Additionally, the significant improvements this material and microfabrication method provide to currently used materials and methods vouch for their use in future microsphere-based *in vitro* models. The following sections discuss the use of agarose and directly compare the microfluidic based approach to published techniques used for microsphere fabrication in 3D neuronal culture.

5.1.1 AGAROSE

In this work, the use of agarose microspheres was explored to support neuronal network growth in 3D. The agarose polysaccharide was chosen for the microsphere material due to its low stiffness, inherent biocompatibility (lack of adverse immune reactions) and previous use in microfluidic-based microsphere fabrication [77]. Furthermore, considering the end use in physiological conditions (aqueous and 37 °C), the thermal hysteretic behaviour of the agarose polysaccharide was ideal to ensure the construct remained robust in culture medium throughout the duration of the cell culture. As expected, agarose was easily prepared at the desired concentration of 1.5% for use in the microfluidic device and no adverse cellular reactions were observed during culture with neurons. Additionally, the agarose microspheres were shown to be robust, with no morphological

changes over several months at 4 °C, or 14 days (cell culture period) at 37°C. Indeed, agarose has been described as having no *in vitro* or *in vivo* basis for degradation [132] and has shown no swelling or shrinkage post microfluidic processing when suspended in PBS or culture medium [133]. The oil phase used for the emulsion at the microfluidic nozzle was also successfully washed away and no residual oil was left on the microsphere surfaces. Overall, the material was simple to manipulate, low cost and behaved as expected throughout the methods of this work.

5.1.2 Comparison with Published Techniques: Soft Microspheres

The monodisperse population of microspheres and consistent geometry achieved using the microfluidic fabrication method is a considerable improvement for microsphere-based 3D scaffolding in neuronal culture. The fabrication method not only allowed employment of a soft polymer to fabricate the microspheres, but also provided high throughput while maintaining precise geometries. Comparing the mean microsphere diameter and associated standard deviation achieved in this work to distributions highlighted in the literature review (Section 2.2.3.3; Figure 2.7), the microfluidic method was shown to reduce both the difference between minimum and maximum diameters, and the standard deviation associated with the mean. For instance, the percent deviation from the mean microsphere diameter is only 2% in this work, where deviations reported in [20] range between 30-40% and 6% in [134]. A quantitative comparison between studies in literature and this work is presented in Table 5.1, highlighting the microsphere materials and method used, mean, minimum and maximum diameters obtained, and associated error.

Table 5.1 | Microsphere dispersity: comparison with literature

Material	Method	Mean ± STDEV (%DEV)	Min – Max Diameter	Ref
1% chitosan	Bulk Emulsion (dropwise addition)	66 ± 20 µm (30%)	40 – 90 µm	[20]
2% chitosan		100 ± 40 µm (40%)	40 -160 µm	
3% chitosan	Electrospray extrusion into ionic solution	*Not reported*	30-100 µm	[55]
PHBV	Bulk, double emulsion	205.2 ± 12.3 µm (6%)	*Not reported*	[134]
1.5% agarose	Emulsion within flow focusing microfluidic device	48 ± 1 µm (2%)	42-54 µm	This work

***STDEV**: standard deviation; **Ref**: reference*

The improvement this work provides over currently published work is likely attributed to the precise microfluidic technology; however, the simplicity and predictability of the agarose polymer presumably played a role in the consistent nature of the method.

5.1.3 Comparison with Published Techniques: Stiff, Manufactured Microspheres

The soft agarose microspheres used in this work also provided critical improvements over studies using rigid glass or plastic microspheres sourced from commercial suppliers to interface with neuronal cultures *in vitro* [24], [56], [57]. For instance, the commercially available glass microspheres used in this study as a control were observed to have geometrical and size irregularities within the microsphere populations, with quantities falling outside the manufacturers specified range of deviation (*specified range*: 42-47 µm). Figure 5.1 shows optical images of glass microspheres taken while carrying out Raman spectroscopic measurements, where geometrical and size irregularities are clear and are indicated by red and yellow arrows, respectively. When quantified, the microsphere diameter irregularities were found to reach up to 13 µm outside the manufacturer's specified range. Figure 5.1B identifies a 28.4 µm diameter microsphere (yellow arrow), and Figure 5.1C identifies 35.2 µm (top yellow arrow) and 31.7 µm (bottom yellow arrow) diameter microspheres. To note, the measured maximum and minimum microsphere diameter differed by ~19 µm in the glass microsphere population, and only 12 µm in the agarose microsphere population fabricated using the microfluidic technology for this work (Figure 3.1). Although the agarose microspheres did have slight deviations, and were not perfectly spherical in geometry, blatant irregularities were not observed, as they were with the commercially manufactured microspheres (Figure 5.1A-C). In this context, the microfluidic approach resulted in a more precise microsphere diameter, compared to the commercially available glass microspheres.

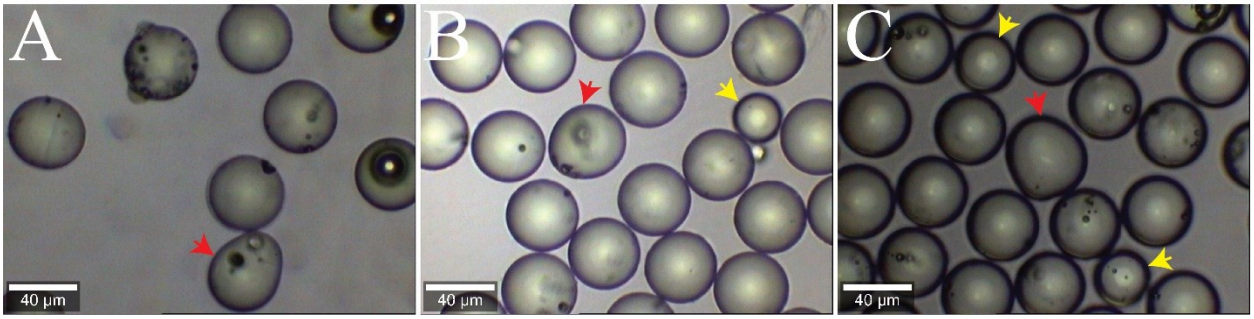

Figure 5.1 | **(A-C)** Size and geometrical inconsistencies in commercially manufactured glass microsphere population; Red arrow: geometrical inconsistency; Yellow arow: outside diameter range specified by manufacturer.

Taken together, the ability of the microfluidic approach to produce soft polymeric microspheres with high-throughput and improved batch to batch reproducibility in comparison to commercially manufactured microspheres bring a promising avenue for microsphere-based scaffolding for *in vitro* use. Of note, the high-throughput and small batch-to-batch variation provide an attractive foundation for potential clinical translation in the future.

5.1.4 MICROSPHERE-BASED 3D CULTURES: PRACTICAL LIMITATION

Prior to obtaining immunofluorescent results shown in Section 4.3, multiple experiments were completed where prepared 3D cultures contained multiple layers of microspheres and required seeding multiple layers of cells. At 14 DIV, fluorescent imaging of the neuronal cultures showed low β-III tubulin and DAPI expression (data not shown). It was determined that the microsphere seeding method was resulting in a non uniform microsphere distribution (i.e. regions of multilayered microspheres) within the culture wells which did not correlate to the theoretical surface area expected for cell seeding. Prior to seeding microspheres in culture wells, calculations were performed such that the volume of microspheres collected using a pipette would yield a calculated number of microspheres within the microwells. The *close packing of equal spheres* lattice packing strategy was considered for this purpose, where the volume occupied by the microspheres within the volume collected by the pipette is described by:

$$V_{sphere\ occupancy} = V_{aspirated}(\pi/3\sqrt{2}) \qquad \text{Eq 5}$$

Considering the total surface area provided by culture wells, the exact volume of microspheres required for a hexagonally close packed system was determined. Theoretically, the mathematics agreed—practically, the method was challenging to execute. Figure 5.2 illustrates the challenges experienced for each microsphere type, with Figure 5.2A showing how microspheres would need to be aspirated for theoretical calculations to be valid experimentally. With glass microspheres, the theoretical seeding scheme was challenging due to the microsphere density compared to the culture medium. When aspirating the microspheres, they would inherently collect at the bottom of the aspirated volume (Figure 5.2B), resulting in a smaller volume/number of microspheres collected than theoretically calculated. Conversely, agarose microspheres were less dense, requiring additional time to settle within the aspirated volume. This resulted in a reduced packing density within the volume and thus a lower number of microspheres within the collected volume than theoretically calculated (Figure 5.2C). An additional challenge with the agarose microspheres was

their translucence, requiring DIC microscopy to see them. Fortunately, the PDA functionalization created a dark coating around the surface of the spheres making them visible after polymerization of PDA on their surface.

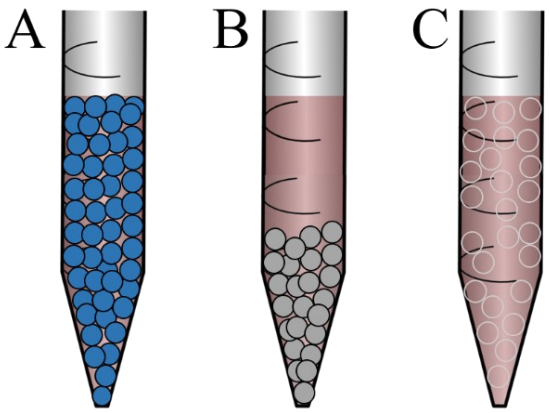

Figure 5.2 | Microsphere seeding practical limitations **(A)** Theoretical close packing of spheres within volume collected by pipette. *Note: Close packing of sphere not perfectly depicted in schematic.* **(B)** Experimental reality of glass microspheres in specified volume collected by pipette. **(C)** Experimental reality of agarose microspheres in specified volume collected by pipette

It was for these reasons that the originally designed multi-layer microsphere construct was reduced to a single monolayer of microspheres—this allowed evaluation of the culture growth at a fundamental level, while ensuring neuronal seeding density remained accurate. During microsphere seeding, brightfield microscopy was used to ensure a uniformly seeded layer of microspheres prior to the addition of neurons to their surface area. This resulted in a more accurate cell seeding density on the surface area provided by the microspheres. Although a monolayer was sought, discrete regions with multi-layer microsphere conglomeration existed within the culture wells. In this way, regions of single layer microsphere depositions allowed evaluation of network connectivity, while multi-layer regions allowed examination of neuronal network growth into the 3D space.

5.2 POLYDOPAMINE FUNCTIONALIZATION

The PDA-functionalization scheme was found to be optimal for the purpose of this work due to its adhesive, and substrate-independent properties. The following sections elaborate on the deposition homogeneity, the effect of polymerization time on resulting substrates for neuronal

culture, and PDAs effectiveness as a single functionalization. Finally, the limitations of the functionalization scheme for pre-clinical models are addressed.

5.2.1 Polydopamine Deposition: Full Surface Coverage

From brightfield and DIC images, PDA-functionalized microspheres (agarose and glass) were shown to have an apparent dark pigment and rough surface morphology (Figure 4.1C-E), while unmodified microspheres had a smooth surface (Figure 4.1B). This difference was more clearly represented on agarose microspheres. To further confirm PDA-deposition, Raman spectroscopy was used. Not only was PDA deposition confirmed but results also show complete coverage on all surfaces, evidenced by the characteristic PDA peaks in all acquired spectra regardless of sample location. Qualitatively, no appreciable differences were identified between PDA deposition on the microsphere compared to on a 2D substrate, nor between PDA deposition on the agarose microsphere compared to the glass microsphere. This speaks to the material independent nature of the PDA-functionalization. However, local band intensity variations were present between samples, which, as suggested in [110], is an indicator of PDA aggregation. The hypothesis that these varying intensities is an indicator of PDA aggregation can be preliminarily confirmed through identification of PDA aggregates in brightfield images Figure 4.2B-C.

5.2.2 Polymerization Time

To functionalize the surface of all substrates (2D and microspheres), a 2-hour dynamic polymerization protocol was used. However, in the optimization phase, an overnight (18-hour) dynamic polymerization scheme was assessed. Figure 4.1C, and Figure 4.1D-E show agarose microspheres functionalized with a 2-hour, and 18-hour dynamic deposition, respectively. Qualitatively, the 18-hour deposition resulted in an increased number of larger PDA aggregates on the surface of the microsphere. This phenomenon was previously reported by our research group [115] and is associated with longer deposition times. The 2-hour deposition time was assessed after evaluating the structure-function relationships between PDA film, aggregates, and neurons. As expected, the shorter deposition time resulted in fewer, and smaller aggregates. The effect of polymerization time for neuronal culture is discussed in further detail in Section 5.4.

5.2.3 USE AS A SINGLE FUNCTIONALIZATION

In literature, the PDA functionalization has been used as an intermediate immobilization scheme due to its catechol and amine groups that provide secondary reaction sites for biomolecules like PDL and laminin [107]. However, studies have since shown the ability of the adhesive polymer to promote neuronal attachment and growth even when used alone [26], [116], [117]. This evidence supported the use and effectiveness of PDA as a single functionalization step without the need for additional biomolecule immobilization. As such, functionalization with PDL and laminin (gold standard in conventional neuronal cultures) was not carried out after PDA deposition to solely focus on the role of PDA in the application. In reference to the results obtained with 2D cultures, neuronal adhesion and network growth was evident on substrates functionalized with PDA alone. In fact, improved neurite outgrowth was demonstrated on surfaces functionalized with PDA compared to those functionalized with PDL and laminin. While confirming previous evidence that the PDA could be used as a bio-effective functionalization approach, PDA also showed improvement over the current gold standard protocol. This ultimately simplified the method and reduced the time required for functionalization of the microspheres. In future work, the addition of PDL and laminin to the PDA functionalization protocol could be evaluated to potentially further improve results obtained in this work.

Furthermore, since PDA has been used successfully to functionalize neuron-electrode interfaces for *in vitro* electrophysiological recordings [111], [120], this model can be seamlessly coupled to MEAs. The functionalization scheme would remain consistent on both the MEA and microspheres, while limiting the risk of affecting the electrophysiological signature of neurons. Importantly, the PDA coating has shown effectiveness as a functionalization without reducing the electrical properties of the electrodes, which is important for accurate electrophysiological recordings [119]. In the case where an MEA would be used to record electrophysiological behaviour of the network, the methods can remain as outlined in Section 3, with only replacement of the glass-bottom plate with a MEA multi-well plate.

Moreover, should the microsphere material need to be replaced with another material (e.g. to modulate the mechanical properties of the construct), the PDA functionalization scheme can remain unchanged because of its substrate-independency.

5.2.4 Limitation and Pre-clinical Application

While there are multiple advantages to the PDA-functionalization, one limitation is the fact that the exact mechanism in which PDA is polymerized, and the specific factors that precisely control it, are still open research questions [109]. In this context, although the PDA deposition can be confirmed, the structure-function relationships and mechanisms through which PDA polymerizes and deposits on the surface of the microspheres is not entirely known. To date, investigation into the chemical mechanisms that result in PDA films and aggregates have largely been limited to deposition on 2D substrates [107], [109], [115]. These studies have shown static vs. dynamic deposition schemes can vastly affect antibacterial properties, film thickness, and aggregate morphology of the polymer coating [115], [135]. As such, the mechanisms and manner in which PDA deposits on the surface of the microsphere vs. 2D substrates could very well be different—specifically when using a dynamic deposition scheme. The rolling action of the microspheres through the PDA solution could potentially produce local turbidity within the PDA solution, influencing the number, size and physiochemical properties of PDA aggregates produced. This is hypothesized since the way PDA deposits on surfaces using different dynamic schemes (e.g. rotation vs. shaking), along with time and speed has been previously shown to affect these features. Unfortunately, investigation into the differences between dynamic deposition of PDA on a round surface vs. a flat substrate has—as far as the author of this thesis is aware—yet to be explored. Although work has been published on the topic of PDA-based colloids [136], no publication has investigated influence of substrate size and geometry on PDA film and aggregate polymerization.

Implementation of this type of functionalization for pre-clinical studies therefore presents challenge, due to the areas of uncertainty and batch-to-batch surface variation. However, with further optimization of PDA deposition on spherical substrates, the potential inconsistencies can be ruled out, while the complex chemical mechanisms involved in PDA polymerization are simultaneously unravelled by chemists around the globe.

5.3 Material Properties

Measuring the physical and mechanical properties of biomaterials interfacing with cells is an imperative step in the evaluation of an *in vitro* model. This allows direct assessment of the degree of recapitulation of the *in vivo* physiology. In this work, the physical and mechanical

properties of the fabricated materials were found to play a significant role in regulating neuronal adhesion and neurite growth in 3D. The following sections discuss material stiffness and Young's modulus for soft samples, and adhesion on all functionalized samples.

5.3.1 Stiffness: Agarose Microsphere vs. 2D Substrate

Results showed a significant increase in stiffness and Young's modulus of 1.5% agarose when measured as a homogenous 2D substrate compared to its microsphere form with a diameter of ~48 μm. Although stiffness is both a material and structure dependent property, the difference seen in stiffness should theoretically not exist for these two substrates at the nanoscale. Since the AFM probe can almost be considered infinitesimally small (*nominal tip radius = 20 nm)* in comparison to the dimensions of both the 2D agarose sample and the microspheres, the geometrical differences between the macroscale 2D sample and microscale spherical sample would not influence the nanoscale measurement. Considering the small deviations associated with the nanoindentation measurements for these sample conditions, the difference in stiffness is likely attributed to a parameter associated with the sample fabrication method.

A possible explanation for this divergence is the fabrication method-specific mechanisms involved in agarose gelation. Within the microfluidic device, a temperature gradient exists along the base of the setup, where the inlet and outlet of the chip were maintained at temperatures of ~37 ºC and ~4 ºC, respectively. This is to prevent premature agarose gelation at the inlet and ensure gelation prior to the microsphere's arrival at the device outlet. As a result of this controlled gradient, the formation of the polymers double helices during the initial gelation state, and/or the aggregation of double helices during the final gel state of the agarose could differ from the gelation behaviour during processing of the 2D substrate. In the microfluidic device, the agarose microsphere experiences this temperature gradient within a few seconds due to the high throughput, however with the agarose deposited manually for 2D substrates, the cooling rate for gelation is much slower. To gel the 2D substates, dishes are also brought to 4 ºC, however the time from deposition (between 90 ºC and room temperature) to 4 ºC occurs over ~1-2 minutes—this is relatively long in comparison to temperature gradient the microsphere experiences within the microfluidic device. With this considered and referencing the effect of cooling rate on agarose gelation [137], the fast cooling rate of the microsphere should induce tighter double helices aggregation resulting in an overall smaller pore size and ultimately a stiffer material. Since the results show the agarose

microsphere has a lower stiffness than the 2D agarose substrates, the cooling rate is likely not root cause of the discrepancy.

Alternatively, this discrepancy could arise from variability in location of nanoindentation measurements on the surface of the microsphere. Due to the spherical geometry of the microspheres, for the force applied by AFM tip to be evenly distributed, the indentation needs to be perfectly executed above the sphere's center of mass. Since the AFM tip is manually manipulated, and the center of the sphere is obstructed by the probes cantilever, executing this measurement perfectly is difficult. Indeed, since the size of the AFM tip is relatively small compared to the microsphere size, a tolerance is acceptable for this location relative to the exact sphere center. However, since the contact mechanics in this work are carried out considering a uniformly distributed applied load across a flat surface, a measurement made outside an acceptable margin from the sphere's center could result in considerable discrepancy. In this case, the curvature of the microsphere would influence nanomechanics of the indentation.

5.3.2 Stiffening: Result of PDA-Functionalization

Consistent with previous studies, [138], [139], results presented in this work showed microsphere stiffening after dynamic, 2-hour PDA deposition on their surface. Correspondingly, the percent difference in stiffness between PDA-functionalized, and non-modified agarose microspheres decreased as the indentation depth increased; the same comparison between PDA-functionalized microspheres and 2D agarose substrates also followed this trend. Interestingly, comparison of measurements between agarose microspheres and 2D agarose substrates (both not functionalized) showed the opposite trend, where the percent differences increased as a function of indentation depth. This confirms PDA influences overall substrate stiffness. Additionally, since the pore size of 1.5% agarose ranges from ~70-150 nm [140], the PDA can polymerize within exposed pores and potentially a few hundred nanometers into the agarose microsphere. Indeed, the results suggest that the PDA solution could be diffusing into the microsphere pores, resulting in stiffening of the microspheres outer layer. Notably, the influence of PDA on the substrate stiffness is the most considerable in the first 300 nm of indentation, and therefore suggests limited diffusion of the PDA solution beyond this depth.

5.3.2.1 *High Standard Deviations Associated with PDA-Functionalization*

Nanoindentation measurements on PDA-functionalized agarose microspheres showed significantly higher standard deviation between measurements than on unmodified surfaces (Figure 4.3). The most likely explanation for the deviation is the non-homogeneous PDA functionalization layer.. Since PDA is known to produce both a homogenous film and variously sized aggregates during polymerization, the resulting surface of the agarose microsphere was topographically and nanomechanically non-homogenous. A schematic depicting the resulting topography of the PDA on the surface of a nano-porous agarose microsphere is shown in Figure 5.2. Additionally, since the PDA is polymerized onto the microspheres while they roll through the solution, the PDA thickness can vary across the surface area of the microsphere [115], thicker regions or locations of PDA aggregation on the microsphere surface would result in local stiffening of the substrate and therefore a steeper force-indentation curve.

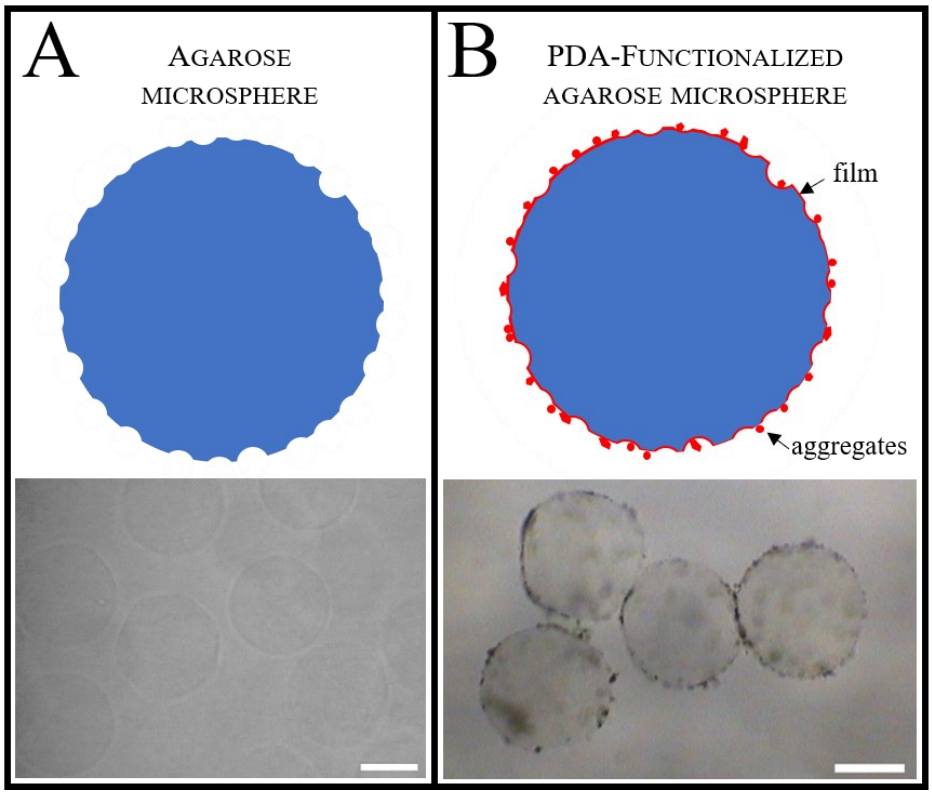

Figure 5.3 | Agarose microsphere functionalization schematic; **(A)** Unmodified agarose microsphere highlighting ~70-150 nm pores exposed on surface; **(B)** PDA-functionalized agarose microsphere, highlighting PDA polymerization as a film and as aggregates; scale bars = 30 µm

To note, nano-topographical changes due to agarose nanopores exposed on the surface of the microsphere were not likely contributors to the deviation since nanoindentation measurements carried out on unmodified agarose microspheres did not show the same result. This suggested the variation in measurements on PDA-functionalized agarose microspheres was attributed to the PDA functionalization only.

Another potential contributor to the deviation in measurements could be due to the noise-inducing combination of the adhesive PDA film and the aqueous measurement medium. Since measurements were performed in an aqueous medium, the noise introduced into the system from motion of the AFM probe is amplified. Therefore, since PDA has shown to significantly increase surface adhesion, the deflection of the cantilever prior to detachment will be considerably larger than with the non-PDA-functionalized samples. Correspondingly, the noise introduced into the system through the aqueous medium as a result of the cantilever oscillation would be cause for increased deviation in measurements.

5.3.3 YOUNG'S MODULUS

To determine the Young's modulus, the first 300 nm of the force-indentation curves was considered since the Hertz/Sneddon extended model is only valid for shallow indentations. This way, the substrate being indented will not influence contact mechanics and the indentation can be characterized by the geometry of the indenter. Figure 4.4B shows the Hertz model adapted for a tetrahedral indenter (Sneddon extended model) converging well with nanoindentation data for each sample, suggesting a accurate estimation of the Young's modulus with respect to the parameters used.

5.3.3.1 2D AGAROSE SUBSTRATE AND MICROSPHERES

Similar to the stiffness, the discrepancies between the 2D agarose substrate and agarose microsphere are also seen in the Young's modulus. As such, they will not be reiterated in this section. Instead, results will be discussed and compared with Young's moduli in literature for 1.5% agarose substrates, and microspheres (of different materials) used in microsphere-based 3D neuronal culture.

Table 5.2 compares the Young's modulus of 1.5% agarose found in this work to values from published work. Unfortunately, in literature to date, the Young's modulus of a 1.5% agarose

microsphere measured using AFM has—to the knowledge of the author of this thesis—yet to be published. The results found in this work are therefore compared to the Young's moduli of flat 1.5% agarose substrates determined through AFM nanoindentation. Based on these comparisons, the Young's modulus quantified in this work falls within a reasonable margin of published data, suggesting relatively accurate AFM measurements. Of note, the Young's modulus estimated for the agarose microsphere in this work differs from values found in [88] by only 14%, which is of particular importance since it indicates the curved microsphere geometry is likely not a major contributor of error to nanoindentation measurements.

Table 5.2 | Young's modulus of 1.5% agarose: comparison with literature

Substrate	**E ± STDEV**	**Indentation Depth**	**Contact Mechanics Model**	**AFM Probe Information**	**Ref**
Flat	5.6 ± 0.9 kPa *(mean)*	400 nm	Hertz	Tip-less, equipped with 5.3µm melamine bead, k=0.1 N/m	[88]
Flat	9.8 ± 1.5 kPa	100 nm	Sneddon extended (Hertz for pyramidal indenter)	Pyramidal (k=0.06 N/m)	[89]
Flat	13.3 ± 5.2 kPa	300 nm	Sneddon extended (Hertz for pyramidal indenter)	Pyramidal (k=0.03 N/m)	This work
~ 48 µm sphere	4.9 ± 0.6 kPa	300 nm	Sneddon extended (Hertz for pyramidal indenter)	Pyramidal (k=0.03 N/m)	This work

***E**: Young's modulus; **STDEV**: standard deviation; **Ref**: reference*

Table 5.3 compares Young's moduli of microspheres in this work, to another study reporting the use of microspheres to interface with neuronal networks *in vitro*. The Young's modulus of the PDA-functionalized agarose microsphere falls within the same range as reported by Tedesco *et al* [20], for 2% chitosan microspheres, while the unmodified agarose microsphere falls closer to the modulus calculated for the 1% chitosan microsphere. To quantify the Young's modulus of the 1% chitosan microsphere however, Tedesco *et al* [20] extrapolated based on normalization to the 2% chitosan microsphere Young's moduli and followed with a statement indicating the 1% chitosan microsphere Young's modulus is within the range of the Young's modulus of brain tissue (0.7 – 1

kPa). Although this could potentially be a valid method of deriving the Young's modulus based on the authors methods, it should be noted that after review of literature for the Young's modulus of chitosan at this concentration, no other study was found to report an Young's modulus as low as 0.8-1.4 kPa [141]–[143]. Interestingly, the method to fabricate the chitosan in [20] was said to be based on methods reported by He *et al* [144], where He *et al* report chitosan Young's moduli on the order of MPa. Additionally, in [20], Tedesco *et al* failed to report any standard deviations for the Young's moduli, leading us to believe there could have been significant errors associated with these values.

Table 5.3 | Young's Modulus of microspheres for *in vitro* neuronal cultures

Material	Ø ± stdev	E ± stdev	Contact Mechanics model	AFM Probe Information	Reference
1% chitosan	66 ± 20 µm	0.8 – 1.4 kPa *+	Hertz	Tipless probe (k = 0.03 N/m)	[20]
2% chitosan	100 ± 40 µm	15 – 25 kPa +	Sneddon (Hertz for conical indenter)	Conical (k = 0.03 N/m)	[20]
1.5% agarose	48 ± 1 µm	4.9 ± 0.6 kPa	Sneddon extended (Hertz for pyramidal indenter)	Pyramidal (k=0.03 N/m)	This work
1.5% agarose w/ 2mg/ml PDA functionalization	48 ± 1 µm	26.8 ± 17.9 kPa	Sneddon extended (Hertz for pyramidal indenter)	Pyramidal (k=0.03 N/m)	This work

E *= Young's modulus;* ***Ø*** *= microsphere diameter;* ***stdev*** *= standard deviation*
*******: Inferred based on extrapolation*
+: stev not reported

With regard to Young's moduli found in this work for agarose microspheres, there is still room for improvement since the values we report fall short of the physiological target range. As previously mentioned in the literature review, the mechanical properties the agarose can be tuned using its concentration (Section 2.3.2). To lower the Young's modulus of an agarose hydrogel, its concentration needs to be reduced. Although seemingly simple, with the agarose microsphere, this becomes a challenge two-fold in origin; first, due to limitations of the microfluidic device and second, due to the nature of molecular-grade agarose. Unfortunately, when using the microfluidic

platform, creating microspheres lower than 1.5% in concentration, resulted in microsphere diameters with high polydispersity. Additionally, with ultra-low gelling temperature molecular biology grade agarose (used in this work), gelation at concentrations lower than 1.5% is not guaranteed by the manufacturer and thus limits further reduction of the Young's modulus of the microspheres. Through numerous tests at different concentrations (0.75%, 1%, 1.5%, 2%), it was found that 1.5% agarose provided both a monodisperse sample while avoiding clumping within the microfluidic device. Consequently, to further lower the Young's modulus, the microfluidic device could be modified, or an alternative synthetic agarose could be sought out.

5.3.3.2 PDA-Functionalized Agarose Microsphere

As with stiffness, an increase in the agarose microsphere Young's modulus occurred after functionalization with PDA. To lower the degree of stiffening caused by the PDA functionalization, the PDA polymerization time can be decreased to reduce the thickness of the resulting coating and lower the number and size of PDA aggregates on the microsphere surface. By reducing the amount of PDA on the surface of the microsphere, the stiffening induced by PDA would be lowered, thus improving the overall Young's modulus. However, prior to reducing polymerization time, the cellular response to the functionalization should be assessed on a 2D substate to confirm network viability.

5.3.3.3 Limitations of the Hertz (Extended Sneddon) Model

The adapted Hertz model (Sneddon extended model [130]) used to quantify the Young's modulus from nanoindentation AFM data has multiple limitations; all of which require the Young's modulus quantity to be taken generally. To start, the Hertz model does not consider surface interaction forces, i.e., forces between atoms and molecules of the tip and the material. Since the PDA surface functionalization is incredibly adhesive, not taking the adhesive forces into account can dramatically influence the Young's modulus estimation. Additionally, the Hertz model is highly dependent on determination of the contact point of the force-indentation curve. Determining the contact point on the force-indentation curve of a soft polymer is not straight forward since the contact point is characterized by only a gradual increase in force associated with increased indentation. As such, potential inconsistencies related to identification of this location on the force-indentation curves can arise.

5.3.3.4 General Misconception in Literature

It should also be noted that within the field, there seems to be a disconnect that should bridge the biological nature of the work, with material property characterization. For instance, some published works report *stiffness* in units of pascals [93], where stiffness is indeed a force per unit length, not per unit area, and defined as resistance to elastic deformation. Although stiffness and Young's modulus can be proportional, they are different properties. Cases such as this, where the Young's modulus and stiffnesses of biomaterials are used interchangeably, make progression and literature benchmarks with regard to biomimetic *in vitro* modeling increasingly difficult. Additionally, almost every published work that uses AFM as a method to determine mechanical properties of a polymer for *in vitro* cell culture reports *only* the Young's modulus. It was for this reason the nanoindentation data was fitted for Young's modulus in this work; since only the Young's modulus is consistently reported in literature, it was required for comparison with previously published data. This is quite interesting, since when using AFM, only sample stiffness can be calculated directly from the acquired measurement—not the Young's modulus. To acquire this property, fitting models are required, and within the field, the model adopted for this purpose (ex: Hertz, JKR, DMT) is not generally consistent. Additionally, as mentioned in Section 5.3.3.3, considerable limitations are associated with all fitting models used for quantification of the Young's modulus.

5.3.4 Adhesion

Sample adhesion was assessed through quantification of maximum force required for tip-sample detachment during retraction portion of nanoindentation measurements. Adhesion was quantified on all samples with functionalization, thus including PDA-functionalized and PDL and laminin functionalized glass microsphere samples. Results obtained were expected, where microspheres with PDA functionalization possessed the highest sample adhesion, requiring the greatest forces for tip-sample detachment, followed by the glass microsphere functionalized with PDL and laminin. Since PDA engages in noncovalent interactions, such as hydrogen bonding and electrostatic interactions, the functionalization increased interfacial adhesion on the surface of the microspheres. As seen with quantification of stiffness and Young's modulus, adhesion on PDA-functionalized substrates was also associated with larger standard deviations in comparison to the other functionalization types. However, as previously stated, the non-homogeneous topography of

the PDA is a likely culprit for deviation in measurements due to variously sized aggregates scattered on the surface of the microsphere. Indeed, it has been demonstrated in literature that PDA film and aggregates are characterized by significantly different adhesion forces [115]. Additionally, the noise introduced into the system as a result of the combination of aqueous measurement medium and the increased adhesion between the AFM tip and PDA (previously explained in Section 5.3.2.1) likely contributed to the increased standard deviation as well.

Important for continued use of the PDA functionalization in this research space is the increased adhesive forces it elicits on both glass and agarose microspheres compared to the current gold standard functionalization for neuronal culture, PDL and laminin. Together with the substate-independent nature of PDA, the improved adhesion observed with this functionalization scheme, allow expansion of the next generation of biomaterials for neuronal culture.

5.3.5 The AFM Technique and Cantilever Calibration

The AFM technique relies heavily on the probe's tip and cantilever for accurate and reliable measurements. As such, it was imperative the tip sensitivity and cantilever spring constant were obtained prior to AFM measurements. The sensitivity of the AFM tip is a measure of how the photodiode responds to deflection of the cantilever, which is a property of the optical alignment of each AFM system and is easily obtained. The spring constant however is a property of the AFM cantilever and more difficult to obtain. Prior to beginning this work, no cantilever spring constant calibration technique was established for the AFM in our lab. Therefore, a protocol was developed during this work to do so using the Sader online tool and thermal noise methods [128] (Section 3.3.3.1). Carrying out this protocol, calculated values for cantilever spring constants were tending toward the lower end of values reported by the manufacturer. Although the measurements using the Sader and thermal noise method should be accurate within 4%, [145], there is a potential that the calibration method needs optimizing for the equipment in our lab. In the case an operating/protocol error existed, the nanomechanical data obtained would show the materials were stiffer and less adhesive than results presented in this work, since the spring constants favoured the lower end of the manufacturer's tolerances. If this is the case, the reported Young's moduli would be further reduced and thus report a softer model, while the PDA functionalization could be more adhesive than reported. Both outcomes would only result in an improvement of the model towards the ideal physiological nano-mechanics.

It should be highlighted, that quantification and processing of nanomechanical measurements on soft polymers in an aqueous environment is not yet standardized within the field. Currently, no comprehensive model exists to account for all relevant variables that contribute to the overall nanomechanical properties of a material, including porosity/water content, curved geometry, homogeneity of porous matrix, and pore size. Further investigation into a model that includes all these variables in would be an invaluable contribution to the field to ensure soft polymers can be reliably tested.

5.4 Neuronal Networks on 2D Polydopamine Functionalized Substrates

As a preliminary assessment of the bioaffinity of neuronal networks to PDA, neurons were cultured for 14 days on 2D substrates functionalized with PDA. As briefly mentioned in Section 5.2.2, an 18-hour dynamic polymerization deposition method was first adopted. Results showed PDA polymerization time had a direct effect on its ability to serve as a functionalization for neuronal cultures (data not shown). Although neuronal adhesion was achieved on substrates functionalized with an 18-hour scheme, neurite outgrowth was absent. Since longer polymerization time is associated with large aggregate formation, and aggregates are known to be stiffer and less adhesive than the PDA film [115], substates that underwent 18-hour deposition presented surfaces with increased stiffness and reduced adhesive forces that likely prevented neurite projection. These local increases in substrate stiffness and reduced adhesion due to increased number and size of PDA aggregates strayed from the soft ECM matrix these substrates were in pursuit of recapitulating. By reducing polymerization time by 16 hours, the number of aggregates decreased significantly, and neurons produced highly interconnected networks. When compared to the current gold standard, the PDA functionalization (2-hour, dynamic scheme) promoted neurite growth after 14 DIV. In fact, neurite projection from nuclei was found to cover 34% more culture surface area per neuron on PDA-functionalized substrates compared to PDL and laminin gold standard functionalization protocol. Interestingly, although the PDA-functionalized substrates improved neurite development, higher number of nuclei were found to adhere to the PDL and laminin functionalized substrates. Considering this result alone, it would be expected for the PDL and laminin functionalized substrate to present superior neurite growth, largely influenced by the biophysical effects of high cell density. Interestingly, neurite outgrowth was partial to the PDA, regardless of the higher cell retention on PDL and laminin substrates. This could suggest the role

of PDA at the molecular level as a catalyst to promote neurite growth. The lower rate of cell body adhesion to the PDA substrate was not an expected result considering the strong adhesive nature of polymer and the available binding sites it provides through catechol and amine groups. In addition to the reasons outlined in Section 5.2.3, the positive neuronal response to PDA-functionalized substrates vouched for the use of PDA alone in the attempt to maximize neurite outgrowth and, in turn, the creation of a complex network when translating the functionalization scheme to 3D.

5.5 Neuronal Networks on Polydopamine Functionalized Microspheres

Overall, results showed improved neuronal network growth on PDA-functionalized agarose microspheres, compared to its glass microsphere counterpart and the previously reported PDL and laminin glass microsphere model [24]. Note that discussion of 3D neuronal network growth on microspheres is partially discussed in the results section (Section 4.3) since direct references to fluorescent images are mentioned. In general, PDA-functionalized agarose microspheres elicited unified growth across the entire culture surface while facilitating functional connections between neurites on microspheres at mid-hemisphere height. Conversely, functionalized glass microspheres were found to serve as regions for growth in discrete areas of the culture wells, with projections extending across the top hemisphere of microspheres and showing a lower degree of network connectivity. Additionally, differences were observed between neuronal networks cultured on functionalized 2D substrates and the microsphere analogue.

5.5.1 Substrate-Mediated Neuronal Network Formation

From qualitative observation, the neurites projecting on the surface, and within the interstitial space of PDA-functionalized agarose microspheres (Figure 4.9) were thicker than neurites observed on 2D PDA-functionalized substrates (Figure 4.6B). This suggests dense bundles of multiple neurites surrounding each microsphere. Interestingly, dense bundles of neurites were not observed on PDA-functionalized glass microspheres (Figure 4.8B), instead, singular neurites projected around and over top of each microsphere as separate entities. Since the difference between these models lies in the substrate stiffness, and Young's modulus, it can be speculated that the soft microsphere played an important role in regulating neurite development. Further, in analyzing the 3D architecture of the glass and agarose microsphere-based cultures, the enhanced

dendritic development observed in agarose microsphere-based cultures showed higher network complexity and thus increased network connections, also leading us to believe that microsphere stiffness is the main driver involved in determination of an overall biomimetic *in vitro* neuronal culture. In future work, a functional readout of this nanomechanical material property-induced difference using a MEA would provide insight on this inference.

While microscale arborizations within the network were clearly visible with confocal microscopy, previous studies have shown that nanoscale extensions can penetrate the surface of hydrogel microspheres resulting in the formation of a compact and well-structured neuronal network [20]. Indeed, the nano-porosity provided by the agarose microsphere surface could have enabled neurites to extend into these surface inhomogeneities for improved adherence to the surface of the microsphere. This is probable considering the network stability and interconnectivity was enhanced on functionalized agarose microspheres in comparison to networks cultured on functionalized glass microspheres—which inherently do not provide nanopores to act as anchors for neurite extensions. In this context, it should also be noted that in cultures on glass microspheres, neurites were shown to traverse across the tops of each microsphere; this was not observed within cultures on agarose microspheres. Considering hydrogel nanopores, the neurites could have preferentially grown onto the top portions of glass microspheres since no nanopores for neurite anchorage were provided on their surface; below the mid-hemisphere height of the microsphere, neurites could have succumbed to gravity if no anchorage points were available for neurite ingrowth.

5.5.2 Microsphere Model Limitation: Immunofluorescent Staining

Through execution of cell culture methods, a limitation of microsphere model was identified at the at the microscopy stage, which stemmed from the staining procedure used to label nuclei and neurites. Since the microsphere model is gravity driven, and the weight of the microspheres is extremely small in comparison to the force required to draw the solution in the culture well up into a pipette, the risk of destroying the network the neurons created during culture was high. As such, washing steps that are commonly relatively vigorous for removal of excess stain to reduce background fluorescence, needed to be done very delicately. This resulted in residual staining solution within the microwells. This was identified as the cause for considerable background noise and fluorescent cell debris in the 3D culture images. For comparison, the 2D culture images shown

in Figure 4.6 have minimal background noise. To improve the 3D culture robustness, the sintering method used in [58] (see Section 2.2.1) can be evaluated for use, where the microsphere collection would be heated above its glass transition temperature to thermally fuse the microspheres together. Although ideal to improve robustness of the scaffolding for immunofluorescent staining steps, fusing the microspheres would result in difficulties in uniform cell seeding within the culture and complicate the PDA functionalization steps.

Granted, since the ultimate goal for the microsphere model is to be utilized as a pre-clinical tool, electrophysiological recordings on MEAs will be the preeminent readout of neuronal behaviour. As shown in previous studies, the microsphere model can be successfully coupled to MEAs [20], [24], thus mitigating the use of immunofluorescence to assess network viability. Consequently, once the model has been sufficiently optimized, staining steps would not be required.

5.5.3 Glass Microsphere Limitation: Optical Clarity

3D *Volume Viewer* (ImageJ) renderings were not possible on networks cultured on glass microspheres due to optical clarity. As a result of increased diffraction events caused by glass microspheres during fluorescent image acquisition, visualization of the β-III tubulin marker was more difficult within neuronal networks cultured on glass microsphere constructs than on agarose microsphere constructs. This limited use of 3D rendering software to visualize neuronal network growth within 3D glass microsphere models. The hypothesis that diffraction events are increased due to the glass microspheres is probable considering Frega & Tedesco *et al* did not show volumetric renderings in their initial paper that reported the use of PDL and laminin functionalized glass microspheres as 3D scaffolding for neuronal networks [24], suggesting authors encountered similar difficulties. Interestingly, in the groups following paper [20] where glass microspheres were replaced with chitosan microspheres functionalized with the same adhesive proteins, volumetric renderings were shown for networks grown on chitosan microspheres, but again, not the glass microspheres which were used as the study control. Of note, other studies that used glass microspheres and showed immunofluorescent images in 3D only showed maximum projections, without full volume views of neuronal networks. This can be deceiving since growth at the bottom of the wells on the flat functionalized substrate could be dominating fluorescence in the image. Therefore, there is a potential that using glass microspheres for 3D scaffolds could hinder the evaluation of neural processes in a 3D fashion after the culture period. As such, soft microspheres

such as chitosan or agarose provides an advantage regarding both improved mechanical properties and reduced diffraction events during imaging.

6 CONCLUSION AND FUTURE DIRECTION

This work provides proof of concept that PDA-functionalized agarose microspheres assembled in unison can serve as 3D growth area for neuronal networks *in vitro*. The adhesive, versatile and robust nature of the PDA functionalization proved exceptionally useful in this work, by adding functional motifs on agarose—a polymer widely classified as *'inert'*. With the biocompatible and adhesive properties PDA possesses, the ideal mechanical properties of agarose hydrogel were able to be capitalized on to better mimic neuronal ECM *in vitro*. Together, this biomaterial-based approach was not only shown to stimulate a positive neuronal response in 3D, but also improves the physiological relevance of the microsphere-based model for *in vitro* cultures. Additionally, the use of microfluidic technology to fabricate the agarose microspheres provided high-throughput and consistency, with considerable improvements upon existing fabrication methods. Moving forward, improvement upon the methodological approach to microsphere seeding for cell culture is required to ensure the neuronal seeding density conforms with growth area provided by microspheres. Additionally, the degree to which the PDA polymerization time can be reduced such that the Young's modulus of the microsphere is lowered, while adhesive properties of the PDA-functionalization are maintained will require further investigation. A study investigating this parameter should include various time points between 1-2 hours. Furthermore, addition of PDL and laminin to the surface of the PDA-functionalized microsphere can be evaluated to assess any potential improvements to the model. Finally, coupling the 3D construct to a MEA to evaluate electrophysiological behaviour of neuronal networks in culture would provide valuable insight into potential bioactive features of the construct.

As stated in the first page of this thesis on the topic of improving the state of neurological disease and disorders:

> *"a coordinated approach to etiologic research and treatment is required to reduce the associated burden of the disease".*

This statement was found to be undoubtably true while carrying out this thesis work. Ensuring all aspects—biological, chemical, bio-mechanical, or clinical—are accounted for within an *in vitro* model is a difficult task, yet imperative to move toward improved pre-clinical models. Evidenced by the literature reviewed and the contribution this work provides to the research space, the field

is indeed moving toward improved biomimetic models for pre-clinical studies. Continued work in this direction will minimize the gap between cell culture, and animal models and ultimately improve therapeutic options for neurological disease and disorder.

REFERENCES

[1] Y. Smith, T. Wichmann, S. A. Factor, and M. R. DeLong, "Parkinson's Disease Therapeutics: New Developments and Challenges Since the Introduction of Levodopa," *Neuropsychopharmacology*, vol. 37, no. 1, Art. no. 1, Jan. 2012, doi: 10.1038/npp.2011.212.

[2] J. Fernández-Ruiz, "The biomedical challenge of neurodegenerative disorders: an opportunity for cannabinoid-based therapies to improve on the poor current therapeutic outcomes," *Br. J. Pharmacol.*, vol. 176, no. 10, pp. 1370–1383, 2019, doi: 10.1111/bph.14382.

[3] D. G. Brown and H. J. Wobst, "Opportunities and Challenges in Phenotypic Screening for Neurodegenerative Disease Research," *J. Med. Chem.*, vol. 63, no. 5, pp. 1823–1840, Mar. 2020, doi: 10.1021/acs.jmedchem.9b00797.

[4] A. Avena-Koenigsberger, B. Misic, and O. Sporns, "Communication dynamics in complex brain networks," *Nat. Rev. Neurosci.*, vol. 19, no. 1, Art. no. 1, Jan. 2018, doi: 10.1038/nrn.2017.149.

[5] O. Sporns, "The human connectome: a complex network: The human connectome," *Ann. N. Y. Acad. Sci.*, vol. 1224, no. 1, pp. 109–125, Apr. 2011, doi: 10.1111/j.1749-6632.2010.05888.x.

[6] H. Zeng and J. R. Sanes, "Neuronal cell-type classification: challenges, opportunities and the path forward," *Nat. Rev. Neurosci.*, vol. 18, no. 9, Art. no. 9, Sep. 2017, doi: 10.1038/nrn.2017.85.

[7] C. Tator, G. Bray, and D. Morin, "The CBANCH Report - The Burden of Neurological Diseases, Disorders, and Injuries in Canada," *Can. J. Neurol. Sci.*, vol. 34, no. 3, pp. 268–269, Aug. 2007, doi: 10.1017/S0317167100006673.

[8] J. Gaskin, J. Gomes, S. Darshan, and D. Krewski, "Burden of neurological conditions in Canada," *NeuroToxicology*, vol. 61, pp. 2–10, Jul. 2017, doi: 10.1016/j.neuro.2016.05.001.

[9] S. C. Government of Canada, "Canadian Community Health Survey - Annual Component (CCHS)," Nov. 22, 2019. https://www23.statcan.gc.ca/imdb/p2SV.pl?Function=getSurvey&SDDS=3226#a1 (accessed Apr. 12, 2021).

[10] W. Dauer and S. Przedborski, "Parkinson's Disease: Mechanisms and Models," *Neuron*, vol. 39, no. 6, pp. 889–909, Sep. 2003, doi: 10.1016/S0896-6273(03)00568-3.

[11] A. B. Reiss, H. A. Arain, M. M. Stecker, N. M. Siegart, and L. J. Kasselman, "Amyloid toxicity in Alzheimer's disease," *Rev. Neurosci.*, vol. 29, no. 6, pp. 613–627, Aug. 2018, doi: 10.1515/revneuro-2017-0063.

[12] S. Saberi, J. E. Stauffer, D. J. Schulte, and J. Ravits, "Neuropathology of Amyotrophic Lateral Sclerosis and Its Variants," *Neurol. Clin.*, vol. 33, no. 4, pp. 855–876, Nov. 2015, doi: 10.1016/j.ncl.2015.07.012.

[13] C. Holmes *et al.*, "Long-term effects of Aβ42 immunisation in Alzheimer's disease: follow-up of a randomised, placebo-controlled phase I trial," *The Lancet*, vol. 372, no. 9634, pp. 216–223, Jul. 2008, doi: 10.1016/S0140-6736(08)61075-2.

[14] "Pioglitazone in early Parkinson's disease: a phase 2, multicentre, double-blind, randomised trial," *Lancet Neurol.*, vol. 14, no. 8, pp. 795–803, Aug. 2015, doi: 10.1016/S1474-4422(15)00144-1.

[15] J. Riancho, F. J. Gil-Bea, A. Santurtun, and A. L. de Munaín, "Amyotrophic lateral sclerosis: a complex syndrome that needs an integrated research approach," *Neural Regen. Res.*, vol. 14, no. 2, pp. 193–196, Feb. 2019, doi: 10.4103/1673-5374.244783.
[16] C. W. Olanow *et al.*, "Gene delivery of neurturin to putamen and substantia nigra in Parkinson disease: A double-blind, randomized, controlled trial," *Ann. Neurol.*, vol. 78, no. 2, pp. 248–257, 2015, doi: 10.1002/ana.24436.
[17] Alzheimer's Association, "2018 Alzheimer's disease facts and figures," *Alzheimers Dement.*, vol. 14, no. 3, pp. 367–429, Mar. 2018, doi: 10.1016/j.jalz.2018.02.001.
[18] M. K. Lee, M. H. Rich, J. Lee, and H. Kong, "A bio-inspired, microchanneled hydrogel with controlled spacing of cell adhesion ligands regulates 3D spatial organization of cells and tissue," *Biomaterials*, vol. 58, pp. 26–34, Jul. 2015, doi: 10.1016/j.biomaterials.2015.04.014.
[19] M. Köpf, D. F. D. Campos, A. Blaeser, K. S. Sen, and H. Fischer, "A tailored three-dimensionally printable agarose–collagen blend allows encapsulation, spreading, and attachment of human umbilical artery smooth muscle cells," *Biofabrication*, vol. 8, no. 2, p. 025011, May 2016, doi: 10.1088/1758-5090/8/2/025011.
[20] M. T. Tedesco *et al.*, "Soft chitosan microbeads scaffold for 3D functional neuronal networks," *Biomaterials*, vol. 156, pp. 159–171, Feb. 2018, doi: 10.1016/j.biomaterials.2017.11.043.
[21] L. A. Struzyna *et al.*, "Tissue engineered nigrostriatal pathway for treatment of Parkinson's disease," *J. Tissue Eng. Regen. Med.*, vol. 12, no. 7, pp. 1702–1716, 2018, doi: 10.1002/term.2698.
[22] M. Katsuno, K. Sahashi, Y. Iguchi, and A. Hashizume, "Preclinical progression of neurodegenerative diseases," *Nagoya J. Med. Sci.*, vol. 80, no. 3, pp. 289–298, Aug. 2018, doi: 10.18999/nagjms.80.3.289.
[23] K. Mullane and M. Williams, "Preclinical Models of Alzheimer's Disease: Relevance and Translational Validity," *Curr. Protoc. Pharmacol.*, vol. 84, no. 1, p. e57, 2019, doi: 10.1002/cpph.57.
[24] M. Frega, M. Tedesco, P. Massobrio, M. Pesce, and S. Martinoia, "Network dynamics of 3D engineered neuronal cultures: a new experimental model for in-vitro electrophysiology," *Sci. Rep.*, vol. 4, no. 1, Art. no. 1, Jun. 2014, doi: 10.1038/srep05489.
[25] K.-H. Park, "Neuronal Differentiation of PC12 Cells Cultured on Growth Factor-Loaded Nanoparticles Coated on PLGA Microspheres," *J. Microbiol. Biotechnol.*, vol. 19, 2009, doi: 10.4014/jmb.0903.300.
[26] K. Yang *et al.*, "Polydopamine-mediated surface modification of scaffold materials for human neural stem cell engineering," *Biomaterials*, vol. 33, no. 29, pp. 6952–6964, Oct. 2012, doi: 10.1016/j.biomaterials.2012.06.067.
[27] S. Li *et al.*, "Improved neuron culture using scaffolds made of three-dimensional PDMS micro-lattices," *Biomed. Mater.*, vol. 13, no. 3, p. 034105, 2018, doi: 10.1088/1748-605X/aaa777.
[28] B. M. Baker and C. S. Chen, "Deconstructing the third dimension – how 3D culture microenvironments alter cellular cues," *J. Cell Sci.*, vol. 125, no. 13, pp. 3015–3024, Jul. 2012, doi: 10.1242/jcs.079509.
[29] Z.-H. Wang *et al.*, "Novel 3D Neuron Regeneration Scaffolds Based on Synthetic Polypeptide Containing Neuron Cue," *Macromol. Biosci.*, vol. 18, no. 3, p. 1700251, 2018, doi: 10.1002/mabi.201700251.

[30] M. D. Tang-Schomer *et al.*, "Bioengineered functional brain-like cortical tissue," *Proc. Natl. Acad. Sci. U. S. A.*, vol. 111, no. 38, pp. 13811–13816, Sep. 2014, doi: 10.1073/pnas.1324214111.
[31] M. J. Landry, F.-G. Rollet, T. E. Kennedy, and C. J. Barrett, "Layers and Multilayers of Self-Assembled Polymers: Tunable Engineered Extracellular Matrix Coatings for Neural Cell Growth," *Langmuir*, vol. 34, no. 30, pp. 8709–8730, Jul. 2018, doi: 10.1021/acs.langmuir.7b04108.
[32] D. Lam *et al.*, "Tissue-specific extracellular matrix accelerates the formation of neural networks and communities in a neuron-glia co-culture on a multi-electrode array," *Sci. Rep.*, vol. 9, no. 1, Art. no. 1, Mar. 2019, doi: 10.1038/s41598-019-40128-1.
[33] F. Azizi *et al.*, "The combined effects of three-dimensional cell culture and natural tissue extract on neural differentiation of P19 embryonal carcinoma stem cells," *J. Tissue Eng. Regen. Med.*, vol. 12, no. 9, pp. 1909–1924, 2018, doi: 10.1002/term.2712.
[34] R. Rauti, N. Renous, and B. M. Maoz, "Mimicking the Brain Extracellular Matrix in Vitro: A Review of Current Methodologies and Challenges," *Isr. J. Chem.*, vol. n/a, no. n/a, 2019, doi: 10.1002/ijch.201900052.
[35] L. W. Lau, R. Cua, M. B. Keough, S. Haylock-Jacobs, and V. W. Yong, "Pathophysiology of the brain extracellular matrix: a new target for remyelination," *Nat. Rev. Neurosci.*, vol. 14, no. 10, Art. no. 10, Oct. 2013, doi: 10.1038/nrn3550.
[36] L. Papadimitriou, P. Manganas, A. Ranella, and E. Stratakis, "Biofabrication for neural tissue engineering applications," *Mater. Today Bio*, vol. 6, p. 100043, Mar. 2020, doi: 10.1016/j.mtbio.2020.100043.
[37] J. Ma *et al.*, "Extracellular Matrix Proteins Involved in Alzheimer's Disease," *Chem. – Eur. J.*, vol. n/a, no. n/a, Mar. 2020, doi: 10.1002/chem.202000782.
[38] N. George and H. M. Geller, "Extracellular Matrix and Traumatic Brain Injury," *J. Neurosci. Res.*, vol. 96, no. 4, pp. 573–588, Apr. 2018, doi: 10.1002/jnr.24151.
[39] P. A. McRae and B. E. Porter, "The perineuronal net component of the extracellular matrix in plasticity and epilepsy," *Neurochem. Int.*, vol. 61, no. 7, pp. 963–972, Dec. 2012, doi: 10.1016/j.neuint.2012.08.007.
[40] K. Franze, "The mechanical control of nervous system development," *Development*, vol. 140, no. 15, pp. 3069–3077, Aug. 2013, doi: 10.1242/dev.079145.
[41] W. J. Tyler, "The mechanobiology of brain function," *Nat. Rev. Neurosci.*, vol. 13, no. 12, Art. no. 12, Dec. 2012, doi: 10.1038/nrn3383.
[42] C. E. Chan and D. J. Odde, "Traction Dynamics of Filopodia on Compliant Substrates," *Science*, vol. 322, no. 5908, pp. 1687–1691, Dec. 2008, doi: 10.1126/science.1163595.
[43] J. M. Barnes, L. Przybyla, and V. M. Weaver, "Tissue mechanics regulate brain development, homeostasis and disease," *J. Cell Sci.*, vol. 130, no. 1, pp. 71–82, Jan. 2017, doi: 10.1242/jcs.191742.
[44] S. Budday *et al.*, "Mechanical properties of gray and white matter brain tissue by indentation," *J. Mech. Behav. Biomed. Mater.*, vol. 46, pp. 318–330, Jun. 2015, doi: 10.1016/j.jmbbm.2015.02.024.
[45] A. Tanaka, Y. Fujii, N. Kasai, T. Okajima, and H. Nakashima, "Regulation of neuritogenesis in hippocampal neurons using stiffness of extracellular microenvironment," *PLoS ONE*, vol. 13, no. 2, Feb. 2018, doi: 10.1371/journal.pone.0191928.
[46] L. M. Y. Yu, N. D. Leipzig, and M. S. Shoichet, "Promoting neuron adhesion and growth," *Mater. Today*, vol. 11, no. 5, pp. 36–43, May 2008, doi: 10.1016/S1369-7021(08)70088-9.

[47] K. R. Ko and J. P. Frampton, “Developments in 3D neural cell culture models: the future of neurotherapeutics testing?,” *Expert Rev. Neurother.*, vol. 16, no. 7, pp. 739–741, Jul. 2016, doi: 10.1586/14737175.2016.1166053.
[48] Y. S. Zhang, C. Zhu, and Y. Xia, “Inverse Opal Scaffolds and Their Biomedical Applications,” *Adv. Mater.*, vol. 29, no. 33, p. 1701115, 2017, doi: 10.1002/adma.201701115.
[49] P. K. Gupta and C. T. Hung, “Albumin Microspheres II: Applications in Drug Delivery,” *J. Microencapsul.*, vol. 6, no. 4, pp. 463–472, Jan. 1989, doi: 10.3109/02652048909031166.
[50] Y. Jun, H. Oh, R. Karpoormath, A. Jha, and R. Patel, “Role of microsphere as drug carrier for osteogenic differentiation,” *Int. J. Polym. Mater. Polym. Biomater.*, vol. 0, no. 0, pp. 1–10, Jan. 2020, doi: 10.1080/00914037.2020.1713783.
[51] S. Freiberg and X. X. Zhu, “Polymer microspheres for controlled drug release,” *Int. J. Pharm.*, vol. 282, no. 1, pp. 1–18, Sep. 2004, doi: 10.1016/j.ijpharm.2004.04.013.
[52] A. Batorsky, J. Liao, A. W. Lund, G. E. Plopper, and J. P. Stegemann, “Encapsulation of adult human mesenchymal stem cells within collagen-agarose microenvironments,” *Biotechnol. Bioeng.*, vol. 92, no. 4, pp. 492–500, 2005, doi: 10.1002/bit.20614.
[53] X. Sun, J. Wang, Y. Wang, and Q. Zhang, “Collagen-based porous scaffolds containing PLGA microspheres for controlled kartogenin release in cartilage tissue engineering,” *Artif. Cells Nanomedicine Biotechnol.*, vol. 46, no. 8, pp. 1957–1966, Nov. 2018, doi: 10.1080/21691401.2017.1397000.
[54] T. Ren, X. Yang, N. Wu, Y. Cai, Z. Liu, and W. Yuan, “Sustained-release formulation of levodopa methyl ester/benserazide for prolonged suppressing dyskinesia expression in 6-OHDA-leisoned rats,” *Neurosci. Lett.*, vol. 502, no. 2, pp. 117–122, Sep. 2011, doi: 10.1016/j.neulet.2011.07.042.
[55] N. B. Skop, F. Calderon, C. H. Cho, C. D. Gandhi, and S. W. Levison, “Optimizing a multifunctional microsphere scaffold to improve neural precursor cell transplantation for traumatic brain injury repair,” *J. Tissue Eng. Regen. Med.*, vol. 10, no. 10, pp. E419–E432, 2013, doi: 10.1002/term.1832.
[56] S. Pautot, C. Wyart, and E. Y. Isacoff, “Colloid-guided assembly of oriented 3D neuronal networks,” *Nat. Methods*, vol. 5, no. 8, Art. no. 8, Aug. 2008, doi: 10.1038/nmeth.1236.
[57] Z. Huang, Y. Sun, W. Liu, W. Zhang, W. Zheng, and X. Jiang, “Assembly of Functional Three-Dimensional Neuronal Networks on a Microchip,” *Small*, vol. 10, no. 13, pp. 2530–2536, 2014, doi: 10.1002/smll.201400513.
[58] C. Laurencin, F. Ko, M. Attawia, and M. Borden, “Studies on the development of a tissue engineered matrix for bone regeneration,” vol. 8, Jan. 1998.
[59] M. Borden, M. Attawia, Y. Khan, and C. T. Laurencin, “Tissue engineered microsphere-based matrices for bone repair:: design and evaluation,” *Biomaterials*, vol. 23, no. 2, pp. 551–559, Jan. 2002, doi: 10.1016/S0142-9612(01)00137-5.
[60] M. Borden, S. F. El-Amin, M. Attawia, and C. T. Laurencin, “Structural and human cellular assessment of a novel microsphere-based tissue engineered scaffold for bone repair,” *Biomaterials*, vol. 24, no. 4, pp. 597–609, Feb. 2003, doi: 10.1016/S0142-9612(02)00374-5.
[61] P. B. Malafaya, A. J. Pedro, A. Peterbauer, C. Gabriel, H. Redl, and R. L. Reis, “Chitosan particles agglomerated scaffolds for cartilage and osteochondral tissue engineering approaches with adipose tissue derived stem cells,” *J. Mater. Sci. Mater. Med.*, vol. 16, no. 12, pp. 1077–1085, Dec. 2005, doi: 10.1007/s10856-005-4709-4.
[62] M. Singh, C. P. Morris, R. J. Ellis, M. S. Detamore, and C. Berkland, “Microsphere-Based Seamless Scaffolds Containing Macroscopic Gradients of Encapsulated Factors for Tissue

Engineering," *Tissue Eng. Part C Methods*, vol. 14, no. 4, pp. 299–309, Sep. 2008, doi: 10.1089/ten.tec.2008.0167.
[63] A. W. Lund, J. A. Bush, G. E. Plopper, and J. P. Stegemann, "Osteogenic differentiation of mesenchymal stem cells in defined protein beads," *J. Biomed. Mater. Res. B Appl. Biomater.*, vol. 87B, no. 1, pp. 213–221, 2008, doi: 10.1002/jbm.b.31098.
[64] I. Gerçek, R. S. Tığlı, and M. Gümüşderelioğlu, "A novel scaffold based on formation and agglomeration of PCL microbeads by freeze-drying," *J. Biomed. Mater. Res. A*, vol. 86A, no. 4, pp. 1012–1022, 2008, doi: 10.1002/jbm.a.31723.
[65] C. Nelson, Y. Khan, and C. T. Laurencin, "Nanofiber–microsphere (nano-micro) matrices for bone regenerative engineering: a convergence approach toward matrix design," *Regen. Biomater.*, vol. 1, no. 1, pp. 3–9, Nov. 2014, doi: 10.1093/rb/rbu002.
[66] J. S. Park, K. Park, D. G. Woo, H. N. Yang, H.-M. Chung, and K.-H. Park, "PLGA Microsphere Construct Coated with TGF-β 3 Loaded Nanoparticles for Neocartilage Formation," *Biomacromolecules*, vol. 9, no. 8, pp. 2162–2169, Aug. 2008, doi: 10.1021/bm800251x.
[67] S.-S. Kim, S.-J. Gwak, C. Y. Choi, and B.-S. Kim, "Skin regeneration using keratinocytes and dermal fibroblasts cultured on biodegradable microspherical polymer scaffolds," *J. Biomed. Mater. Res. B Appl. Biomater.*, vol. 75B, no. 2, pp. 369–377, 2005, doi: 10.1002/jbm.b.30302.
[68] A. W. Smith, C. E. Segar, P. K. Nguyen, M. R. MacEwan, I. R. Efimov, and D. L. Elbert, "Long-term culture of HL-1 cardiomyocytes in modular poly(ethylene glycol) microsphere-based scaffolds crosslinked in the phase-separated state," *Acta Biomater.*, vol. 8, no. 1, pp. 31–40, Jan. 2012, doi: 10.1016/j.actbio.2011.08.021.
[69] R. Roux, C. Ladavière, A. Montembault, and T. Delair, "Particle assemblies: Toward new tools for regenerative medicine," *Mater. Sci. Eng. C*, vol. 33, no. 3, pp. 997–1007, Apr. 2013, doi: 10.1016/j.msec.2012.12.002.
[70] V. Gupta, Y. Khan, C. J. Berkland, C. T. Laurencin, and M. S. Detamore, "Microsphere-Based Scaffolds in Regenerative Engineering," *Annu. Rev. Biomed. Eng.*, vol. 19, no. 1, pp. 135–161, Jun. 2017, doi: 10.1146/annurev-bioeng-071516-044712.
[71] W. Li *et al.*, "Microfluidic fabrication of microparticles for biomedical applications," *Chem. Soc. Rev.*, vol. 47, no. 15, pp. 5646–5683, Jul. 2018, doi: 10.1039/C7CS00263G.
[72] K. Saralidze, L. H. Koole, and M. L. W. Knetsch, "Polymeric Microspheres for Medical Applications," *Materials*, vol. 3, no. 6, Art. no. 6, Jun. 2010, doi: 10.3390/ma3063537.
[73] E. Jacques *et al.*, "Collagen-Based Microcapsules As Therapeutic Materials for Stem Cell Therapies in Infarcted Myocardium," *ACS Biomater. Sci. Eng.*, vol. 6, no. 8, pp. 4614–4622, Aug. 2020, doi: 10.1021/acsbiomaterials.0c00245.
[74] N. B. Skop, F. Calderon, S. W. Levison, C. D. Gandhi, and C. H. Cho, "Heparin crosslinked chitosan microspheres for the delivery of neural stem cells and growth factors for central nervous system repair," *Acta Biomater.*, vol. 9, no. 6, pp. 6834–6843, Jun. 2013, doi: 10.1016/j.actbio.2013.02.043.
[75] P. Garstecki, I. Gitlin, W. DiLuzio, G. M. Whitesides, E. Kumacheva, and H. A. Stone, "Formation of monodisperse bubbles in a microfluidic flow-focusing device," *Appl. Phys. Lett.*, vol. 85, no. 13, pp. 2649–2651, Sep. 2004, doi: 10.1063/1.1796526.
[76] T. Fu, Y. Wu, Y. Ma, and H. Z. Li, "Droplet formation and breakup dynamics in microfluidic flow-focusing devices: From dripping to jetting," *Chem. Eng. Sci.*, vol. 84, pp. 207–217, Dec. 2012, doi: 10.1016/j.ces.2012.08.039.

[77] P. Kanda *et al.*, "Deterministic paracrine repair of injured myocardium using microfluidic-based cocooning of heart explant-derived cells," *Biomaterials*, vol. 247, p. 120010, Jul. 2020, doi: 10.1016/j.biomaterials.2020.120010.
[78] C. Godugu, A. R. Patel, U. Desai, T. Andey, A. Sams, and M. Singh, "AlgiMatrix^{TM} Based 3D Cell Culture System as an In-Vitro Tumor Model for Anticancer Studies," *PLOS ONE*, vol. 8, no. 1, p. e53708, Jan. 2013, doi: 10.1371/journal.pone.0053708.
[79] S. Nath and G. R. Devi, "Three-Dimensional Culture Systems in Cancer Research: Focus on Tumor Spheroid Model," *Pharmacol. Ther.*, vol. 163, pp. 94–108, Jul. 2016, doi: 10.1016/j.pharmthera.2016.03.013.
[80] M. M. Baksh, C. Dean, S. Pautot, S. DeMaria, E. Isacoff, and J. T. Groves, "Neuronal Activation by GPI-Linked Neuroligin-1 Displayed in Synthetic Lipid Bilayer Membranes," *Langmuir*, vol. 21, no. 23, pp. 10693–10698, Nov. 2005, doi: 10.1021/la051243d.
[81] M. Tedesco, M. Frega, S. Martinoia, M. Pesce, and P. Massobrio, "Interfacing 3D Engineered Neuronal Cultures to Micro-Electrode Arrays: An Innovative In Vitro Experimental Model," *JoVE J. Vis. Exp.*, no. 104, p. e53080, Oct. 2015, doi: 10.3791/53080.
[82] N. Reddy, R. Reddy, and Q. Jiang, "Crosslinking biopolymers for biomedical applications," *Trends Biotechnol.*, vol. 33, no. 6, pp. 362–369, Jun. 2015, doi: 10.1016/j.tibtech.2015.03.008.
[83] J. E. Gough, C. A. Scotchford, and S. Downes, "Cytotoxicity of glutaraldehyde crosslinked collagen/poly(vinyl alcohol) films is by the mechanism of apoptosis," *J. Biomed. Mater. Res.*, vol. 61, no. 1, pp. 121–130, 2002, doi: 10.1002/jbm.10145.
[84] J.-Y. Xiong, J. Narayanan, X.-Y. Liu, T. K. Chong, S. B. Chen, and T.-S. Chung, "Topology Evolution and Gelation Mechanism of Agarose Gel," *J. Phys. Chem. B*, vol. 109, no. 12, pp. 5638–5643, Mar. 2005, doi: 10.1021/jp044473u.
[85] R. Weinberger, "CHAPTER 6 - Size Separations in Capillary Gels and Polymer Networks," in *Practical Capillary Electrophoresis (Second Edition)*, R. Weinberger, Ed. San Diego: Academic Press, 2000, pp. 245–292.
[86] P. L. Indovina, E. Tettamanti, M. S. Micciancio-Giammarinaro, and M. U. Palma, "Thermal hysteresis and reversibility of gel–sol transition in agarose–water systemsa)," *J. Chem. Phys.*, vol. 70, no. 6, pp. 2841–2847, Mar. 1979, doi: 10.1063/1.437817.
[87] A. Ed-Daoui, M. Benelmostafa, and M. Dahmani, "Study of the viscoelastic properties of the agarose gel," *Mater. Today Proc.*, vol. 13, pp. 746–751, Jan. 2019, doi: 10.1016/j.matpr.2019.04.036.
[88] C. Markert *et al.*, "Characterizing the micro-scale elastic modulus of hydrogels for use in regenerative medicine," *J. Mech. Behav. Biomed. Mater.*, vol. 27, Jul. 2013, doi: 10.1016/j.jmbbm.2013.07.008.
[89] K. D. Costa, M. M. Y. Ho, and C. T. Hung, "Multi-Scale Measurement Of Mechanical Properties Of Soft Samples With Atomic Force Microscopy," p. 2, 2003.
[90] S. Park, K. D. Costa, G. A. Ateshian, and K.-S. Hong, "Mechanical properties of bovine articular cartilage under microscale indentation loading from atomic force microscopy," *Proc. Inst. Mech. Eng. [H]*, vol. 223, no. 3, pp. 339–347, Mar. 2009, doi: 10.1243/09544119JEIM516.
[91] M. Stolz, R. Raiteri, A. U. Daniels, M. R. VanLandingham, W. Baschong, and U. Aebi, "Dynamic Elastic Modulus of Porcine Articular Cartilage Determined at Two Different Levels of Tissue Organization by Indentation-Type Atomic Force Microscopy," *Biophys. J.*, vol. 86, no. 5, pp. 3269–3283, May 2004.

[92] S. Park, C.-T. Duong, J.-H. Lee, S.-S. Lee, and K. Son, "Effect of tip geometry of atomic force microscope on mechanical responses of bovine articular cartilage and agarose gel," *Int. J. Precis. Eng. Manuf.*, vol. 11, no. 1, pp. 129–136, Feb. 2010, doi: 10.1007/s12541-010-0016-1.

[93] M. Iwashita, T. Nomura, T. Suetsugu, F. Matsuzaki, S. Kojima, and Y. Kosodo, "Comparative Analysis of Brain Stiffness Among Amniotes Using Glyoxal Fixation and Atomic Force Microscopy," *Front. Cell Dev. Biol.*, vol. 8, 2020, doi: 10.3389/fcell.2020.574619.

[94] P. Zarrintaj *et al.*, "Agarose-based biomaterials for tissue engineering," *Carbohydr. Polym.*, vol. 187, pp. 66–84, May 2018, doi: 10.1016/j.carbpol.2018.01.060.

[95] S. J. Yoo, J. Kim, C.-S. Lee, and Y. Nam, "Simple and Novel Three Dimensional Neuronal Cell Culture Using a Micro Mesh Scaffold," *Exp. Neurobiol.*, vol. 20, no. 2, pp. 110–115, Jun. 2011, doi: 10.5607/en.2011.20.2.110.

[96] Z. Cao, R. J. Gilbert, and W. He, "Simple Agarose−Chitosan Gel Composite System for Enhanced Neuronal Growth in Three Dimensions," *Biomacromolecules*, vol. 10, no. 10, pp. 2954–2959, Oct. 2009, doi: 10.1021/bm900670n.

[97] Q. Gu *et al.*, "Functional 3D Neural Mini-Tissues from Printed Gel-Based Bioink and Human Neural Stem Cells," *Adv. Healthc. Mater.*, vol. 5, no. 12, pp. 1429–1438, 2016, doi: 10.1002/adhm.201600095.

[98] B. C. Martin, E. J. Minner, S. L. Wiseman, R. L. Klank, and R. J. Gilbert, "Agarose and methylcellulose hydrogel blends for nerve regeneration applications," *J. Neural Eng.*, vol. 5, no. 2, pp. 221–231, Jun. 2008, doi: 10.1088/1741-2560/5/2/013.

[99] P. Zarrintaj, B. Bakhshandeh, I. Rezaeian, B. Heshmatian, and M. R. Ganjali, "A Novel Electroactive Agarose-Aniline Pentamer Platform as a Potential Candidate for Neural Tissue Engineering," *Sci. Rep.*, vol. 7, no. 1, pp. 1–12, Dec. 2017, doi: 10.1038/s41598-017-17486-9.

[100] A. Kunze, M. Giugliano, A. Valero, and P. Renaud, "Micropatterning neural cell cultures in 3D with a multi-layered scaffold," *Biomaterials*, vol. 32, no. 8, pp. 2088–2098, Mar. 2011, doi: 10.1016/j.biomaterials.2010.11.047.

[101] Z. Lu, M. Piechowicz, and S. Qiu, "A Simplified Method for Ultra-Low Density, Long-Term Primary Hippocampal Neuron Culture," *J. Vis. Exp. JoVE*, no. 109, Mar. 2016, doi: 10.3791/53797.

[102] Y. H. Kim, N. S. Baek, Y. H. Han, M.-A. Chung, and S.-D. Jung, "Enhancement of neuronal cell adhesion by covalent binding of poly-d-lysine," *J. Neurosci. Methods*, vol. 202, no. 1, pp. 38–44, Oct. 2011, doi: 10.1016/j.jneumeth.2011.08.036.

[103] N. Li and A. Folch, "Integration of topographical and biochemical cues by axons during growth on microfabricated 3-D substrates," *Exp. Cell Res.*, vol. 311, no. 2, pp. 307–316, Dec. 2005, doi: 10.1016/j.yexcr.2005.10.007.

[104] S. Varon, "The culture of chick embryo dorsal root ganglionic cells on polylysine-coated plastic," *Neurochem. Res.*, vol. 4, no. 2, pp. 155–173, Apr. 1979, doi: 10.1007/BF00964141.

[105] T. Sasaki, R. Fässler, and E. Hohenester, "Laminin," *J. Cell Biol.*, vol. 164, no. 7, pp. 959–963, Mar. 2004, doi: 10.1083/jcb.200401058.

[106] J. H. Ryu, P. B. Messersmith, and H. Lee, "Polydopamine Surface Chemistry: A Decade of Discovery," *ACS Appl. Mater. Interfaces*, vol. 10, no. 9, pp. 7523–7540, Mar. 2018, doi: 10.1021/acsami.7b19865.

[107] H. Lee, S. M. Dellatore, W. M. Miller, and P. B. Messersmith, “Mussel-Inspired Surface Chemistry for Multifunctional Coatings,” *Science*, vol. 318, no. 5849, pp. 426–430, Oct. 2007, doi: 10.1126/science.1147241.
[108] Y. Liu, K. Ai, and L. Lu, “Polydopamine and Its Derivative Materials: Synthesis and Promising Applications in Energy, Environmental, and Biomedical Fields,” *Chem. Rev.*, vol. 114, no. 9, pp. 5057–5115, May 2014, doi: 10.1021/cr400407a.
[109] Q. Lyu, N. Hsueh, and C. L. L. Chai, “Unravelling the polydopamine mystery: is the end in sight?,” *Polym. Chem.*, vol. 10, no. 42, pp. 5771–5777, Oct. 2019, doi: 10.1039/C9PY01372E.
[110] A. J. Steeves, A. Atwal, S. C. Schock, and F. Variola, “Evaluation of the direct effects of poly(dopamine) on the in vitro response of human osteoblastic cells,” *J. Mater. Chem. B*, vol. 4, no. 18, pp. 3145–3156, May 2016, doi: 10.1039/C5TB02510A.
[111] K. Kang, I. S. Choi, and Y. Nam, “A biofunctionalization scheme for neural interfaces using polydopamine polymer,” *Biomaterials*, vol. 32, no. 27, pp. 6374–6380, Sep. 2011, doi: 10.1016/j.biomaterials.2011.05.028.
[112] X. Wang *et al.*, “A high-sensitivity immunosensor for detection of tumor marker based on functionalized mesoporous silica nanoparticles,” *Electrochimica Acta*, vol. 112, pp. 473–479, Dec. 2013, doi: 10.1016/j.electacta.2013.08.099.
[113] D. Hauser, D. Septiadi, J. Turner, A. Petri-Fink, and B. Rothen-Rutishauser, “From Bioinspired Glue to Medicine: Polydopamine as a Biomedical Material,” *Materials*, vol. 13, no. 7, Art. no. 7, Jan. 2020, doi: 10.3390/ma13071730.
[114] P. Liesi, D. Dahl, and A. Vaheri, “Neurons cultured from developing rat brain attach and spread preferentially to laminin,” *J. Neurosci. Res.*, vol. 11, no. 3, pp. 241–251, 1984, doi: 10.1002/jnr.490110304.
[115] A. J. Steeves and F. Variola, “Elucidating structure–function relationships governing the interfacial response of human mesenchymal stem cells to polydopamine coatings,” *J. Mater. Chem. B*, vol. 8, no. 2, pp. 199–215, Jan. 2020, doi: 10.1039/C9TB02188D.
[116] C.-H. Chen, C.-C. Tsai, P.-T. Wu, I.-K. Wang, J. Yu, and W.-B. Tsai, “Modulation of Neural Differentiation through Submicron-Grooved Topography Surface with Modified Polydopamine,” *ACS Appl. Bio Mater.*, vol. 2, no. 1, pp. 205–216, Jan. 2019, doi: 10.1021/acsabm.8b00556.
[117] S. H. Bhang *et al.*, “Enhanced neuronal differentiation of pheochromocytoma 12 cells on polydopamine-modified surface,” *Biochem. Biophys. Res. Commun.*, vol. 430, no. 4, pp. 1294–1300, Jan. 2013, doi: 10.1016/j.bbrc.2012.11.123.
[118] S. E. Park, A. Georgescu, J. M. Oh, K. W. Kwon, and D. Huh, “Polydopamine-Based Interfacial Engineering of Extracellular Matrix Hydrogels for the Construction and Long-Term Maintenance of Living Three-Dimensional Tissues,” *ACS Appl. Mater. Interfaces*, vol. 11, no. 27, pp. 23919–23925, Jul. 2019, doi: 10.1021/acsami.9b07912.
[119] K. Kang, S. Lee, R. Kim, I. S. Choi, and Y. Nam, “Electrochemically Driven, Electrode-Addressable Formation of Functionalized Polydopamine Films for Neural Interfaces,” *Angew. Chem.*, vol. 124, no. 52, pp. 13278–13281, 2012, doi: 10.1002/ange.201207129.
[120] R. Kim and Y. Nam, “Polydopamine-doped conductive polymer microelectrodes for neural recording and stimulation,” *J. Neurosci. Methods*, vol. 326, p. 108369, Oct. 2019, doi: 10.1016/j.jneumeth.2019.108369.
[121] L. Tian, M. P. Prabhakaran, J. Hu, M. Chen, F. Besenbacher, and S. Ramakrishna, “Synergistic effect of topography, surface chemistry and conductivity of the electrospun

nanofibrous scaffold on cellular response of PC12 cells," *Colloids Surf. B Biointerfaces*, vol. 145, pp. 420–429, Sep. 2016, doi: 10.1016/j.colsurfb.2016.05.032.
[122] H. Zhang *et al.*, "Design and Applications of Cell-Selective Surfaces and Interfaces," *Biomacromolecules*, vol. 19, no. 6, pp. 1746–1763, 11 2018, doi: 10.1021/acs.biomac.8b00264.
[123] A. Stylianou, S.-V. Kontomaris, C. Grant, and E. Alexandratou, "Atomic Force Microscopy on Biological Materials Related to Pathological Conditions," *Scanning*, vol. 2019, May 2019, doi: 10.1155/2019/8452851.
[124] C. A. Grant, D. J. Brockwell, S. E. Radford, and N. H. Thomson, "Effects of hydration on the mechanical response of individual collagen fibrils," *Appl. Phys. Lett.*, vol. 92, no. 23, p. 233902, Jun. 2008, doi: 10.1063/1.2937001.
[125] N. Monette-Catafard, "HIGH-THROUGHPUT CELL ENCAPSULATION IN MONODISPERSE AGAROSE MICROCAPSULES USING A MICROFLUIDIC DEVICE," p. 86.
[126] N. Soucy, "Hollow Hydrogel Cocoons for the Encapsulation of Therapeutic Cells Using a Microfluidic Platform," University of Ottawa, Ottawa, Ontario Canada, 2020.
[127] M. Martín, P. Salazar, S. Campuzano, R. Villalonga, J. M. Pingarrón, and J. L. González-Mora, "Amperometric magnetobiosensors using poly(dopamine)-modified Fe3O4 magnetic nanoparticles for the detection of phenolic compounds," *Anal. Methods*, vol. 7, no. 20, pp. 8801–8808, Oct. 2015, doi: 10.1039/C5AY01996F.
[128] J. E. Sader *et al.*, "A virtual instrument to standardise the calibration of atomic force microscope cantilevers," *Rev. Sci. Instrum.*, vol. 87, no. 9, p. 093711, Sep. 2016, doi: 10.1063/1.4962866.
[129] P. J. Eaton and P. West, *Atomic force microscopy*. Oxford ; New York: Oxford University Press, 2010.
[130] F. Rico, P. Roca-Cusachs, N. Gavara, R. Farré, M. Rotger, and D. Navajas, "Probing mechanical properties of living cells by atomic force microscopy with blunted pyramidal cantilever tips," *Phys. Rev. E*, vol. 72, no. 2, p. 021914, Aug. 2005, doi: 10.1103/PhysRevE.72.021914.
[131] L. Jiang *et al.*, "Surface characteristics of mussel-inspired polydopamine coating on titanium substrates," *J. Wuhan Univ. Technol.-Mater Sci Ed*, vol. 29, no. 1, pp. 197–200, Feb. 2014, doi: 10.1007/s11595-014-0892-9.
[132] J. J. Roberts and P. J. Martens, "9 - Engineering biosynthetic cell encapsulation systems," in *Biosynthetic Polymers for Medical Applications*, L. Poole-Warren, P. Martens, and R. Green, Eds. Woodhead Publishing, 2016, pp. 205–239.
[133] N. Monette-Catafard, "HIGH-THROUGHPUT CELL ENCAPSULATION IN MONODISPERSE AGAROSE MICROCAPSULES USING A MICROFLUIDIC DEVICE," University of Ottawa, Ottawa, Ontario Canada, 2014.
[134] W. Chen and Y. W. Tong, "PHBV microspheres as neural tissue engineering scaffold support neuronal cell growth and axon–dendrite polarization," *Acta Biomater.*, vol. 8, no. 2, pp. 540–548, Feb. 2012, doi: 10.1016/j.actbio.2011.09.026.
[135] L. Su, Y. Yu, Y. Zhao, F. Liang, and X. Zhang, "Strong Antibacterial Polydopamine Coatings Prepared by a Shaking-assisted Method," *Sci. Rep.*, vol. 6, no. 1, Art. no. 1, Apr. 2016, doi: 10.1038/srep24420.
[136] Z. Deng, B. Shang, and B. Peng, "Polydopamine Based Colloidal Materials: Synthesis and Applications," *Chem. Rec.*, vol. 18, no. 4, pp. 410–432, 2018, doi: 10.1002/tcr.201700051.

[137] C. Chen *et al.*, "Precise control of agarose media pore structure by regulating cooling rate," *J. Sep. Sci.*, vol. 40, no. 22, pp. 4467–4474, Nov. 2017, doi: 10.1002/jssc.201700546.
[138] D. Sharma *et al.*, "Polydopamine and collagen coated micro-grated polydimethylsiloxane for human mesenchymal stem cell culture," *Bioact. Mater.*, vol. 4, pp. 142–150, Dec. 2019, doi: 10.1016/j.bioactmat.2019.02.002.
[139] Y. H. Ding, M. Floren, and W. Tan, "Mussel-inspired polydopamine for bio-surface functionalization," *Biosurface Biotribology*, vol. 2, no. 4, pp. 121–136, Dec. 2016, doi: 10.1016/j.bsbt.2016.11.001.
[140] J. Narayanan, J.-Y. Xiong, and X.-Y. Liu, "Determination of agarose gel pore size: Absorbance measurements vis a vis other techniques," *J. Phys. Conf. Ser.*, vol. 28, pp. 83–86, Jan. 2006, doi: 10.1088/1742-6596/28/1/017.
[141] A. Aryaei, A. H. Jayatissa, and A. C. Jayasuriya, "Nano and micro mechanical properties of uncross-linked and cross-linked chitosan films," *J. Mech. Behav. Biomed. Mater.*, vol. 5, no. 1, pp. 82–89, Jan. 2012, doi: 10.1016/j.jmbbm.2011.08.006.
[142] J. Duan, X. Liang, Y. Cao, S. Wang, and L. Zhang, "High Strength Chitosan Hydrogels with Biocompatibility via New Avenue Based on Constructing Nanofibrous Architecture," *Macromolecules*, vol. 48, no. 8, pp. 2706–2714, Apr. 2015, doi: 10.1021/acs.macromol.5b00117.
[143] K. D. Yao, W. G. Liu, Z. Lin, and X. H. Qiu, "In situ atomic force microscopy measurement of the dynamic variation in the elastic modulus of swollen chitosan/gelatin hybrid polymer network gels in media of different pH," *Polym. Int.*, vol. 48, no. 9, pp. 794–798, 1999, doi: https://doi.org/10.1002/(SICI)1097-0126(199909)48:9<794::AID-PI220>3.0.CO;2-8.
[144] Q. He, Q. Ao, Y. Gong, and X. Zhang, "Preparation of chitosan films using different neutralizing solutions to improve endothelial cell compatibility," *J. Mater. Sci. Mater. Med.*, vol. 22, no. 12, pp. 2791–2802, Dec. 2011, doi: 10.1007/s10856-011-4444-y.
[145] S. M. Cook, K. M. Lang, K. M. Chynoweth, M. Wigton, R. W. Simmonds, and T. E. Schäffer, "Practical implementation of dynamic methods for measuring atomic force microscope cantilever spring constants," *Nanotechnology*, vol. 17, no. 9, pp. 2135–2145, May 2006, doi: 10.1088/0957-4484/17/9/010.
[146] S. Shin *et al.*, "Alginate–marine collagen–agarose composite hydrogels as matrices for biomimetic 3D cell spheroid formation," *RSC Adv.*, vol. 6, no. 52, pp. 46952–46965, May 2016, doi: 10.1039/C6RA01937D.
[147] X. Yi, G. Jin, M. Tian, W. Mao, and J. Qin, "Porous chitosan scaffold and NGF promote neuronal differentiation of neural stem cells in vitro," p. 6, 2011.
[148] S. Guan, X.-L. Zhang, X.-M. Lin, T.-Q. Liu, X.-H. Ma, and Z.-F. Cui, "Chitosan/gelatin porous scaffolds containing hyaluronic acid and heparan sulfate for neural tissue engineering," *J. Biomater. Sci. Polym. Ed.*, vol. 24, no. 8, pp. 999–1014, Jun. 2013, doi: 10.1080/09205063.2012.731374.
[149] D. K. Cullen *et al.*, "Microtissue Engineered Constructs with Living Axons for Targeted Nervous System Reconstruction," *Tissue Eng. Part A*, vol. 18, no. 21–22, pp. 2280–2289, Jun. 2012, doi: 10.1089/ten.tea.2011.0534.
[150] R. W. N. Nugroho *et al.*, "Quantifying the interactions between biomimetic biomaterials – collagen I, collagen IV, laminin 521 and cellulose nanofibrils – by colloidal probe microscopy," *Colloids Surf. B Biointerfaces*, vol. 173, pp. 571–580, Jan. 2019, doi: 10.1016/j.colsurfb.2018.09.073.

[151] X. Song *et al.*, "A Novel Human-Like Collagen Hydrogel Scaffold with Porous Structure and Sponge-Like Properties," *Polymers*, vol. 9, no. 12, p. 638, Dec. 2017, doi: 10.3390/polym9120638.
[152] A. Kourgiantaki *et al.*, "Neural stem cell delivery via porous collagen scaffolds promotes neuronal differentiation and locomotion recovery in spinal cord injury," *Npj Regen. Med.*, vol. 5, no. 1, Art. no. 1, Jun. 2020, doi: 10.1038/s41536-020-0097-0.
[153] E. M. Steel, J.-Y. Azar, and H. G. Sundararaghavan, "Electrospun hyaluronic acid-carbon nanotube nanofibers for neural engineering," *Materialia*, vol. 9, p. 100581, Mar. 2020, doi: 10.1016/j.mtla.2019.100581.
[154] Y. Ji *et al.*, "Electrospun three-dimensional hyaluronic acid nanofibrous scaffolds," *Biomaterials*, vol. 27, no. 20, pp. 3782–3792, Jul. 2006, doi: 10.1016/j.biomaterials.2006.02.037.
[155] C. Zhu, D. Fan, and Y. Wang, "Human-like collagen/hyaluronic acid 3D scaffolds for vascular tissue engineering," *Mater. Sci. Eng. C*, vol. 34, pp. 393–401, Jan. 2014, doi: 10.1016/j.msec.2013.09.044.
[156] Y. H. Kim *et al.*, "A 3D human neural cell culture system for modeling Alzheimer's disease," *Nat. Protoc.*, vol. 10, no. 7, pp. 985–1006, Jul. 2015, doi: 10.1038/nprot.2015.065.
[157] A. Bastiaens, S. Xie, and R. Luttge, "Nanogroove-Enhanced Hydrogel Scaffolds for 3D Neuronal Cell Culture: An Easy Access Brain-on-Chip Model," *Micromachines*, vol. 10, no. 10, Sep. 2019, doi: 10.3390/mi10100638.
[158] S. E. Stabenfeldt and M. C. LaPlaca, "Variations in rigidity and ligand density influence neuronal response in methylcellulose–laminin hydrogels," *Acta Biomater.*, vol. 7, no. 12, pp. 4102–4108, Dec. 2011, doi: 10.1016/j.actbio.2011.07.026.
[159] T. Ahlfeld *et al.*, "Methylcellulose – a versatile printing material that enables biofabrication of tissue equivalents with high shape fidelity," *Biomater. Sci.*, vol. 8, no. 8, pp. 2102–2110, 2020, doi: 10.1039/D0BM00027B.
[160] B. B. Patel, F. Sharifi, D. P. Stroud, R. Montazami, N. N. Hashemi, and D. S. Sakaguchi, "3D Microfibrous Scaffolds Selectively Promotes Proliferation and Glial Differentiation of Adult Neural Stem Cells: A Platform to Tune Cellular Behavior in Neural Tissue Engineering," *Macromol. Biosci.*, vol. 19, no. 2, p. 1800236, 2019, doi: 10.1002/mabi.201800236.
[161] S. Vijayavenkataraman, S. Kannan, T. Cao, J. Y. H. Fuh, G. Sriram, and W. F. Lu, "3D-Printed PCL/PPy Conductive Scaffolds as Three-Dimensional Porous Nerve Guide Conduits (NGCs) for Peripheral Nerve Injury Repair," *Front. Bioeng. Biotechnol.*, vol. 7, 2019, doi: 10.3389/fbioe.2019.00266.
[162] S.-J. Lee, M. Nowicki, B. Harris, and L. G. Zhang, "Fabrication of a Highly Aligned Neural Scaffold via a Table Top Stereolithography 3D Printing and Electrospinning<sup/>," *Tissue Eng. Part A*, vol. 23, no. 11–12, pp. 491–502, 2017, doi: 10.1089/ten.TEA.2016.0353.
[163] N. Antill-O'Brien, J. Bourke, and C. D. O'Connell, "Layer-By-Layer: The Case for 3D Bioprinting Neurons to Create Patient-Specific Epilepsy Models," *Materials*, vol. 12, no. 19, Oct. 2019, doi: 10.3390/ma12193218.
[164] M. Thomas and S. M. Willerth, "3-D Bioprinting of Neural Tissue for Applications in Cell Therapy and Drug Screening," *Front. Bioeng. Biotechnol.*, vol. 5, 2017, doi: 10.3389/fbioe.2017.00069.

[165] A. L. Carlson *et al.*, “Generation and transplantation of reprogrammed human neurons in the brain using 3D microtopographic scaffolds,” *Nat. Commun.*, vol. 7, no. 1, Art. no. 1, Mar. 2016, doi: 10.1038/ncomms10862.
[166] A. Jakobsson, M. Ottosson, M. C. Zalis, D. O’Carroll, U. E. Johansson, and F. Johansson, “Three-dimensional functional human neuronal networks in uncompressed low-density electrospun fiber scaffolds,” *Nanomedicine Nanotechnol. Biol. Med.*, vol. 13, no. 4, pp. 1563–1573, May 2017, doi: 10.1016/j.nano.2016.12.023.
[167] M. C. Serrano *et al.*, “3D free-standing porous scaffolds made of graphene oxide as substrates for neural cell growth,” *J. Mater. Chem. B*, vol. 2, no. 34, pp. 5698–5706, Aug. 2014, doi: 10.1039/C4TB00652F.
[168] F. Khayyatan, S. Nemati, S. Kiani, S. Hojjati Emami, and H. Baharvand, “Behaviour of Human Induced Pluripotent Stem Cell-Derived Neural Progenitors on Collagen Scaffolds Varied in Freezing Temperature and Laminin Concentration,” *Cell J. Yakhteh*, vol. 16, no. 1, pp. 53–62, 2014.
[169] K. Tan, X. Wang, J. Zhang, Z. Zhuang, and T. Dong, “[Effect of chitosan porous scaffolds combined with bone marrow mesenchymal stem cells in repair of neurological deficit after traumatic brain injury in rats],” *Zhongguo Xiu Fu Chong Jian Wai Ke Za Zhi Zhongguo Xiufu Chongjian Waike Zazhi Chin. J. Reparative Reconstr. Surg.*, vol. 32, no. 6, pp. 745–752, 15 2018, doi: 10.7507/1002-1892.201712047.
[170] G. Binnig, C. F. Quate, and Ch. Gerber, “Atomic Force Microscope,” *Phys. Rev. Lett.*, vol. 56, no. 9, pp. 930–933, Mar. 1986, doi: 10.1103/PhysRevLett.56.930.
[171] E. Thormann, T. Pettersson, and P. M. Claesson, “How to measure forces with atomic force microscopy without significant influence from nonlinear optical lever sensitivity,” *Rev. Sci. Instrum.*, vol. 80, no. 9, p. 093701, Sep. 2009, doi: 10.1063/1.3194048.
[172] “AFM || WITec Raman Imaging.” https://www.witec.de/techniques/afm/ (accessed Jan. 03, 2021).
[173] A. Smekal, “Zur Quantentheorie der Dispersion,” *Naturwissenschaften*, vol. 11, no. 43, pp. 873–875, Oct. 1923, doi: 10.1007/BF01576902.
[174] C. V. Raman and K. S. Krishnan, “A New Type of Secondary Radiation,” *Nature*, vol. 121, no. 3048, Art. no. 3048, Mar. 1928, doi: 10.1038/121501c0.
[175] U. Wehrmeister, A. L. Soldati, D. E. Jacob, T. Häger, and W. Hofmeister, “Raman spectroscopy of synthetic, geological and biological vaterite: a Raman spectroscopic study,” *J. Raman Spectrosc.*, vol. 41, no. 2, pp. 193–201, 2010, doi: 10.1002/jrs.2438.
[176] K. J. I. Ember *et al.*, “Raman spectroscopy and regenerative medicine: a review,” *Npj Regen. Med.*, vol. 2, no. 1, Art. no. 1, May 2017, doi: 10.1038/s41536-017-0014-3.
[177] “Bruker AFM Probes - MLCT-BIO.” https://www.brukerafmprobes.com/p-3945-mlct-bio.aspx (accessed Dec. 18, 2020).

APPENDIX A: 3D NEURONAL CULTURE

A.1 BIOMATERIALS FOR NEURONAL CELL CULTURE

Table A.1 | Biomaterials used as scaffolding for 3D neuronal cell culture

Material	Description	Advantageous Characteristics	Scaffold Types Used in	Publications
Agarose	Naturally occurring, neutral, thermo-reversible polysaccharide	- Thermoreversible with hysteric properties (ideal for cell culture conditions) - Soluble in water - Biocompatible and non-toxic - Tunable mechanical properties	- Hydrogel - 3D printed - Electrospun	[19], [95], [96], [98], [99]
Alginate	Naturally occurring anionic polymer	- Biocompatible - Hydrophilic - Biodegradable under physiological pH	- Hydrogel - Beads for drug delivery	[100], [146]
Chitosan	A cationic polymer, and the N-deacetylated derivative of chitin, which is abundant in nature	- Biocompatible and non-toxic - Hydrophilic - Biodegradable	- Hydrogel - Microspheric (gravity driven) - Porous scaffolds (freeze-dried)	[20], [96], [147], [148]
Collagen Type I	Fibrillar protein found in the ECM of most tissues	-Naturally occurring - Regenerative capabilities - Expensive - Does not require functionalization	- Hydrogel - Porous (freeze dried) - Electrospun - Used as functionalization on surface of scaffolds	[21], [53], [149]–[152]
Hyaluronic Acid (*or hyaluronan)*	Unsulfated glycosaminoglycan abundant in ECM of most tissues	- Naturally occurring - Ideal viscoelastic properties	- Electrospun - Porous (freeze dried) - 3D printed hydrogel	[153]–[155]
Matrigel	ECM protein mixture derived from extracts of from Engelbreth-Holm-Swarm mouse tumors.	- Resembles the basement membrane of *in vivo* ECM	- Hydrogel - Used as functionalization on surface of scaffolds	[156], [157]
Methylcellulose	A methyl ester of cellulose containing 27-32% methoxy groups	- Biocompatible/non-toxic - Sol-gel transition around body temp - Soluble in water - Tunable mechanical properties	- Hydrogel - 3D printed hydrogel	[98], [158], [159]

Polycaprolactone (PCL)	Biodegradable, semicrystalline, linear polyester with low melting and glass transition temperatures	- Slow degradation
		- PCL fibers can be fabricated without a crosslinking process
			- 3D printed porous scaffold
			- Fibrous
			  - Electrospun
			  - Microfluidics
				[160]–[162]

Polydimethylsiloxane (PDMS)	Silicon elastomer used extensively in microfluidics	- Non-toxic - Young's Modulus 0.4-4 MPa - High optical transparency (ideal for assessing cells via microscopy)	- Hydrogel - Micropatterned lattice	[27]

*Note that most references listed use the material in conjunction with other materials (some listed here, some not) for composite scaffolds

A.2 3D Scaffold Fabrication Methods Used in Neuronal Culture

Table A.2 | Current methods used for 3D neuronal cell culture

Technique	Description	Advantages	Disadvantages	Publications
Bioprinting	Layer-by-layer additive manufacturing. The fabrication technique combines 3D printing and bioinks (composed of polymers, cells, crosslinking agents, growth factors, etc.)	- High throughput - Consistent - High resolution - Intricate geometry	- High upfront costs - High shear force on cells during fabrication	[97], [163], [164]
Electrospinning and Electrospraying	Electrically charged jet of polymer solution is released from a syringe pump in a spiral formation due to the electrostatic force from high-voltage power source resisting surface tension on the collector. Solvent evaporates and polymer solidifies creating a scaffold of nanofibers.	- Fibers promote neurite outgrowth - Nanoscale features - Precise control of fiber diameter - Structurally similar to ECM	- Use of toxic solvents - Insufficient cell infiltration - Inhomogeneous cell distribution	[153], [165], [166]
Hydrogels	Network of polymer swollen in water. A cell suspension is mixed with the polymer solution when in its liquid phase (commonly at 4°C) and then encapsulates the cells within the polymer matrix when gelled at 37°C	- Easily fabricated - Continuous matrix - Structurally similar to ECM	- Non-uniform diffusion of additives - Difficult O_2 and CO_2 exchange throughout culture - Slightly more difficult optical imaging	[18], [21], [95], [151]
Microsphere sintering or gravity driven chamber	Monodisperse emulsions (using microfluidics) or bulk emulsification (vortex mixing or stirring) is used to fabricate polymeric microspheres. Microspheres can also be obtained commercially. Microspheres are functionalized and added to a small chamber where they naturally form a close-packed scaffold. Microsphere scaffold can be heated above the material's glass transition temperature allowing polymer chains to intertwine and connect with adjacent microspheres for a rigid matrix	- Uniform diffusion of additives - Efficient Difficult O_2 and CO_2 exchange throughout culture - Predictable and tunable growth area - Many commercially available microspheres - Can use microspheres as drug	- Structurally dissimilar to ECM - Requires a pre-seeding of cells on spheres prior 3D build.	[20], [24], [25], [55]–[57]
Freeze-drying	Polymer dissolved in a solvent then frozen (below triple point) and lyophilized under high vacuum. Ice crystals are evaporated (under low pressure ice sublimates from solid phase to gas phase) to create voids.	- Highly porous - Water can be used as the solvent instead of toxic materials (ie. more biocompatible) - Can be combined with other methods (ex; gas foaming)	- Initial essential equipment is expensive - Long processing time	[147], [148], [167]–[169]

APPENDIX B: BIOMATERIAL CHARACTERIZATION

B.1 ATOMIC FORCE MICROSCOPY

Discovered in 1985 through the combination of scanning tunneling microscope and stylus profilometer principles [170], atomic force microscopy (AFM) has become a widely used technique for material characterization in a variety of applications. Falling into the scanning probe microscopy (SPM) category, AFM permits 3D imaging of sample structure or topography with simultaneous extraction of mechanical properties by capitalizing on the basic principles of material interactions occurring at the atomic level. The technique enables image acquisition ranging from a few atoms in size, to measure crystallographic structure of a material, to a few hundred micrometers in size to evaluate a material' topography and mechanical properties. With its versatility and angstrom level resolution, AFM has found application in many fields, including the biomedical engineering field for biomaterial development.

B.1.1 WORKING PRINCIPLE AND THE FORCE-DISTANCE CURVE

Unlike the classic optical or electron microscopes which use glass or magnetic lenses to image a sample, SPM microscopes—like the AFM—employ a cantilevered tip (probe) which interacts directly, or indirectly with a sample surface. In the present work, direct interaction (contact AFM) is used and will therefore be the method elaborated on. Specifically, single indentation measurements will be discussed.

To obtain information about a sample in contact mode, the user can either perform single indentations on the sample surface or image scans of larger regions of the sample. Both methods provide the user with important information on the stiffness and adhesion of the sample, with the latter providing information on the sample topography. From here, only the single indentation method will be discussed. To perform an indentation, the AFM apparatus first approaches the probe to the sample surface. When the probe becomes close enough to the sample, interatomic repulsion and attractive forces existing at the tip-sample interface will result in deflections of the cantilever. To track the dynamics of the cantilever, a laser is directed on the backside of the cantilever which reflects onto a photodiode (Figure B.1A). Prior to approaching a sample surface,

the laser is positioned such that it is centered and focused on the cantilever beam and centered on the photodiode quadrant. Therefore, any deflections of the cantilever caused by the tip-sample interaction will cause the laser to be reflected to a new location on the photodiode. The system registers these changes and uses this information to construct force distance curves (Figure B.1B). The deflection of the cantilever can be approximated using Hooke's Law, where deflections are proportional to the force between the tip and the sample surface [171]. Since the probe's cantilever is of known stiffness, the interaction dynamics within the force-distance curve can be further analyzed. By systematically unravelling this interaction, and capitalizing on the known properties cantilever being used, sample stiffness, elasticity, adhesion, and more can be determined.

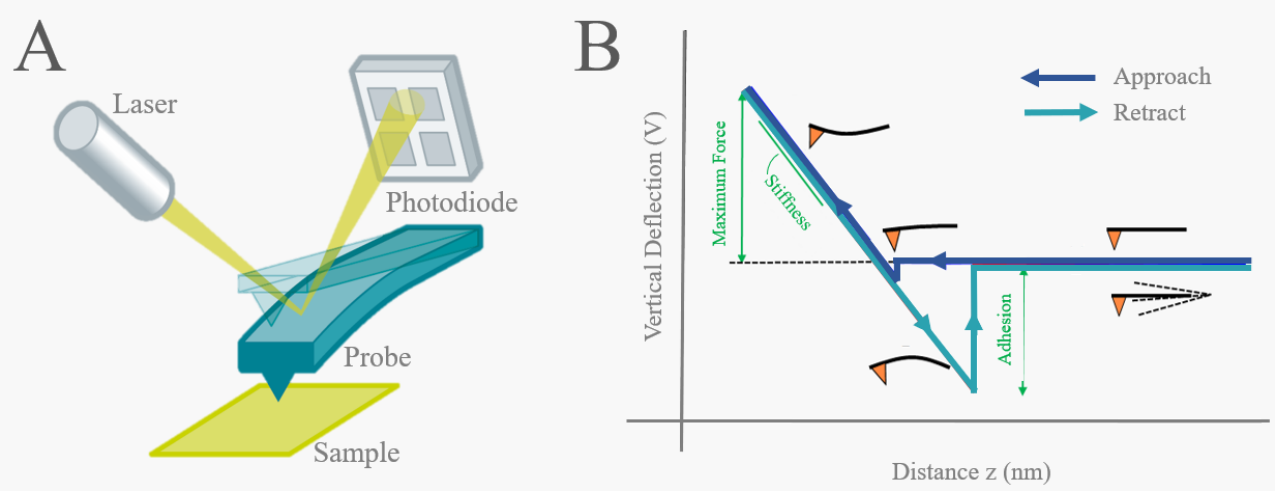

Figure B.1 | AFM working principle **(A)** Schematic [172] and **(B)** Force distance curve

B.2 RAMAN SPECTROSCOPY

Raman spectroscopy is a non-invasive, non-destructive, and label-free analytical method by which the chemical/molecular fingerprint of a material can be determined by capturing the inelastic (now termed Raman) scattering of light. Initially hypothesized by Adolf Smekal in 1923 [173], and first observed by C.V Raman in 1928 [174], the current use of Raman spectroscopy ranges from geological [175] to biomedical [176] application.

B.2.1 WORKING PRINCIPLE

When incident light from a high intensity laser light source interacts with a molecule in a sample, the molecules of that sample can enter a virtual energy state. Most of the incident light is absorbed or transmitted thorough the sample, however, a portion of the light is scattered. This scattered light can be detected using spectroscopy, revealing important information about a sample based how the light is scattered. If the scattered light has a frequency equal to the incident light frequency, the scattered light is referred to as Rayleigh scattering ($v_o = v$; Figure B.2B). Conversely, if the scattered light has a frequency different from the incident light, Raman scattering is observed ($v_o \neq v$; Figure B.2B). Raman scattering can be divided into two types: Stokes, and Anti-Stokes scattering (Figure B.2C). Stokes scattering describes the instances where an incident photon has greater energy than the scattered photon (energy transferred to molecule from incident photon), while Anti-Stokes scattering describes the instances where the incident photon has lower energy than the scattered photon (energy is transferred from the molecule to the incident photon) [176]. Raman scattering is the scattered light that material scientists and engineers are interested in since it provides information about a material's chemical make-up. Each material has a characteristic Raman spectrum which is sometimes referred to as a materials Raman fingerprint. These spectra make it easy to identify a material or confirm its presence.

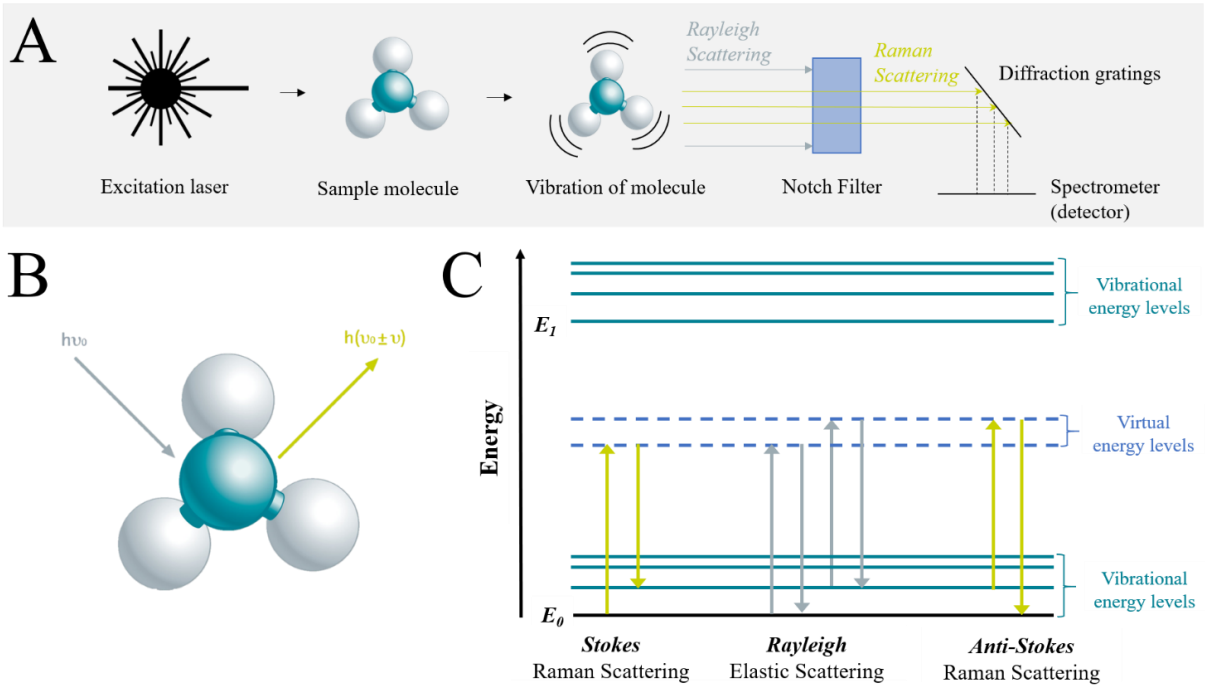

Figure B.2 | Raman spectroscopy working principle

(A) Raman spectroscopy energy path; **(B)** Scattering of light from molecule in a virtual energy state. If $v_o = v$, Rayleigh scattering observed, if $v_o \neq v$, Raman scattering is observed [172]. **(C)** Graphical depiction of molecule energy after interaction with a high intensity incident light source (laser). If molecule returns to its initial ground state, the energy emitted is equal to the energy of incident photon from the laser (equal vibrational frequency), resulting in Rayleigh scattering of the light. When a molecule releases a different quantity of energy compared to the incident photon, the molecule will fall back to a different vibrational/energy level resulting in Raman scattering (Graph adapted from: [176]).

APPENDIX C: MLCT-BIO PROBE SPECIFICATIONS

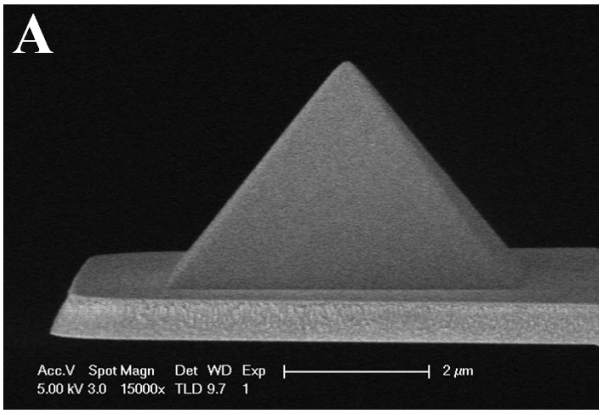

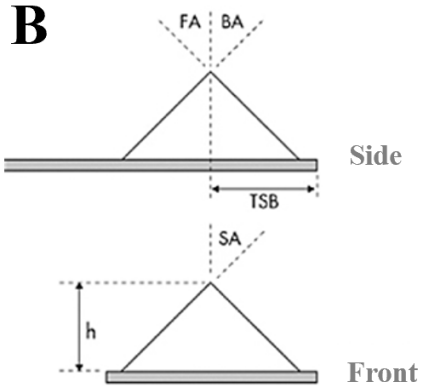

C

Geometry:	Standard (Steep)
Tip Height (h):	2.5 – 4.5 µm
Front Angle (FA):	35 ± 2°
Back Angle (BA):	35 ± 2°
Side Angle (SA):	35 ± 2°
Tip Radius (Nom):	20 nm

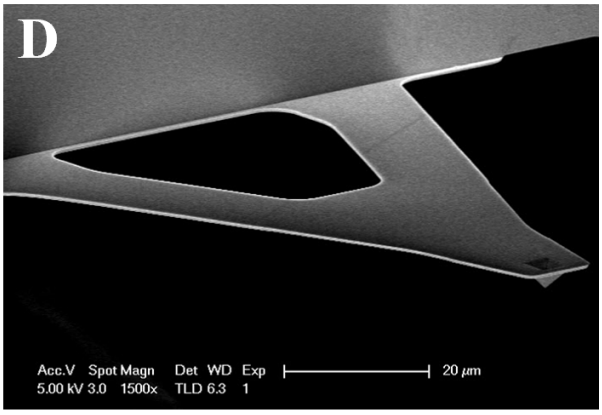

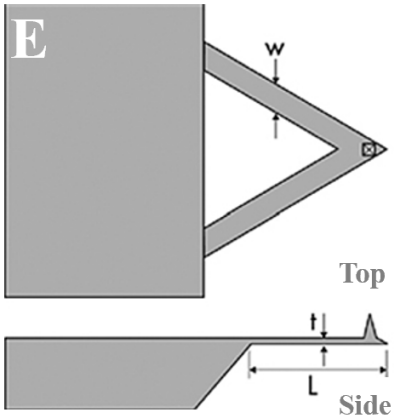

F

Material:	Silicon Nitride
Geometry:	Triangular and Rectangular
Cantilevers Number:	6
Cantilever Thickness (Nom):	0.55 µm
Cantilever Thickness (RNG):	0.5 – 0.6 µm
Back Side Coating:	Reflective Gold

Figure C.1 | MLCT-BIO probe schematic and specifications for cantilever F; **(A&B)** Tip schematic. **(C)** tip specifications **(D&E)** cantilever schematic. **(F)** cantilever specifications. Figure prepared using images and tables courtesy of Bruker AFM Probes product information website [177].